Glacial isostatic adjustment and sea-level change

State of the art report

Pippa Whitehouse, Durham University

April 2009

SKB

Glacial isostatic adjustment and sea-level change

State of the art report

Pippa Whitehouse, Durham University

April 2009

Preface

This document contains information on the process of glacial isostatic adjustment (GIA) and how this affects sea-level and shore-line displacement, and the methods which are employed by researchers to study and understand these processes. The information will be used in e.g. the report "Climate and climate-related issues for the safety assessment SR-Site".

Stockholm, April 2009

Jens-Ove Näslund
Person in charge of the SKB climate programme

Contents

1 Introduction

1.1 Structure and purpose of this report

This report outlines the physics of glacial isostatic adjustment (GIA), how this affects sea-level, and the methods which are employed by researchers to study and understand these processes. The report describes the scientific background into the processes and methods presented in /SKB 2006, section 3.3/. The purpose of this report is to provide a reference document for people who require a more in-depth understanding of GIA processes than is presented in the SKB report. The key components of the GIA system are described, and this is followed by a concise description of the processes that take place within and between these components during a glacial cycle. The report contains 4 chapters:

- "Introduction" (chapter 1)
- "GIA systems" (chapter 2)
- "Governing equations" (chapter 3)
- "State-of-the-art GIA models" (chapter 4)

Chapter 2, "GIA systems", describes the three main systems which are involved in the GIA process; the solid Earth, the hydrosphere and the cryosphere. The various parameters which govern the behaviour of these systems, and must be known in order to model GIA processes, are defined.

Chapter 3, "Governing equations", lays out the physics of GIA and derives the equations which must be solved to determine the redistribution of water over the surface of the Earth, and the solid Earth response. Secondary processes, such as ocean syphoning, are also described. The driving forces behind glacial cycles are briefly discussed.

The methods used to solve these equations are laid out in chapter 4, "State-of-the-art GIA models". In this chapter, the different approaches used by different groups of researchers are discussed, as are the relative accuracy of the methods. Recent improvements to the theory are described, as are current shortcomings of the models. The various data sets used to calibrate and verify the accuracy of the modelling are also briefly described in this chapter.

In the past few years advances in computational speed have enabled researchers to develop models which attempt to account for the effects 3-D Earth structure upon GIA processes. The preliminary results from this research are also discussed within chapter 4.

1.2 A brief introduction to GIA

1.2.1 Overview/general description

Glacial isostatic adjustment (GIA) is the response of the solid Earth to mass redistribution during a glacial cycle. For the past ~700,000 years the Earth's climate has followed a cycle of alternating glacial and interglacial conditions, with a periodicity on the order of 100,000 years. During a glacial period the lower temperatures result in the growth of ice sheets at higher latitudes, and consequently water is removed from the oceans and relative sea-level falls. Conversely, during interglacial conditions several of these ice sheets have melted, water is returned to the oceans, and relative sea-level rises. The movement of water over the surface of the Earth, both as water and as ice, during a glacial cycle acts as a load upon the lithosphere. The Earth deforms in response to this force; subsiding under the load of an ice sheet or full oceanic basin, and rebounding once the ice sheets melt or water is removed from the oceanic basins.

The deformation that takes place is isostatic. Isostasy refers to a concept whereby deformation takes place in an attempt to return the Earth to a state of equilibrium. In isostatic equilibrium the elevation of a column of the Earth's crust is a consequence of its density profile, which defines how that column 'floats' upon the Earth's mantle. The process of *glacial* isostatic adjustment refers to isostatic deformation related to ice and water loading during a glacial cycle.

There are many feedbacks within a glacial cycle, relating both to GIA and relative sea-level change, and the climate system. However, feedbacks relating to the climate system are beyond the scope of this report, and are not discussed in detail further. The principle feedback relating to GIA concerns the redistribution of water following the melting of an ice sheet. Water is distributed over the surface of the Earth according to the shape of the geoid; an equipotential gravitational surface defined by the distribution of mass both upon the surface of, and within, the Earth. Therefore both the solid deformation of the Earth and the distribution of surface loads, such as ice sheets and ocean water, must be taken into consideration when determining the instantaneous shape of the geoid, and hence the distribution of water over the surface of the Earth and changes in relative sea-level.

The most important concept to grasp in relation to GIA is that relative sea-level change is *not uniform* over the surface of the Earth: The change in the distribution of internal and surface masses following the melting of an ice sheet alters the shape of the geoid, and consequently the resulting meltwater is distributed non-uniformly throughout the oceans.

Relative sea-level is a height which is defined by the position of the interface between the ocean and the land (Figure 1-1). A rise in relative sea-level can occur due to an increase in the height of the ocean surface (for example, due to a change in the shape of the geoid, an increase in the volume of water in the oceans, or a decrease in the storage capacity of the oceans) and/or a drop in the height of the land (for example due to ice sheet loading, or tectonic activity). Conversely, a fall in relative sea-level can occur due to a fall in the height of the ocean and/or a rise in the height of the land surface, brought about by the opposite processes to those described above. At any point in time the rate of relative sea-level change is governed by a combination of these factors.

The shoreline is also related to the position of the land-sea interface, and is defined by the latitudinal and longitudinal position of this interface upon the surface of the Earth. The shoreline migrates laterally as a result of changes in relative sea-level. It will not migrate uniformly, but is dependent upon the topography of the surface of the Earth.

1.2.2   Governing factors

There are two primary factors that govern the magnitude and spatial distribution of GIA:

- The evolution of surface loading determines the forces applied to the surface of the Earth;
- The rheological structure of the Earth defines its isostatic response to this loading.

Surface loading may consist of the transport of water or sediment, or the growth and decay of ice sheets. Variations in the volume and distribution of ice are the principal cause of sea-level change and GIA-related solid Earth deformation, and the temporal and spatial evolution of ice sheets must be accurately known in order to understand the GIA response to loading during a glacial cycle. A secondary loading effect arises due to the redistribution of meltwater in the oceans. As a by-product of the surface loading, the shape of the geoid, and hence the global distribution of water and rates of relative sea-level change, are altered.

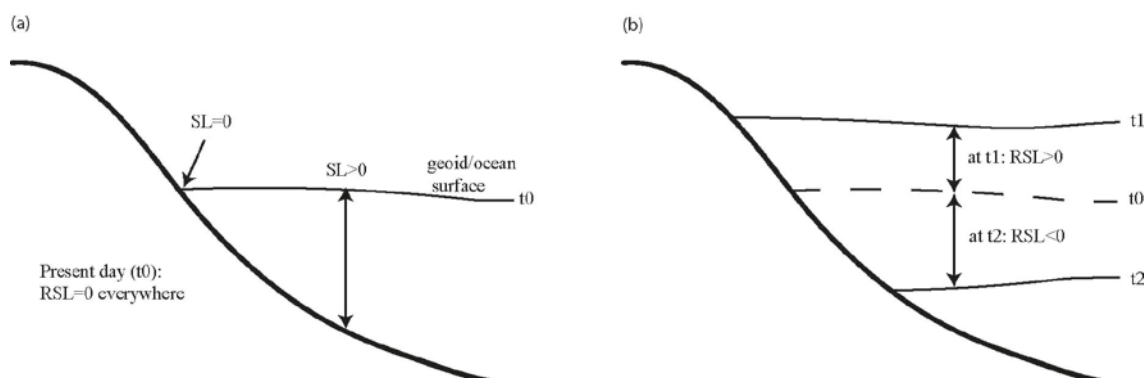***Figure 1-1.*** *(a) At time t0 sea-level (SL) is zero where the depth of the sea is zero, and positive where the depth of the sea is positive. Sea-level is defined to be zero on land. (b) At time t1 and t2 relative sea-level (RSL) is higher and lower respectively, as a result of the processes described in the text. Note that the change in relative sea-level is not uniform over the oceans, due to changes in the shape of the geoid.*

The rheology of the Earth refers to its elastic and viscous properties. These govern the magnitude and temporal evolution of deformation. To first order they vary with depth, but the Earth is strongly heterogeneous, and to a lesser degree these properties also vary laterally.

A secondary factor which governs GIA is the climate. The climate determines the timing and severity of a glacial cycle, and hence the evolution of ice sheet growth and decay. In turn, the climate is driven by a complex combination of factors; including variations in solar radiation, cycles in the Earth's orbit, anthropogenic activity, and, over longer time scales, tectonic forcing.

1.2.3   Observations of glacial isostatic adjustment

The deformation of the solid Earth is a key process of GIA. It may be observed in the present day using Global Positioning System (GPS) receivers to measure vertical and horizontal deformation rates relative to the centre of the Earth /e.g. Johansson et al. 2002/.

A by-product of solid Earth deformation is relative sea-level change. Present-day rates of relative sea-level change are measured using tide gauges. However, in order to understand the temporal evolution of GIA it is also useful to make observations which relate to past relative sea-level positions. These are recorded as raised or submerged shorelines, or in terms of salinity changes as determined from diatom analysis of lake sediments. It is important to be able to determine both the height and the age of any relative sea-level marker for it to be of use in reconstructing relative sea-level change over time.

A third observable relates to changes in the gravity field. As isostatic relaxation takes place mass movement takes place within the interior of the Earth. This signal is observable in the rate of change of the present-day gravity field, such as that measured by the GRACE satellite /e.g. Tamisiea et al. 2007/ and by terrestrial gravity surveys /e.g. Lambert et al. 2001/.

1.2.4   Time scales

For the past ~700,000 years glacial cycles have had a periodicity of ~100 ka. Prior to this, for the preceding ~1.5 Ma, they had a shorter periodicity of ~40 ka. Both time scales are determined by the Earth's orbital parameters. Changes in ice volume during a glacial cycle tend to follow an asymmetric pattern, with the growth of ice taking place gradually over several tens of thousands of years due to the slow response of ice sheets to external forcing, and deglaciation taking place much more rapidly over a few thousand years.

Loading on these time scales excites both elastic and viscous deformation within the solid Earth. Following unloading, the elastic deformation is recovered instantaneously; however viscous deformation recovers according to the relaxation time of the underlying mantle. For realistic mantle viscosities (η) of 10^{20}–10^{22} Pa s and a rigidity (μ) of ~7 × 10^{10} Pa, relaxation times ($\tau=\eta/\mu$) are on the order of a few thousand years. Therefore, following the removal of surface ice loads from high latitude continental land masses, the system will take a few tens of thousands of years to return to isostatic equilibrium. In practice this relaxation is generally cut short by the initiation of another ice age; therefore the deformation that we observe today is the overprinted result of a series of glacial cycles.

Maximum rates of solid Earth rebound due to GIA at present are ~10 mm/yr for vertical motion and ~3 mm/yr for horizontal motion; these values are found at the centre of the former Laurentian (north-east Canada) /e.g. Sella et al. 2007/ and Fennoscandian /e.g. Lidberg et al. 2007/ ice sheets. Immediately following deglaciation, rebound rates were up to an order of magnitude greater; they decay approximately exponentially with time according to the viscous properties of the Earth.

GIA is strongly dependent upon the global deglaciation history. The primary constraints upon the timing and location of deglaciation come from geomorphology (moraines etc.) and relative sea-level data. Past rates of relative sea-level change allow us to place constraints upon the rate at which deglaciation took place following the Last Glacial Maximum (LGM), and make inferences about ice sheet dynamics. Present-day eustatic rates of relative sea-level change are estimated at 3.1 ± 0.4 mm/yr /Cazenave and Nerem 2004/, but during peak deglaciation eustatic rates will have reached 10 mm/yr. The term 'eustatic rate' attempts to describe a mean global rate of relative sea-level change. However, as will become apparent in chapter 3, sea-level change is not globally uniform.

2 Glacial isostatic adjustment systems

2.1 Introduction

The key components of the Earth systems involved in GIA are discussed. The parameters which govern the behaviour of these systems are defined, and a description of their internal dynamics is given. Finally, a summary of the methods used to represent the systems within GIA modelling is presented. Further details of this are given in chapter 4.

2.2 The solid Earth

2.2.1 General description

From a geophysical point of view, the solid Earth is a heterogeneous, multi-layered, oblate spheroid. Its outer layer is the crust, which has an average thickness of 35 km beneath the continents and 7–8 km beneath the oceans. The crust forms the upper part of the lithosphere, which is typically ~100 km thick, and is the section of the Earth that participates in plate tectonics. Beneath the lithosphere lies the mantle, which extends down to ~2,900 km (Figure 2-1). It may be sub-divided into two layers, the upper and lower mantle. The transition is marked by a change in density and chemical composition. At the base of the lower mantle lies the core-mantle boundary, beneath which lies the iron-rich core which comprises an outer liquid core and an inner solid core.

The time scale and magnitude of loading during a glacial cycle excites deformation from the crust to the lower mantle. The transition at the core-mantle boundary from solid to liquid means that the core plays no part in influencing GIA processes.

Glacial inception occurs on land, and while ice sheets may extend offshore and be grounded as far as the edge of the continental shelf, they do not extend onto oceanic crust. The major global ice sheets form upon old cratonic lithosphere, and in the following section I focus on the material properties of such regions. However, there are exceptions: ice sheets that form on Iceland are situated upon very young crust above a low viscosity mantle. GIA models of this region should take account of its unusual geodynamic setting.
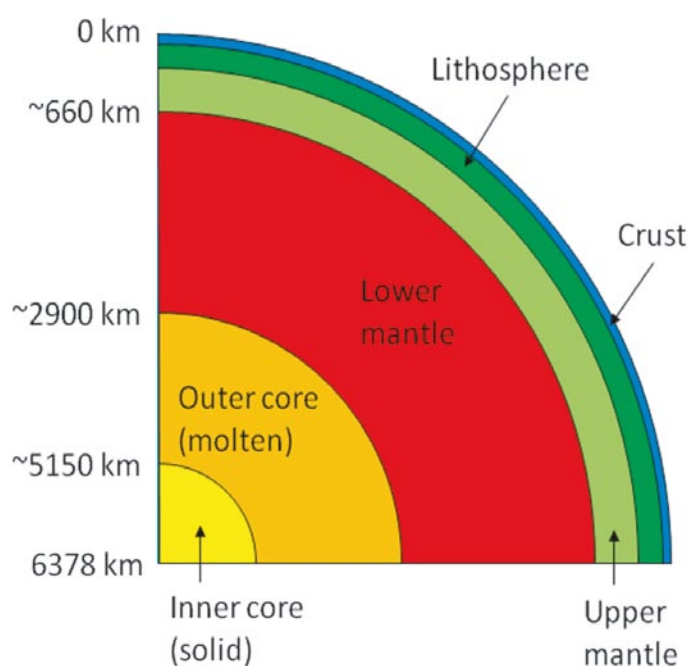

Figure 2-1. *Simple diagram of the Earth's interior. See text for details of layer thicknesses.*

2.2.2 Governing parameters and system dynamics

The material properties of the crust, lithosphere and mantle determine the response of the solid Earth to GIA-related surface loading.

The transition from crust to mantle takes place across the Mohorovičić discontinuity (or the Moho) and is defined in terms of a change in chemical composition. It occurs at depths of 5–40 km depending on whether the crust is oceanic or continental.

Crustal material is silica-rich, and is classified as mafic or felsic depending on its chemical composition. Oceanic crust is formed from mafic material at spreading ridges, which means that it is rich in magnesium and iron and is denser than continental crust. Principal mafic minerals are olivine and pyroxene, and common mafic rocks are gabbro and basalt. Oceanic crust is generally younger than 150 Ma, and it responds approximately elastically to surface loading. As it cools it thickens and becomes denser, eventually becoming denser than the underlying mantle material. The resulting gravitational instability results in the recycling of oceanic crust via subduction zones.

In contrast, continental crust is strongly heterogeneous in terms of composition, age, thickness and strength. Continental crust is predominantly felsic, which means that it is enriched with lighter elements such as silicon and aluminium, and is less dense than oceanic crust. The most common mafic mineral is quartz, which is one of the principle constituents of granite. Continental crust is, on average, thicker and older than oceanic crust, although its age may vary from a few million years to several billion years.

Beneath the crust, the Moho marks the transition from silica-rich crustal material to ultramafic mantle material. Ultramafic material has a very low silica content (< 45%) and is predominantly composed of mafic minerals (> 90%), making it denser than the crust.

It is important to understand the difference between definitions of the crust and the lithosphere. The lithosphere is the solid outer layer of the Earth, and comprises the crust and uppermost mantle. The transition from crust to mantle is defined by a change in *chemical composition*, whereas the transition from lithosphere to asthenosphere (the name given to non-lithospheric mantle material) is defined in terms of *mechanical* and *physical* properties, and often approximately coincides with the melting point of mantle material. The base of the lithosphere is not uniquely defined; it may be delimited by a change in seismic, thermal, or mechanical properties. Each definition results in a different estimate for lithospheric thickness. The lithosphere-asthenosphere system may be thought of as a rigid elastic shell enclosing a viscous fluid.

When placed under stress, the Earth exhibits both elastic and viscous behaviour. A material that behaves elastically deforms instantaneously when a force is applied, and returns to its original state immediately after the force is removed, e.g. a spring. A viscous material, such as honey, undergoes transient, permanent deformation when a force is applied. This deformation will have either linear (Newtonian), or non-linear (non-Newtonian), time dependence. A material that behaves both elastically and viscously is called a viscoelastic material; it will experience both instantaneous and transient deformation upon the application of a force.

Over time periods of several million years, continental lithosphere has been shown to deform viscously when placed under stress /England and Houseman 1986/. However, stresses on the time scale of a glacial cycle (~100,000 years) principally excite elastic deformation throughout the lithosphere. Within the upper crust high stresses are often accommodated by brittle faulting resulting in earthquakes. The stress related to ice-loading can cause brittle failure immediately following loading or unloading /Lund 2005/, but over the time scale of a whole glacial cycle it is the elastic deformation of the entire lithosphere, combined with the viscoelastic deformation of the underlying mantle, that are of most interest. Therefore, we must determine the parameters relating to the bulk properties of the lithosphere in order to understand the response of this region of the Earth to loading during a glacial cycle.

Conversely, the mantle behaves viscoelastically over the time scale of a glacial cycle. Over longer time scales the dominant process is viscous convection, driven by temperature and density gradients, but this may be perturbed by lithospheric processes. When the lithosphere is deformed by glacially-related surface loading, mantle flow plays a part in compensating for, and driving, the resulting isostatic response of the lithosphere. The depth to which the mantle responds to surface loading is dependent upon the size of the load; the largest ice sheets excite deformation in the lower mantle.

The viscosity of the mantle is a measure of its strength, and determines to what degree surface loading is supported. Estimates of mantle viscosity for non-rift regions lie in the range 10^{19} to 10^{24} Pa s. This large variation highlights the dependence of mantle viscosity upon depth, temperature, composition and stress, and has been derived from a range of observational studies including those relating to postglacial rebound /e.g. Cathles 1975, Peltier 1976, 1998a/, continental deformation /England and Houseman 1986/, long wavelength geoid anomalies /Richards and Hager 1984/ and seismic velocity perturbations (where physical scaling laws are used to translate velocity perturbations into perturbations of density, temperature and finally viscosity). GIA data are a particularly good indicator of absolute viscosity values due to their time-varying nature.

The transition from the upper to lower mantle at a depth of ~660 km is poorly understood, but is probably related to changes in the composition of the mantle, resulting in apparent changes in the density and elastic properties of the mantle, and an abrupt change in seismic velocities at this depth. For the purposes of GIA it is sufficient to note that it is highly likely that surface-loading excites a signal in the lower mantle, which is generally understood to have a slightly higher viscosity than the upper mantle by 1 to 2 orders of magnitude /Lambeck et al. 1990, Mitrovica and Forte 1997, Simons and Hager 1997/.

This overview of the structure of the Earth is simplistic in that, apart from differences between oceanic and continental crust, it only considers radial variations in material properties such as viscosity. The Earth is laterally heterogeneous at all depths: To first order continental lithosphere is generally weaker and less viscous than oceanic lithosphere, and therefore they should exhibit different styles of deformation under the same load. Similarly, mantle viscosity probably varies laterally by 1 to 2 orders of magnitude, and this will influence the pattern and magnitude of the resulting deformation. GIA studies should take these variations into account when attempting to understand the global relationship between surface loading and solid Earth deformation.

All of our understanding relating to the material properties of the Earth comes from previous geophysical studies, including early GIA studies. Tomography and seismology provide the key to understanding the deep Earth, and the seminal work of /Dziewonski and Anderson 1981/ in defining a Preliminary Reference Earth Model (PREM) has provided the basis of the radial elastic and density structure of the Earth used in the overwhelming majority of subsequent work, while studies of lithospheric flexure /e.g. Watts 2001/ and continental deformation /e.g. England and Houseman 1986/ have provided insights into lithospheric structure /Jackson et al. 2008/. However it must be stressed that values for all of the material parameters defined above are estimates, and this must be taken into account when analysing attempts to model GIA.

2.2.3   Representation in GIA models

The simplest Earth models used in GIA studies consist of two layers; an elastic lithosphere of constant thickness, and a viscous half space that represents the mantle. Such models are generally used in regional studies or sensitivity tests, and adopt a flat, 2-D (Cartesian or axisymmetric) geometry. However, they do not solve the full sea-level equation since they do not consider the redistribution of water over the whole surface of the Earth.

The most common Earth models used in GIA studies use spherical geometry to represent the whole Earth. This allows solutions to the full sea-level equation to be obtained. These models consist of an elastic lithosphere of constant thickness, then between 1 and ~20 viscoelastic mantle layers, depending upon whether the mantle is represented as a single layer of uniform viscosity, whether it is divided into the upper and lower mantle (the most common scenario), or whether a multi-layer structure is adopted. In each case, the viscosity in each layer is usually taken to be uniform.

In all models which use spherical geometry, the PREM /Dziewonski and Anderson 1981/ is used to determine the Earth's radial elastic and density structure. Viscosity values are then either obtained by inversion, or estimated from independent geophysical studies. Continental lithospheric thicknesses typically range between 70 km and 200 km, while mantle viscosities typically range between 10^{19} and 10^{24} Pa s.

The Earth's mantle is commonly approximated to behave viscoelastically on time scales relevant to GIA /Wu and Peltier 1982/. Other material approximations have been used in GIA models, including combinations of brittle, elastic and viscous behaviour. A few models include compressibility /e.g. Latychev et al. 2005a/, and there is also ongoing debate as to whether a linear (Newtonian), non-linear, or transient power law should be used to describe the rheology /Gasperini et al. 2004, Wu and Wang 2008/. However, given the still reasonable fit to the data using Newtonian rheology models (one where there is a linear relationship between the stress, or force, applied to the material and the resulting strain) it seems that such models are adequate for use in current GIA modelling /e.g. Wu 2002a/.

The spherical models described above are essentially 1-D; they only vary in the radial direction. However, recent Earth models have been developed that are fully 3-D: They permit lateral variations in lithospheric thickness and/or lateral variations in viscosity at each depth. GIA models either employ spectral methods, or are defined in terms of finite element or finite volume models (see section 4.3).

It should be noted that alterations to the underlying topography of the Earth, for example as a result of glacial erosion or deposition, are neglected in current GIA models. The resulting effect upon, e.g. shoreline migration, is assumed to be negligible.

2.3 The hydrosphere

2.3.1 General description

The hydrosphere comprises all liquid water on the Earth, including groundwater, surface water in lakes and rivers, and water in the oceans. Around 70% of the Earth's surface is covered by oceans, which play an important part in the climate system due to their ability to store and transport heat, as well as carbon dioxide.

During a glacial cycle water is transferred between the hydrosphere and the cryosphere. During the last glacial maximum (LGM) the ocean equivalent of 115–135 m of water was stored within ice sheets /e.g. Milne et al. 2002/, and ocean levels were at a minimum. During interglacial periods, such as the present day, ocean levels are at a maximum.

During ice sheet build-up, water is taken directly from the oceans by evaporation and deposited as snow, which may then be incorporated into the ice sheets. As water is converted from ice back into liquid form during melting it will often be temporarily stored as surface water in rivers, and potentially for longer in topographic or ice-dammed lakes. Therefore there will be a delay between ice sheet melting and an increase in ocean volume and sea-level height. Ice-dammed lakes can exist for several hundred years before they are breached, leading to a rapid pulse in the rate of sea-level rise.

The volume and timescale of water stored as groundwater is poorly constrained and highly spatially variable. However it is unlikely that these volumes will change sufficiently over a period of 100 ka to generate a GIA response, therefore forces due to groundwater loading are neglected in GIA models.

2.3.2 Governing parameters and system dynamics

The most important dynamical feature of the hydrosphere is its shape. Since it is liquid, the surface of the ocean adjusts to follow an equipotential surface, which is referred to as the reference surface of the Earth, or the geoid. At all points on the surface of the geoid, the gravity field will have the same value, and will be perpendicular to the surface. The shape of the geoid alters as mass is redistributed throughout the Earth's solid and fluid envelopes, and hence the shape of the ocean surface is time-varying.

The gravitational attraction of a land-based ice sheet perturbs the local height of the geoid, and hence sea-level, upwards (Figure 2-2a). As the ice sheet melts, mass is removed from the land and this lowers the local height of the geoid (see the near-field ocean, Figure 2-2b). The resulting meltwater will be distributed throughout the oceans gravitationally-consistently according to the new shape of the geoid. Globally this results in a small eustatic sea-level rise (see the far-field ocean, Figure 2-2b), but locally this rise is masked by the geoid fall due to the removal of the surface mass, and the relative sea-level fall due to solid Earth rebound. The cumulative effect in this region is relative sea-level fall.
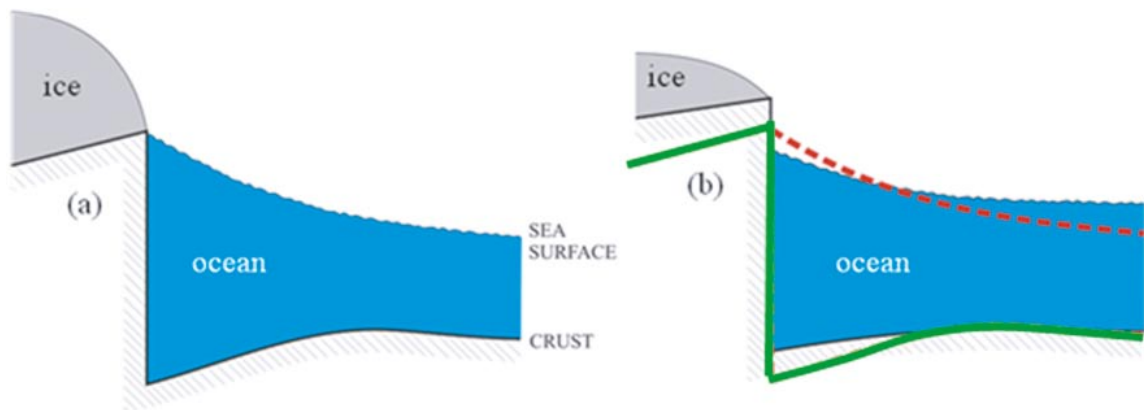
Figure 2-2. *(a) Ocean height is perturbed upwards due to the gravitational attraction of the ice sheet. Solid Earth is depressed downwards due to the mass of the ice sheet. (b) Local relative sea-level fall due to a decrease in gravitational attraction by the ice (red dashed line shows previous position), combined with solid Earth rebound (green line shows previous positions) due to the ice sheet having a smaller mass. Far-field sea-level rise is due to the addition of meltwater into the ocean. Adapted from /Tamisiea et al. 2003/.*

Ocean circulation and ocean currents can perturb the height of the ocean surface away from the predicted geoid height by several metres. Over short time scales, pressure changes in the atmosphere and lunar tides alter the height of the sea surface by a similar amount. Ocean circulation is driven by density gradients within the ocean, which exist due to variations in the temperature and salinity, giving rise to the term 'thermohaline circulation'. Ocean currents are also driven by the wind, and the rotation of the Earth. During a glacial cycle the temperature and salinity structure of the ocean is altered, for example, due to inputs of cold, freshwater from melting ice sheets, while ocean currents may be perturbed by the presence of a land bridge during a glacial low-stand. These changes may be sufficient to fundamentally alter the pattern of the thermohaline circulation, and hence the distribution of perturbations to the height of the ocean surface.

Sea-level height can also be altered as a result of density changes, related to variations in temperature or salinity. This is known as the *steric* effect. There is no input or output of water; volume changes are purely due to an increase or decrease in density. For example, as water is heated it becomes less dense and expands, thus its volume increases. In the present-day increasing ocean temperatures are thought to contribute ~1.6 ± 0.5 mm/yr to eustatic sea-level rise /IPCC 2007/ via the steric effect.

The final factor which controls the distribution of water over the surface of the Earth is the underlying bathymetry of the ocean basins. The time-dependent nature of isostatic deformation means that the shape of the ocean basins is continually changing. This results in ongoing relative sea-level change and the migration of shorelines.

In terms of GIA, surface water acts as a time-varying load. Within the water cycle, water is also present in the atmosphere (in solid, liquid or gaseous form), on the Earth's surface (as snow and ice), and as groundwater. The volumes of water involved in precipitation, evaporation, and transpiration, and the volume stored as groundwater do not vary over long time scales, and they have a minimal loading effect upon the solid Earth. The role of water in the form of ice is discussed in section 2.4.

2.3.3   Representation in GIA models

Conservation of mass is used to determine the timing and mass of water that is transferred from ice sheets into the oceans during a glacial cycle. This calculation is determined by the ice-loading history used in the GIA model (see section 2.4). Water is redistributed gravitationally-consistently throughout the oceans according to the sea-level equation (see section 3.3).

Early GIA models used a fixed ocean area to calculate approximate solutions for the redistribution of water throughout the oceans. Current models use bathymetry and topography data in order to determine changes in ocean surface area during glacial cycles. This feeds back into the sea-level equation and is used to calculate how water is distributed throughout the oceans, the ocean-loading function, and the position of the shoreline.

Ocean circulation and sea-level changes due to steric effects are neglected in present GIA models. Perturbations to the height of the ocean surface away from the reference geoid due to ocean dynamics are negligible compared to the magnitude of relative sea-level change over a whole glacial cycle. In light of this assumption, a constant value is used for the density of ocean water in GIA calculations. Perturbations to the height of the ocean surface due atmospheric pressure variations take place on a much shorter time scale than those involved with GIA, and may also be neglected in the modelling.

Another factor that is currently neglected in GIA models is the delay between the melting of ice and the time at which the meltwater enters the ocean. If the meltwater flows continuously from the edge of the ice sheet to the ocean then this interval is very small on the time scale of a glacial cycle, and errors to the surface loading functions will be negligible. However, if large bodies of meltwater are stored for several hundred years in proglacial lakes then ocean-loading will be overestimated. The error due to neglecting this factor needs to be quantified in future GIA models.

2.4   The cryosphere

2.4.1   General description

The cryosphere comprises all frozen water on the Earth, including snow and ice, glaciers, ice sheets, sea ice, ice shelves and permafrost. During the present interglacial, ice sheets persist where there are suitable climate conditions; in Antarctica and Greenland, while glaciers exist in high mountain ranges such as the Andes, the Himalaya, the Rockies, the Alps and the Scandinavian mountain range. During a glacial, existing ice sheets expand and new ice sheets grow across high latitude continental land masses where there are suitable climatic conditions. During the LGM, large areas of North America and northern Eurasia were glaciated, and the Antarctic and Greenland ice sheets contained considerably larger volumes of ice than at present.

The volume of ice within the cryosphere reaches a maximum sometime during the glacial phase. There are strong feedbacks to the climate system which variously enhance or restrict the build-up of ice. A detailed discussion of these is beyond the scope of this report, but it is worth noting that it is not sufficient for a region to have an average temperature below a certain value; there must also be sufficient precipitation for ice build-up, and inter-annular climate variations must be favourable to support permanent ice sheets.

Ice sheets store large volumes of freshwater. Variations in these volumes throughout a glacial cycle alter relative sea-level, and the distribution of salinity within the oceans.

In GIA studies, the parts of the cryosphere of principal interest are those which apply a sufficient load upon the Earth as to produce solid Earth deformation, and are of sufficient size to cause tens of metres of eustatic sea-level change when they grow or melt. This includes ice sheets, glaciers, and grounded sea ice. Where ice sheets meet the ocean they may continue to be grounded for tens of kilometres on the continental shelf, thus considerably extending the area of loading.

2.4.2   Governing parameters and system dynamics

Ice sheets gain mass in accumulation zones where snow is transformed to ice. This takes place mainly at higher altitudes. Mass is lost in ablation zones at lower altitudes due to melting at the surface. Basal melting may occur under large portions of an ice sheet, both under accumulation and ablation areas. Water is removed as runoff upon, within and beneath the ice sheet. If ice sheets end at the coast then mass is lost as the tongue begins to float and eventually iceberg calving takes place. There are many factors that influence the internal dynamics of ice sheets and their resulting topographic ice profile. Fast-moving parts of ice sheets will tend to have a gentler profile and smaller maximum thickness than parts that are frozen at their base which results in slow ice movement. Many factors influence whether or not an ice sheet is frozen at its bed, e.g. climatic conditions, ice thickness, geothermal heat flow at the Earth's surface, ice dynamics, the topography and gradient of the bed, and the bed material (e.g. glacial till or solid rock). Ice sheets that form in present day temperate regions are more susceptible to climatic variations; therefore it is the growth and decay of ice sheets in these regions – such as Fennoscandia and North America – that provide the greatest contribution to sea-level changes during a glacial cycle.

Conditions at the terminus of an ice sheet can also strongly influence the dynamics of the ice sheet, especially if the ice sheet extends to the coast. Here, ocean temperatures or sea surface conditions can influence the rate of iceberg calving, or the longevity of an ice shelf. The collapse of an ice shelf due to warming temperatures can affect the dynamics of a large portion of the ice sheet.

Further discussion of the dynamics of ice sheets is beyond the scope of this report; for a detailed overview of this topic, see e.g. /SKB 2006/.

2.4.3   Representation in GIA models

Ice-loading in GIA models is generally applied in a series of time steps, with each time step covering between ~500 years and ~10,000 years, depending upon the temporal and spatial resolution required. Ice extent and thickness are defined at each time step.

Sensitivity studies often use a simplified, axisymmetric ice sheet where accumulation and melting takes place linearly over time. The majority of global GIA models use ice histories that cover the whole of the last glacial cycle. Ice margin positions prior to the LGM are in these models often poorly constrained. Early ice models defined the loads as a series of discs /e.g. Tushingham and Peltier 1991/, whereas more recent models /e.g. Lambeck et al. 1998a, Peltier 2004/ give the thickness of ice at a given position and at a given time. This distribution of loading is then transformed into the spectral domain in order to compute solutions to the sea-level equation (see section 4.3.2).

A few studies have used the output from dynamic ice models to define the pattern of ice-loading during a glacial cycle /e.g. Tarasov and Peltier 2004/. In such cases climatic and basal conditions, and the physics of ice flow, are the primary factors controlling the growth and decay of the ice sheet. However, the majority of GIA studies use ice histories that are constrained in time and space by geomorphology (dated moraine positions), and in volume by observations of relative sea-level change /e.g. Lambeck et al. 1998a/. Such models are often less 'physical' than the dynamic models, especially with regard to the profile of the ice sheet, but they have the advantage that they are usually constrained by observations. Furthermore, dynamic ice sheet models may also be constrained by glacial geological observations, /e.g. SKB 2006/.

Future GIA modelling should adopt an iterative approach, and provide feedback about the accuracy of the dynamic models in predicting GIA observables so that they may be tuned to fit the vast array of data available.

3 Governing equations

3.1 Introduction

In this chapter the physics governing GIA processes is described. The equations that determine the redistribution of water over the surface of the Earth, and the solid Earth response to loading, are derived. These equations have been modified as our understanding of GIA has increased, in order to more accurately reflect the physical processes that take place during a glacial cycle. A brief description is given, explaining each of these modifications, and how their inclusion increases the accuracy of the modelling. In order to test that the equations accurately represent GIA processes suitable output must be generated in order to compare predictions with observations. The form of solutions to the governing equations is described, and the potential output variables are listed.

Sea-level change is dependent upon several factors, described by:

$$\Delta\xi_{rsl}(x,t) = \Delta\xi_{eus}(t) + \Delta\xi_{isos}(x,t) + \Delta\xi_{local}(x,t) \qquad \text{3-1}$$

In equation 3-1 $\Delta\xi$ represents a change in sea-level. The subscript *rsl* refers to relative sea-level; relative sea-level changes vary both over time (*t*) and in space (*x*), and their cause may be divided into three distinct categories. Eustatic sea-level change (subscript *eus*) is the spatially uniform change in sea-level that occurs when a volume of water is taken from the ocean and locked into an ice sheet, or vice versa. Isostatic sea-level change (subscript *isos*) varies in both space and time, and is the result of perturbations to the shape of the solid Earth and the geoid due to temporal variations in loading by ice and water. These two components represent the change in sea-level that takes place as a result of GIA, and they form the basis of the sea-level equation, as discussed below.

The third term in equation 3-1 refers to local factors (subscript *local*) that cause sea-level change. These include the local tidal regime, atmosphere and ocean dynamics, the consolidation of sediments, and tectonic processes. These factors are neglected in this report and do not contribute to the sea-level equation as derived below. However, it may be noted, that all these processes have a negligible effect upon sea-level variations within the Baltic due to the fact that it is an enclosed sea, it is not fed by any large, sediment-laden rivers, and it is located in a stable cratonic region.

3.2 Key definitions

In the following derivations (section 3.3), the notation of /Mitrovica and Milne 2003/ has been adopted. Key variables and terms are defined below.

SL(x,t), ΔSL(x,t)	Sea-level, or a change in sea-level, at a given position, *x*, and a given time, *t*. This is equivalent to relative sea-level, as defined in section 1.2.1. For the purposes of these derivations, sea-level is referenced to the local height of the solid surface and is positive when the geoid lies above the solid surface (*G(x,t)–R(x,t)> 0*) and negative when it lies below (*G(x,t)–R(x,t) < 0*). Sea-level is therefore always positive in oceanic regions and always negative on land (see Figure 3-1). The situation is more complex in the presence of marine-grounded ice: here sea-level is positive, but for the purposes of re-distributing meltwater this location is not part of the ocean (see section 3.5.2 for further discussions on this issue). Within oceanic regions sea-level is equivalent to ocean height.
C(x,t)	The ocean function /Munk and MacDonald 1960/. This takes the value 1 over the ocean and 0 elsewhere (see Figure 3-1).
S(x,t), ΔS(x,t)	Ocean height, or a change in ocean height. This is the projection of sea-level onto the ocean function (*S(x,t)=SL(x,t).C(x,t)*). Within oceanic regions ocean height is equivalent to sea-level, elsewhere it is zero (see Figure 3-1).
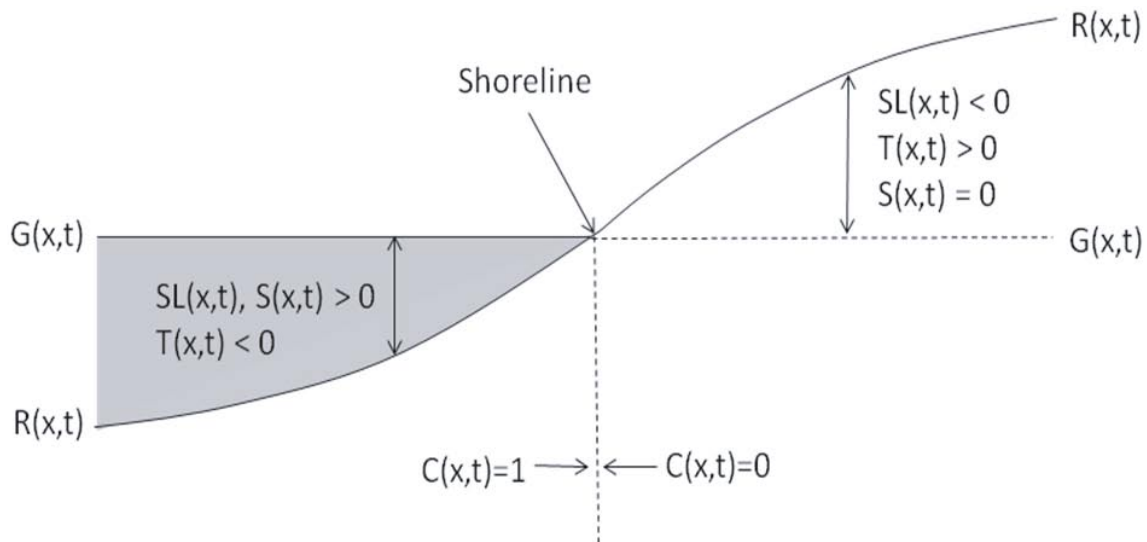
Figure 3-1. *Diagram showing sea-level (SL(x,t)) as the difference between the height of the geoid, G(x,t), and the solid surface, R(x,t). Other principle variables used in the derivation of the sea-level equation are labelled; see text for details. Ocean height is given by the vertical height of the shaded region; it is zero on land where C(x,t)=0.*

$G(x,t)$	The height of the geoid, relative to e.g. the centre of the Earth (see Figure 3-1). The geoid is an equipotential gravitational surface, as defined in section 1.2.1.
$\Phi(x,t)$	The gravitational potential, which defines the shape and height of the geoid. The value of Φ is constant over the surface of the ocean for a given ocean volume. The gravitational potential is related to the geoid by the expression $G(x,t)=\Phi(x,t)/g$, where g is the acceleration due to gravity.
$R(x,t)$	The height of the solid surface, relative to e.g. the centre of the Earth. Sea-level is defined to be the difference between the height of the geoid and the height of the solid surface (see Figure 3-1).
$T(x,t)$	Topography. For the purposes of this derivation, topography is referenced to the height of the geoid and is defined to be the negative of sea-level: $T(x,t)=R(x,t)–G(x,t)=–SL(x,t)$. (See Figure 3-1).
ρ_I, ρ_W, ρ_E	The density of ice (*I*), water (*W*), and the Earth (*E*), respectively.
A_O	The surface area of the oceans (*O*).
$V_{OW}(t)$	The change in ocean volume between time *t* and some initial time t_0.
$V_I(t)$	The change in ice volume between time *t* and some initial time t_0.
$GF(x,t)$	Green's function (sometimes the gravitational potential, Φ, is used as the Green's function).
Eustatic sea-level change	Hypothetical uniform sea-level change arising from a change in ocean volume, traditionally expressed in terms of the global mean change in sea-level.
Isostatic sea-level change	Non-uniform sea-level changes arising from local isostatic processes, in this case related to GIA processes.

20

3.3 Derivation of the sea-level equation

The sea-level equation is derived following the approach of /Farrell and Clark 1976/. First, the simple case of a point load on a rigid Earth is considered, and then a method to deal with more complex melt geometries and histories in the presence of gravitating surface masses is presented.

Secondly, calculations relating to the loading of an elastic Earth are considered. In this case changes to the gravitational potential due to solid Earth deformation (as a result of loading by ice and ocean water) must be accounted for, as well as perturbations due to the movement of surface masses. These expressions are combined with the effect of first order changes in ocean volume to determine changes in relative sea-level.

Finally calculations assuming a viscoelastic Earth are considered, resulting in the derivation of the original sea-level equation that underpins all subsequent GIA studies. Viscoelastic flow within the Earth results in a delayed, continuous response to unloading; hence the gravitational potential will change continuously, as will relative sea-level, thus time-dependence is introduced into the equation.

Further insight into the derivation of the integral form of the sea-level equation, as presented here, can be found in /Clark et al. 1978, Peltier et al. 1978, Mitrovica and Peltier 1991a, Milne and Mitrovica 1998a, Johnston and Lambeck 1999, Milne et al. 1999, Mitrovica and Milne 2003/.

3.3.1 Conservation of momentum, mass, and ocean geometry

Momentum must be conserved when calculating the deformation of the solid Earth in response to loading. Conservation of momentum is governed by the following equation:

$$\nabla \cdot \sigma - \rho g \nabla w = 0 \qquad\qquad 3\text{-}2$$

σ is the incremental stress tensor, ρ is the density of the Earth, g is gravitational acceleration, and w is vertical displacement. The first term in equation 3-2 is the divergence of stress; this is the force that acts to deform the Earth. It is balanced with the second term which is the gradient of the advected pre-stress. This is a buoyancy force which acts to restore hydrostatic equilibrium to the system; without it there would be no viscous gravitational relaxation.

Within the sea-level equation, the momentum equation is used to calculate the deformation of the solid Earth at each time step. This deformation arises due to the redistribution of ice and ocean water over the surface of the Earth. The volume of water within the Earth system must be conserved.

Conservation of mass is used to define a closed hydrological cycle. Mass lost due to melting of the cryosphere is assumed to be instantaneously added to the ocean. The ocean is assumed to be 'connected', meaning that meltwater is freely distributed throughout the oceans according to the physics of the sea-level equation.

Defining $V_{OW}(t)$ to be the volume of water added to the oceans between some initial time t_0 and time t, and $V_I(t)$ to be the change in ice volume for the same period, conservation of mass yields the following equation:

$$V_{OW}(t) = -\frac{\rho_I}{\rho_W} V_I(t) \qquad\qquad 3\text{-}3$$

where ρ_I is the density of ice (~920 kg/m³), and ρ_W is the density of water (~1,000 kg/m³).

For the derivation of the original sea-level equation (sections 3.3.2 and 3.3.3) ocean geometry is assumed constant and shorelines are assumed to be fixed. In reality, the portion of the Earth covered by ocean varies with the volume of water contained within the ocean and the deformation of the solid surface. The assumption of fixed shorelines by /Farrell and Clark 1976/ is analogous to the case where the ocean is bounded by steep cliffs that prevent onlap (the inland migration of the shoreline) or offlap (the oceanward migration of the shoreline) during sea-level change.

Since the work of /Farrell and Clark 1976/ the sea-level equation has been refined /e.g. Johnston 1993/ to account for changes in shoreline position. In present-day GIA calculations, the time-dependent ocean function, $C(x,t)$, is used to restrict ocean-loading to those areas covered by ocean at a given time, and thus accurately account for shoreline migration following meltwater re-distribution and solid Earth deformation. The ocean function takes the value 1 in ocean-covered regions, and 0 elsewhere. A time-invariant version of the ocean function, $C(x)$, is used in the original sea-level equation.

3.3.2 Perturbations to sea-level on a rigid Earth

Point source

The perturbation to the gravitational potential, Φ, due to an idealised point ice load, of mass M_I, on the surface of an ocean-covered, rigid, spherical Earth is derived in /Farrell and Clark 1976/. This expression for the geoid perturbation is used to determine the resulting change in sea-level at all points on the surface of the Earth. By initially considering the simplified case of a rigid Earth, complications due to the deformation of the solid Earth are avoided. The change in sea-level height an angular distance, θ, from the location of the point load is described by:

$$\Delta SL(\theta) = \frac{M_I a}{M_E}\left(\frac{1}{2\sin(\theta/2)} - 1 - \frac{\rho_E}{3\rho_w}\right) \qquad \text{3-4}$$

where M_I and M_E are the mass of the ice load and the Earth respectively, ρ_E is the mean density of the Earth ($\sim 5{,}520$ kg/m³), ρ_W is the density of the water, and a is the radius of the Earth ($\sim 6{,}378$ km). Throughout this report, θ will be used to denote the spatial variable on the surface of the Earth. However, it is acknowledged that two variables, the latitude and longitude, must be defined in order to uniquely identify a location on the surface of a sphere of given radius. Sometimes the variable x is also used to define a general position in space.

The first two terms in equation 3-4 represent the distortion of the shape of the ocean surface due to the attraction of the ice load upon the water. The result of this distortion is that despite the net removal of water from the ocean, sea-level rises within an angular distance of $\sim 20°$ of the ice load (Figure 2-2a). The last term in equation 3-4 represents a uniform fall in sea-level due to the removal of mass M_I from the oceans; it is determined by invoking mass conservation.

For the complementary case of the melting of a point load of mass M_I, the negative of equation 3-4 defines the resulting change in sea-level. Despite the net addition of water to the oceans, close to the melt source there is a net fall in sea-level (Figure 2-2b).

Realistic ice distribution

In order to calculate sea-level change due to a realistic ice distribution that melts instantaneously, a surface mass distribution function is defined: $\rho_I \Delta I(x)$. ρ_I is the density of ice, and $\Delta I(x)$ is the change in ice thickness, taken to be positive during ice build-up and negative during melting. This mass function is convolved with a Green's function that expresses the influence of a point mass on the change in sea-level an angular distance θ away (see equation 3-4). This expression is integrated over the surface of the Earth to give sea-level change:

$$\Delta SL(x) = \iint\limits_{ice}\left\{\frac{a}{M_E}\left(\frac{1}{2\sin(\theta/2)} - 1 - \frac{\rho_E}{3\rho_W}\right)\right\}\rho_I \Delta I(x')d\Omega \qquad \text{3-5}$$

$d\Omega$ is an element of area, and θ is the arc length between fixed position x and variable position x' on the surface of the Earth. Once again, conservation of mass is invoked, enabling the change in sea-level to be expressed in terms of a spatially-varying term, $GF*\Delta I$, and two constant terms representing the change in ocean mass:

$$\Delta SL(x) = \rho_I GF \underset{I}{*} \Delta I - \rho_I \left\langle GF \underset{I}{*} \Delta I \right\rangle_O - \frac{M_I}{A_O \rho_W} \qquad \text{3-6}$$

In equation 3-6 the * symbol with subscript I has been used to represent a convolution integral over the ice-covered surface of the Earth (as in equation 3-5), A_0 is the area covered by the oceans, the notation $<x>_O$ is used to denote the mean of variable x over the oceans, and the substitution:

$$GF(\theta) = \frac{a}{2M_E \sin(\theta/2)} \qquad \text{3-7}$$

has been made; this is the Green's function in the convolution integral. In general, a subscript O refers to integration over the surface of the ocean, and a subscript I refers to integration over all ice-covered areas. GF will be used to represent the Green's function in convolution integrals, however it should be noted that the form of the Green's function varies with the context in which it is used. See /Farrell and Clark 1976/ for a more detailed derivation of how the conservation of mass has been used to derive equation 3-6.

Gravitating surface masses

Finally in this section, the perturbation to the gravitational potential due to the reconfiguration of ice and water surface masses, and their mutual gravitational attraction, is taken into account when determining the change in sea-level. A Green's function

$$GF^R(\theta) = \frac{ag}{2M_E \sin(\theta/2)} \qquad \text{3-8}$$

is used, where the superscript R refers to the case of a rigid Earth, a is the radius of the Earth, and g is the acceleration of gravity. This expression is the perturbation to the gravitational potential field caused by a unit mass located an angular distance θ away. This is convolved with all masses, both ice and water, in order to determine the net change in the gravitational potential due to all changes to the surface mass configuration on $r=a$:

$$\Phi(x) = \rho_I GF^R \underset{I}{*} \Delta I + \rho_W GF^R \underset{O}{*} \Delta SL \qquad \text{3-9}$$

Subscript O refers to convolution over the surface of the ocean, ΔSL is sea-level change, and ΔI is ice thickness change. This alteration to the potential in turn causes a change in sea-level $\Delta SL = \Phi/g + c$ where constant c follows from the conservation of mass:

$$\Delta SL(x) = \frac{\rho_I}{g} GF^R \underset{I}{*} \Delta I + \frac{\rho_W}{g} GF^R \underset{O}{*} \Delta SL - \frac{M_I}{A_O \rho_W} - \frac{\rho_I}{g} \left\langle GF^R \underset{I}{*} \Delta I \right\rangle_O - \frac{\rho_W}{g} \left\langle GF^R \underset{O}{*} \Delta SL \right\rangle_O$$

$$\text{3-10}$$

This is an integral equation because ΔSL appears on the right-hand side in a convolution integral, and therefore the change in sea-level must be determined by iterative methods.

3.3.3 Perturbations to sea-level on an elastic/viscoelastic Earth

When considering perturbations to sea-level due to mass redistribution on an elastic/viscoelastic Earth, the deformation of the solid surface, as well as the ocean surface, must be taken into account. As in the case of a rigid Earth, a Green's function for the perturbation to the geoid due to the redistribution of *surface* masses is used. In addition, a Green's function for the redistribution of *internal* masses, arising due to the depression of the solid surface by the surface masses, is derived.

Elastic Earth

Considering the case of an elastic Earth and a unit point ice mass located at $r=a$, the perturbation potential at surface point (r,θ) is /Farrell and Clark 1976/:

$$\Phi(r,\theta) = \frac{a^2 g}{M_E \sqrt{(a^2 + r^2 - 2ar\cos\theta)}} = \frac{ag}{M_E} \sum_{n=0}^{\infty} \left(\frac{a}{r}\right)^{n+1} P_n(\cos\theta) \qquad \text{3-11}$$

The rearrangement arises due to the fact that the denominator of the first expression contains the generating function for the Legendre polynomials:

$$g(t,x) = (1 - 2xt + t^2)^{-1/2}$$

$$= \sum_{n=0}^{\infty} P_n(x)t^n \qquad \text{3-12}$$

Therefore the Green's functions for surface and internal masses may both be expanded as a Legendre series. For each Legendre degree n, a solution for the static equilibrium state of the Earth under all elastic and gravitational forces may be found for appropriate boundary conditions. The solutions are characterised by three constants, k_n, h_n and l_n, called Love numbers. The Love numbers are dependent upon n, and the elastic and density structure of the Earth.

Considering one term in the expansion of Φ:

$$\Phi_n(\theta) = \frac{ag}{M_E} P_n(\cos\theta) \qquad\qquad 3\text{-}13$$

a physical interpretation of the Love numbers follows: $k_n\Phi_n$ is the perturbation to the gravitational potential of degree n on $r=a$ due to the elastic deformation of matter within the Earth, l_n refers to tangential displacement (not required to calculate the Green's functions for surface loading /Peltier 1974/), and $h_n\Phi_n/g$ is the radial displacement of the solid surface away from $r=a$.

When determining changes in sea-level on a deforming Earth, the displacement of the solid surface must be subtracted from the change in geoid height to yield a measure of sea-level change with respect to the solid surface as opposed to e.g. the centre of the Earth. Using a superscript E to denote the case of an elastic Earth model, the Green's function for the perturbation potential on the deformed boundary of an elastic Earth due to a unit point mass applied at the surface is:

$$\Phi^E(\theta) = \frac{ag}{M_E} \sum_{n=0}^{\infty}(1+k_n-h_n)P_n(\cos\theta) \qquad\qquad 3\text{-}14$$

The polynomials are usually expanded to degree 256 when the pseudospectral approach is used (see section 4.3.2), in response to convergence tests by /Mitrovica and Peltier 1991a/. In order to calculate sea-level changes for realistic ice loads on an elastic Earth, this Green's function must be convolved with the mass distribution function, and this expression integrated over the surface of the Earth, as described in section 3.3.2, equation 3-10.

Viscoelastic Earth

All of the above calculations assume that the Earth deforms instantaneously following a redistribution of surface masses in order to maintain a state of isostatic equilibrium. In reality, the viscous properties of the mantle result in a delayed response to loading/unloading as material flows back into the area beneath a deglaciated region, or away from a glaciated region. This results in transient deformation taking place in an attempt to restore equilibrium to the system. The velocity field of this transient deformation is governed by the balance between elastic, viscous and gravitational forces. Not only does this result in time-varying solid surface deformation, but also a time-varying gravitational potential. Therefore sea-level change is a continuous process through time, both during changes to the ice distribution, and for several thousand years following the cessation of changes in ice distribution.

One material that displays both viscous and elastic properties is a Maxwell solid. This rheology is predominantly used in GIA models, and for simplicity, incompressibility is normally assumed. Unlike the elastic case, the constitutive relationship associated with a Maxwell rheology is time dependent:

$$\frac{\partial\sigma}{\partial t} = \frac{\partial\tau}{\partial t} - \frac{\mu}{\eta}\left[\sigma - \frac{1}{3}Tr(\sigma)\right] \qquad\qquad 3\text{-}15$$

where τ is the elastic part of the stress tensor, σ, η is the dynamic viscosity, μ is the shear modulus, and Tr is the trace of the stress tensor. The elastic part of the stress-strain relationship is given by Hooke's law:

$$\tau = (\kappa - \frac{2}{3}\mu)(\nabla.s)I + \mu[\nabla s + (\nabla s)^T] \qquad\qquad 3\text{-}16$$

where, κ is the bulk modulus of the material, I is the identity tensor, and s is the displacement vector. Equation 3-15 is used to define the Green's function related to the response of a viscoelastic material to loading.

In order to calculate sea-level changes on a viscoelastic Earth, we must use a Green's function for the perturbation to the gravitational potential that depends on both the distance from a point mass, and the time that has elapsed since the mass was applied to the Earth's surface. The Green's function contains all the necessary information relating to the rheological structure of the Earth. Green's functions for a range of Maxwell Earth models were originally determined by /Peltier 1974, 1976/ by using the correspondence principle in conjunction with classical elastodynamics.

Time evolution

The Green's function for the perturbation to the gravitational potential a distance θ from a unit point mass, and time t after it is instantaneously applied, comprises an elastic and a viscous part:

$$GF(\theta,t) = \Phi^E(\theta)\delta(t) + \Phi^V(\theta,t) \qquad \text{3-17}$$

where the superscripts E and V refer to elastic and viscous, respectively. This function is convolved with the loading function, $L(\theta,t)$, which takes the value $\rho_w \Delta SL$ over the ocean and $\rho_I \Delta I$ over ice-covered regions. Solutions in response to a load function that is continuous in time have not yet been derived, and a time-stepping approach is adopted when applying a time-varying load:

$$L(\theta,t) = \sum_i L_i(\theta)H(t-t_i) \qquad \text{3-18}$$

where $H(t–t_i)$ is the Heaviside function:

$$H(t-t_i) = \begin{cases} 0 & t-t_i < 0 \\ \frac{1}{2} & t-t_i = 0 \\ 1 & t-t_i > 0 \end{cases} \qquad \text{3-19}$$

Convolving the loading function (equation 3-18) with the Green's function (equation 3-17) yields a convolution integral for the perturbation to the gravitational potential:

$$\Phi(\theta,t) = \sum_i \left\{ \int_{-\infty}^t \delta(t-\tau)H(\tau-t_i)d\tau \right\} \Phi^E * L_i + \sum_i \left\{ \int_{-\infty}^t \Phi^V(\alpha,t-\tau)H(\tau-t_i)d\tau \right\} * L_i$$

$$= \Phi^E * L + \sum_i \Phi^{HV}(\Delta t_i) * L_i \qquad \text{3-20}$$

where α is the spatial variable in the convolution integral, δ is the Dirac delta function, $\Delta t_i = t–t_i$, and

$$\Phi^{HV}(\alpha,\Delta t_i) = \int_0^{\Delta t_i} \Phi^V(\alpha,\Delta t_i - \tau)d\tau \qquad \text{3-21}$$

The potential perturbation, $\Phi(\theta,t)$ (equation 3-20), is used to calculate the change in sea-level, $\Delta SL(\theta,t)=\Phi/g+c$, between an initial isostatic state and the state at time t. Constant c ensures that mass is conserved:

$$\Delta SL(\theta,t) = \frac{\Phi^E}{g} * (\rho_I \Delta I + \rho_W \Delta SL) + \sum_i \frac{\Phi^{HV}}{g} * (\rho_I \Delta I_i + \rho_W \Delta SL_i) - \frac{M_I}{A_O \rho_W} - \langle c \rangle_O$$

$$\text{3-22}$$

where

$$\langle c \rangle_O = \left\langle \frac{\Phi^E}{g} * (\rho_I \Delta I + \rho_W \Delta SL) + \sum_i \frac{\Phi^{HV}}{g} * (\rho_I \Delta I_i + \rho_S \Delta SL_i) \right\rangle_O \qquad \text{3-23}$$

25

M_I is the total change in the mass of the ice sheets from the start of melting to time t, the subscript O implies that integration takes place over oceanic regions only, and subscript i refers to terms in the time-incremental loading function. ΔI and ΔSL are the total change in ice thickness and sea-level from the start of melting to time t, while ΔI_i and ΔSL_i represent the change in ice or sea-level thickness between times t_{i-1} and t_i. In the first case, the elastic Green's function is convolved with the total change in load over time. In the second case, where the load is convolved with the viscous Green's function, time-stepping is required to solve the viscous part of the equation.

The solution of equation 3-22 describes the evolution of sea-level on a spherical viscoelastic Earth through time, for a loading history defined using the Heaviside function. Mass is conserved, and the calculations account for the change in the shape of the solid surface as well as the shape of the ocean surface, due to mass redistribution. As before, this is an integral equation because ΔSL appears on the right-hand side in a convolution integral, and therefore equation 3-22 must be solved by iterative methods. Physically, this reflects the fact that sea-level change alters the gravitational field of the Earth, via direct gravitational effects and load-induced deformation, yet is also governed by the gravitational field.

3.3.4   Reconstruction of palaeotopography and shoreline migration

Solutions for the evolution of sea-level enable palaeotopography to be determined, if the present-day underlying topography is known. This is useful, for example, for determining the palaeo-height of sills that defined the extent of the Baltic Ice Lake during deglaciation /Björck 1995/. First recall that topography is defined to be the inverse of sea-level:

$$T(\theta,t) = -SL(\theta,t) \qquad\qquad 3\text{-}24$$

We wish to determine palaeotopography at some time, t_j, in the past:

$$T(\theta,t_j) = T(\theta,t_p) + \Delta T(\theta,t_j) \qquad\qquad 3\text{-}25$$

$T(\theta,t_p)$ is present-day topography at position θ, and $\Delta T(\theta,t_j)$ refers to the change in topography between present time, t_p, and time t_j. Present-day topography is positive on land and negative over the oceans. From equation 3-24:

$$\Delta T(\theta,t_j) = -\Delta SL(\theta,t_j) \qquad\qquad 3\text{-}26$$

Substituting for $\Delta T(\theta,t_j)$ in equation 3-25 using 3-26 yields.

$$T(\theta,t_j) = T(\theta,t_p) - \Delta SL(\theta,t_j) \qquad\qquad 3\text{-}27$$

Therefore, in order to determine palaeotopography at time t_j the present-day topography distribution must be known, as well as the change in sea-level, as determined by solving the sea-level equation. Palaeotopography is defined over the whole surface of the Earth, and will be positive on land and negative across the oceans. The distribution of palaeotopography at each discrete time step can be used to determine shoreline position at that time by tracing the zero-topography contour. Shoreline migration can be determined by studying the change in shoreline position between each loading time step. This idea may be developed to define a time-dependent ocean function (see section 3.5.1).

3.4   Physical processes contributing to relative sea-level change

The mechanisms by which GIA causes sea-level change are described. Firstly in terms of spatially-uniform and spatially-varying changes to the height of the surfaces that bound the ocean. Secondly, in terms of the physical processes that take place in the 'near-field', and 'far-field' of the former ice sheets. A summary of the processes that contribute to relative sea-level change is given in Figure 3-2. The feedback associated with rotational effects is discussed in section 3.5.3.
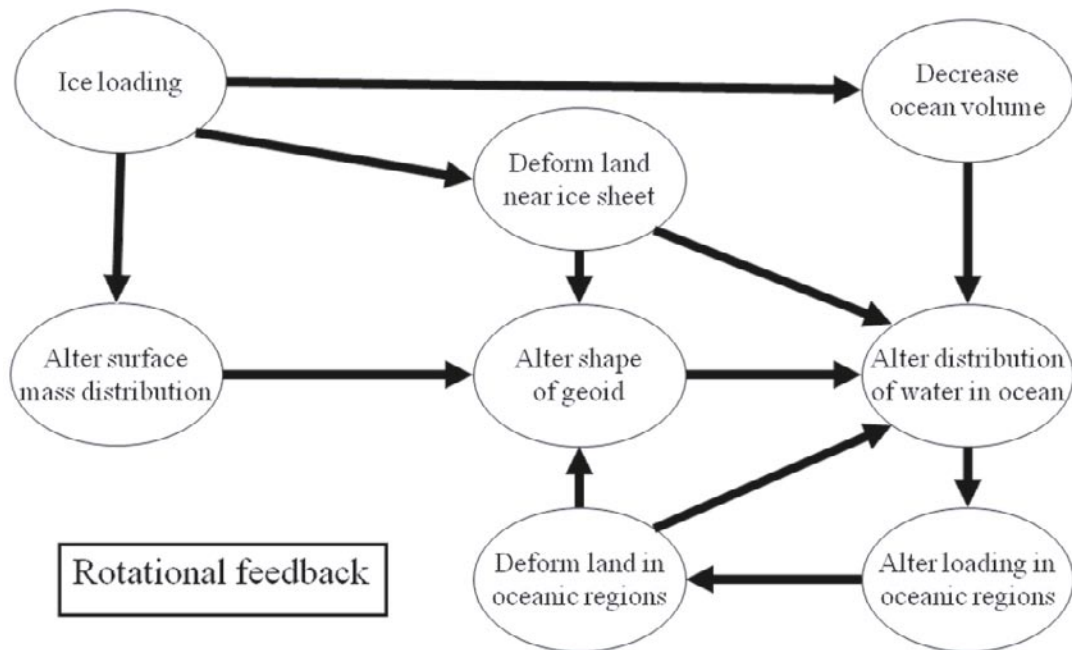
Figure 3-2. *Processes contributing to relative sea-level change.*

3.4.1 Sea-level change due to deformation of the ocean's bounding surfaces

Sea-level change is a non-uniform process. Although the total amount of ice that melts is equal to the total amount of water added to the oceans, the redistribution of the meltwater is, as previously mentioned, not uniform. Local and far-field factors relating to ice-loading, ocean-loading and Earth structure determine whether sea-level rises or falls in a given location. Relative sea-level change is governed by changes to the height of the solid surface (R) and the ocean surface or geoid (G):

$$\Delta SL(\theta,t) = \Delta G(\theta,t) - \Delta R(\theta,t) \tag{3-28}$$

The movement of a surface away from the Earth's centre of mass is taken to be positive, and the movement of a surface towards the Earth's centre of mass is taken to be negative. For example, in Figure 3-3 $\Delta G(\theta,t)$ is positive with respect to the centre of the Earth and $\Delta R(\theta,t)$ is negative, so the change in sea-level is represented by the sum of the length of the arrows.
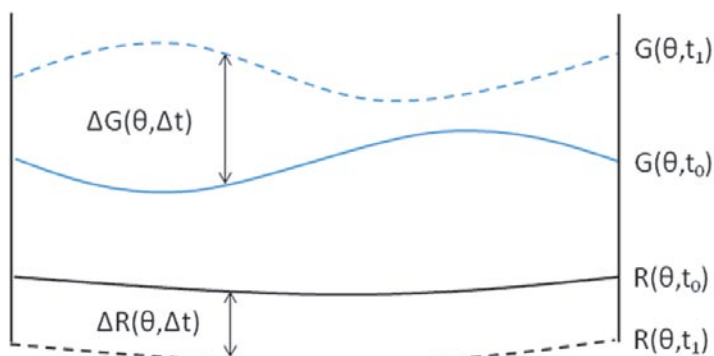
Figure 3-3. *The change in sea-level, $\Delta SL(\theta,t)$, is the difference between the change in the height of the geoid, $\Delta G(\theta,t)$, and the change in the height of the solid surface, $\Delta R(\theta,t)$.*

The term 'ocean height change', $\Delta S(\theta,t)$, is used to define the change in sea-level in oceanic regions only. The ocean function, $C(\theta)$ /Munk and MacDonald 1960/, is used to relate relative sea-level change to ocean height change:

$$\Delta S(\theta,t) = C(\theta)[\Delta SL(\theta,t)]$$
$$= C(\theta)[\Delta G(\theta,t) - \Delta R(\theta,t)]$$

3-29

$C(\theta)$ takes the value 1 over the oceans and 0 elsewhere. Note that it is defined to be time-invariant: this is a consequence of the assumption in the original sea-level equation that ocean geometry does not change during a glacial cycle. This is clearly a false assumption, and this issue is addressed in section 3.5.1, along with a discussion into the magnitude of error introduced by ignoring shoreline migration.

Solid surface deformation

The height of the solid surface (R) will be depressed when a load is applied to it, or it may be elevated due to the inflow of mantle material from adjacent areas that are depressed. The loading may be due to *ice-loading* or *ocean-loading*. Following the removal of loading viscous relaxation takes place, and the solid surface will gradually return to its original position, until a situation of isostatic equilibrium is restored.

Deformation of the geoid

The height of the ocean surface is determined by the shape of the geoid and the height of the equipotential surface that defines the ocean. The height of this equipotential undergoes a spatially-uniform shift ($\Delta G^{SU}(t)$) when the volume of water in the ocean changes, or when the capacity of the ocean basins change due to deformation of the solid surface or the geoid.

The spatially-uniform term can be derived by considering two expressions for the change in ocean volume. The first expression (equation 3-30) follows from the conservation of mass. The second (equation 3-31) is derived by integrating the change in relative sea-level over the surface of the ocean (see equation 3-28), and splitting the geoid term into spatially-uniform (SU) and spatially-varying (SV) parts.

$$V_{OW}(t) = -\frac{\rho_I}{\rho_W} V_I(t)$$

3-30

$$V_{OW}(t) = \left\langle \Delta G(\theta,t) - \Delta R(\theta,t) \right\rangle_O$$
$$= \left\langle \Delta G^{SV}(\theta,t) - \Delta R(\theta,t) \right\rangle_O + A_O \Delta G^{SU}(t)$$

3-31

Equating equations 3-30 and 3-31 yields:

$$\Delta G^{SU}(t) = -\frac{\rho_I}{\rho_W} \frac{V_I(t)}{A_O} - \frac{\left\langle \Delta G^{SV}(\theta,t) - \Delta R(\theta,t) \right\rangle_O}{A_O}$$

3-32

The first term in equation 3-32 is the eustatic change in sea-level due to the addition of a volume $V_I(t)$ of melted ice into the ocean. Note that if water is added to the ocean $V_I(t)$ will be negative, and hence the whole term will be positive. The second term in this equation is the uniform change in *ocean height* arising from the difference between the change in the capacity of the ocean basins due to ice- and ocean-loading (ΔR), and the spatially-varying redistribution of water into the new ocean basin configuration (ΔG^{SV}), averaged over the ocean (Figure 3-4).

In addition to this uniform change in ocean surface height, there is a spatially-varying component of ocean height change ($\Delta G^{SV}(\theta,t)$) which arises due to perturbations to the shape of the geoid by direct and indirect effects (see section 3.4.2 and Figure 3-2) associated with changes to the Earth's mass configuration.
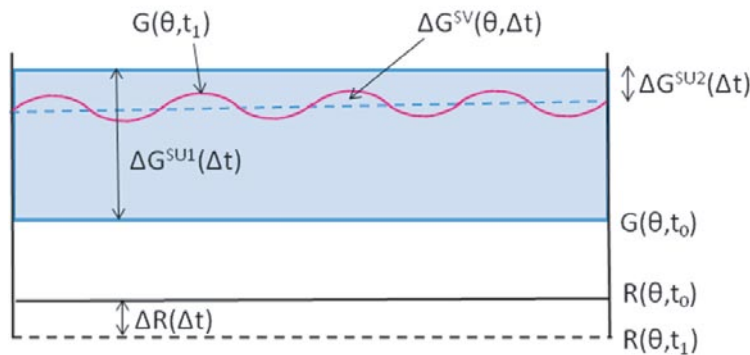
28

Figure 3-4. $\Delta G^{SU1}(\Delta t)$ represents the first term in equation 3-32: the increase in the height of the geoid due to an increase in the volume of water (shaded area). $\Delta G^{SU2}(\Delta t)$ represents the second term in equation 3-32: the decrease in the height of the geoid due to the mean change in ocean height. $\Delta R(\Delta t)$ is the mean change in the height of the solid surface. $\Delta G^{SV}(\theta, \Delta t)$ is the spatially-varying change in the height of the geoid, defined to be the distance between the dashed blue line and the pink line.

For the case shown in Figure 3-4, the uniform decrease in the height of the geoid due to the mean change in ocean height ($\Delta G^{SU2}(\Delta t)$) is equal to the mean change in the height of the solid surface ($\Delta R(\Delta t)$) since in this case ΔR is taken to be spatially-uniform and the spatially-varying term is assumed to sum to zero over the surface of the ocean. The dashed blue line in Figure 3-4 is the new height of the geoid at t_1 due to the sum of the spatially-uniform terms. The pink line is the height of the geoid at t_1 when the spatially-varying term is added.

3.4.2 Near-field relative sea-level changes

The '*near-field*' consists of sites that were covered by ice sheets at the LGM, and regions within a few hundred kilometres of the former ice margins. The simplest sea-level history is found in regions of former ice-loading. As soon as such locations become ice-free they will experience relative sea-level fall because the rebound of the solid Earth will be faster than any sea-level rise due to ongoing melting. Within the margins of the former ice-sheets, solid Earth deformation will continue for several thousands of years after the cessation of melting, resulting in monotonic sea-level fall until the solid Earth reaches a state of isostatic equilibrium. Present-day relative sea-level fall due to solid Earth rebound reaches ~10 mm/yr at the centre of formerly-glaciated regions.

The solid Earth depression beneath an ice sheet results in an internal redistribution of mantle material to the periphery of the loaded region. The surface expression of this mass flow is the growth of a peripheral bulge, generally a few hundred kilometres wide and up to ~100 m high (Figure 3-5a). Deglaciation results in the unloading of the Earth in ice-covered areas, thus allowing a return-flow of mantle material to the formerly-glaciated regions (Figure 3-5b). This not only results in uplift in the formerly-glaciated regions, but also subsidence in the peripheral regions. The combined effect of this peripheral subsidence, and sea-level rise due to the addition of meltwater to the ocean, means that peripheral locations experience monotonic sea-level rise from the initiation of melting until a return to isostatic equilibrium. Present-day relative sea-level rise reaches ~5 mm/yr within the collapsing forebulges of the former ice sheets, for example along the southern coast of the Baltic Sea, and the north-eastern United States.
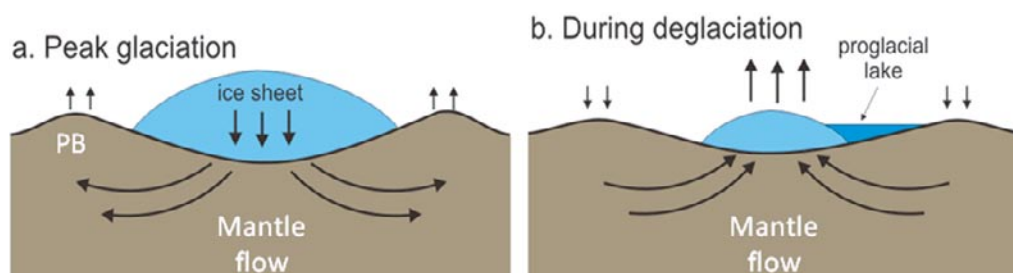

Figure 3-5. *Factors contributing to (a) the growth and (b) the decay of a peripheral bulge (PB). Adapted from http://gsc.nrcan.gc.ca/geodyn/rebound_e.php#load.*

These two cases represent the simplest scenarios of relative sea-level change during deglaciation, and highlight the importance of knowing both solid Earth deformation rates and the rate of ocean height change in order to determine rates of relative sea-level change. Relative sea-level change at the margin of the former ice-sheets is more complicated. Solid Earth deformation is related to the local deglaciation history, while perturbations to the geoid height depend upon a combination of factors which may be divided into 'direct' effects and 'indirect' effects.

Direct effects

Direct effects refer to perturbations to the gravitational potential, and hence the geoid and ocean surface, due to the direct gravitational attraction of surface mass loads (see Figure 3-2). For example, the gravitational attraction between an ice sheet and ocean water results in the height of the gravitational potential being raised in the vicinity of an ice sheet (see Figure 2-1a). When the ice sheet melts the removal of the ice load leads to a relative lowering of the gravitational potential in the region (see Figure 2-1b). Direct effects may be divided into *ice-loading* effects, and *ocean-loading* effects. Ocean water is also a surface mass, and the redistribution of water, for example into regions vacated by melting ice, also perturbs the shape of the gravitational potential.

Indirect effects

Indirect effects refer to perturbations to the gravitational potential due to surface load-induced deformation (see Figure 3-2). Once again effects may be divided into *ice-loading* and *ocean-loading* effects. Both ice- and ocean-loads act to deform the solid Earth. The associated, internal, mass redistribution and resulting surface deformation perturb the gravitational potential, and hence the shape of the geoid and the ocean surface.

Relative contributions to sea-level change

In the near-field, solid surface deformation due to ice-loading is the dominant GIA process: predictions of LGM relative sea-level change due to this effect peak at ~800 m in the centre of loading, and are typically nearly an order of magnitude greater than the predicted relative sea-level change due to ocean loading /Lambeck et al. 1998a/. It is interesting to note that due to the dramatic changes in surface mass distribution in the near-field, the spatially-varying contribution to ocean loading may be as large as the spatially-uniform contribution /Milne et al. 2002/. During deglaciation, solid Earth rebound in formerly-glaciated regions was faster than the rate of 'eustatic' sea-level rise, resulting in relative sea-level fall. In the present-day, ongoing rebound continues to dominate, and rates of relative-sea level fall reach 10 mm/yr in the centre of rebound, while peripheral bulge subsidence immediately outside the formerly-glaciated regions results in sea-level rise at up to 5 mm/yr /Mitrovica and Milne 2002/.

3.4.3 Far-field relative sea-level changes

The '*far-field*' refers to locations far from the major LGM ice sheets, where relative sea-level change is dominated by the eustatic signal, and GIA-related solid Earth deformation is minimal. During deglaciation, far-field sea-level changes are dominated by sea-level rise due to the addition of meltwater to the oceans. Once deglaciation is over, far-field relative sea-level change still takes place on the order of ~0.3 mm/yr /Douglas and Peltier 2002/ due to GIA. The two main processes that contribute to far-field relative sea-level change during periods when there is no change to global ice or water volumes are '*ocean syphoning*' and '*continental levering*'. /Mitrovica and Milne 2002/ provide a detailed overview of both these processes.

Ocean syphoning

Ocean syphoning is a residual effect of ice-loading. It refers to the redistribution of water from far-field oceanic basins to the site of collapsing peripheral bulges /Mitrovica and Peltier 1991a/. The bulges were formed as a result of ice-loading in adjacent continental regions; therefore they are commonly located within the oceans. From the start of deglaciation, the bulges begin to subside; a process that continues beyond the end of melting due to the viscous properties of the mantle. As they subside additional space is created within the oceans, and water is redistributed to these regions (which experience relative sea-level rise), resulting in relative sea-level fall in far-field oceanic basins (Figure 3-6). The process is enhanced by ocean-loading within the subsiding regions.
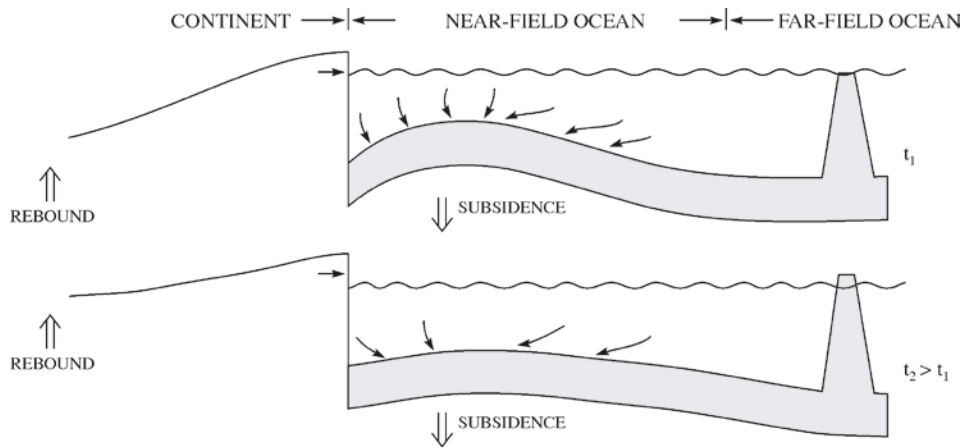
Figure 3-6. *Processes contributing to ocean syphoning. The upper figure illustrates the situation immediately following deglaciation. The lower figure illustrates the situation at a later time. Near-field peripheral bulge subsidence results in local relative sea-level fall. Syphoning of water from the far-field results in far-field relative sea-level fall. Adapted from /Mitrovica and Milne 2002/.*

Continental levering

Continental levering /Walcott 1972, Clark et al. 1978, Nakada and Lambeck 1989/ is associated purely with ocean-loading. Following deglaciation the ocean basins will contain a greater volume, and therefore mass, of water. Large portions of the continental margins will also be newly exposed to ocean-loading following the migration of shorelines onshore during deglaciation. This redistribution of loading results in an effect analogous to the depression of continents by ice-loading and the associated growth of a peripheral bulge: along the submerged margins of the continents, subsidence takes place due to ocean-loading, leading to a decrease in relative sea-level both in the near- and far-fields. At the same time the continental margins are tilted upwards as a result of increased ocean-loading following deglaciation, resulting in relative sea-level fall (Figure 3-7).

Continental levering is a viscoelastic process, and continues for several thousand years following the end of deglaciation. It leaves a clear fingerprint in the sea-level record. Following a period of rapid sea-level rise during deglaciation a highstand is observed at ~5 ka BP in the far-field record. A subsequent gradual fall in relative sea-level is recorded as the land is isostatically uplifted.

Following deglaciation, relative sea-level change in oceanic basins is difficult to interpret as it will be due to a combination of competing processes; both ocean syphoning and continental levering.
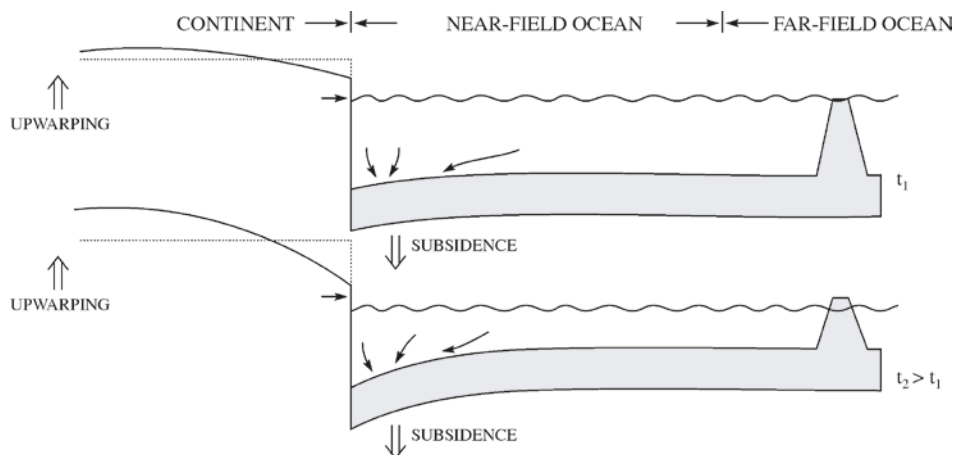
Figure 3-7. *Increased ocean-loading following deglaciation results in a tilting of the continental margins. The upper figure illustrates the situation immediately following deglaciation. The lower figure illustrates the situation at a later time. Relative sea-level fall takes place in the near-field due to subsidence, and the far-field due to the movement of water from the far-field to the near-field. Adapted from /Mitrovica and Milne 2002/.*

Relative contributions to sea-level change

In the far-field, the addition of meltwater into the oceans dominated sea-level change during deglaciation, and was responsible for almost all of the ~125 m of sea-level rise predicted to have taken place since the LGM. Spatially-uniform sea-level changes due to ice-loading processes (e.g. perturbations to the geoid and solid surface) are predicted to have caused ~30 m of sea-level *fall* since the LGM, but this is balanced in the far-field by the contribution to sea-level *rise* from the spatially-varying signal. The spatially-varying signal is the sum of local perturbations to the geopotential and solid surface due to ice-loading, ocean-loading, and rotational-feedback processes, with the dominant signal once again related to ice-loading /Milne et al. 2002/.

In the present-day, solid Earth deformation due to ocean-loading is the dominant factor controlling relative sea-level change in the far-field. Ocean syphoning results in relative sea-level fall at up to 0.5 mm/yr in the major ocean basins, while continental levering results in relative sea-level rise/fall off/onshore at rates of 0.2–0.3 m/yr /Mitrovica and Milne 2002/.

3.5   Modifications to the sea-level equation

Several important processes are neglected in the original definition of the sea-level equation. These have been progressively included in subsequent GIA studies. The treatment of shoreline migration, the presence of grounded or floating ice, rotational feedback, and 3-D Earth structure within the sea-level equation are described below.

3.5.1   Shoreline migration

Early formulations of the sea-level equation assumed a constant area for the oceanic basins. However, as sea-level rises, onlap takes place and shorelines migrate inland, while as sea-level falls, offlap takes place and shorelines migrate oceanwards. A consequence of these processes is that the areal extent of the Earth's surface which is subjected to loading by the ocean varies over time.

The first studies to implement time-varying ocean geometry in the context of GIA were performed by /Lambeck and Nakada 1990/ and /Johnston 1993/. Subsequent studies have developed increasingly accurate techniques to deal with shoreline migration /Peltier 1994, Milne 1998, Milne and Mitrovica 1998a, Milne et al. 1999, Mitrovica and Milne 2003, Lambeck et al. 2003, Kendall et al. 2005/, and it has become standard practice to use a time-varying version of the ocean function, $C(\theta,t)$, within the sea-level equation to keep track of ocean and non-ocean regions. As described in section 3.3.1, the function takes the value 1 in the oceans and 0 otherwise. The application of this function ensures that ocean-loading is applied only if that location lies within the ocean at a given time.

Using the time-varying ocean function, the sea-level equation may be written in an alternative form that will be more useful when it comes to calculating changes in relative sea-level. Ocean height is redefined using the time-varying ocean function:

$$S(\theta,t) = C(\theta,t)SL(\theta,t) \qquad\qquad \text{3-33}$$

The change in ocean height from the initiation of loading at time t_0, to time t_j is therefore

$$\begin{aligned}\Delta S(\theta,t) &= S(\theta,t) - S(\theta,t_0)\\ &= C(\theta,t)SL(\theta,t) - C(\theta,t_0)SL(\theta,t_0)\\ &= [SL(\theta,t_0) + \Delta SL(\theta,t)]C(\theta,t) - [SL(\theta,t_0)]C(\theta,t_0)\\ &= \Delta SL(\theta,t)C(\theta,t) + SL(\theta,t_0)[C(\theta,t) - C(\theta,t_0)]\end{aligned} \qquad\qquad \text{3-34}$$

using the fact that $\Delta SL(\theta,t_0)=0$.

Figure 3-8 illustrates the near-shore change in ocean volume from time t_0 to time t following a rise in sea-level (from $G(t_0)$ to $G(t)$) and a lowering of the land (from $R(t_0)$ to $R(t)$). Letter A indicates the region that contains water at time t_0. Letters B, C, D, and E indicate the regions which do not contain water at time t_0, but do contain water at time t.

In early attempts to account for shoreline migration /e.g. Peltier 1994/ the approximation $\Delta S(\theta,t)=\Delta SL(\theta,t)C(\theta,t)$ was used to determine the cumulative change in ocean height between t_0 and t. The error introduced by neglecting the last term in equation 3-34 is equivalent to overestimating ocean-loading by up to ~130 m (i.e. eustatic sea-level change since the LGM) in the region affected by shoreline migration. The error in ocean height change in the near-shore region is represented by regions D, F, and G in Figure 3-8. This area can be thought of as the topography (R-G) at time t_0 within the region of shoreline migration from time t_0 to t.

Now consider the incremental change in ocean height across a shorter time step, from t_{j-1} to t_j:

$$\delta S(\theta,t_j) = S(\theta,t_j) - S(\theta,t_{j-1})$$
$$= \delta SL(\theta,t_j)C(\theta,t_j) + SL(\theta,t_{j-1})[C(\theta,t_j) - C(\theta,t_{j-1})]$$

$$3\text{-}35$$

Recent studies /e.g. Milne 1998/ use a time-stepping approach, where the period $t_0 \rightarrow t$ is divided into N smaller time steps. Incremental changes in ocean-loading are calculated and applied at each time step, and their cumulative effect gives the change in ocean height from t_0 to t. In this time-stepping approach the approximation $\delta S(\theta,t_j)=\delta SL(\theta,t_j)C(\theta,t_j)$ is commonly used. The error due to the neglect of the last term in equation 3-35 is an order of magnitude smaller than the error introduced in the earlier approximation since the sum of the topography bounded by each time step is much smaller than the topography bounded by the step from t_0 to t (see Figure 3-9).

The numerical methods used to solve the sea-level equation necessitate the use of such approximations. For a more detailed discussion of the numerical methods used to implement shoreline migration see /Milne et al. 1999, Mitrovica 2003, Mitrovica and Milne 2003, Lambeck et al. 2003, Kendall et al. 2005/.

The areal extent of the change in ocean coverage for a given sea-level change depends upon the underlying topography/bathymetry. At steep continental margins the horizontal migration of the shoreline will be small in comparison to the migration of shorelines across a low gradient continental shelf for the same incremental change in relative sea-level. Therefore knowledge of solid Earth topography (which will vary with time due to surface loading) is necessary to determine the geometry of the time-varying ocean function.
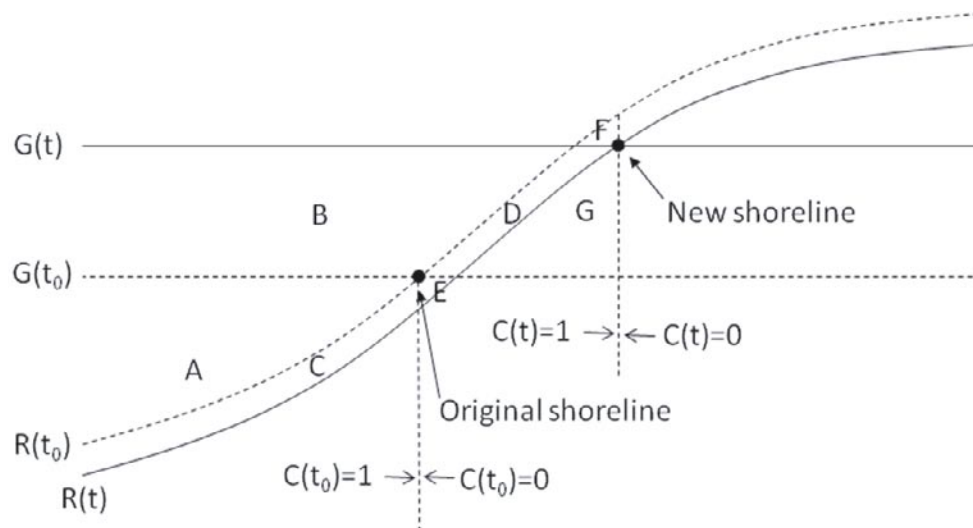
Figure 3-8. *Change in water loading following a rise in sea-level and lowering of the land. Dashed curve: original land surface (R), at time t_0. Solid curve: new land surface, at later time t. Dashed horizontal line: original sea-level/geoid height (G), at time t_0. Solid horizontal line: new sea-level/geoid height, at later time t. Filled circles mark the original and new shoreline positions. Vertical dashed lines indicate the location of the transitions from ocean (C=1) to land (C=0) at times t_0 and t. See text for explanation of the lettered regions. Adapted from /Mitrovica and Milne 2003/.*
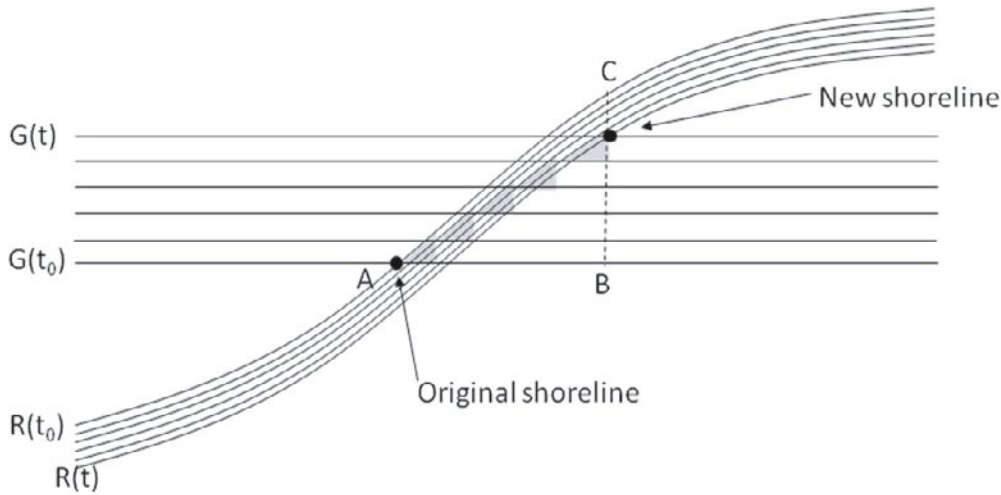
Figure 3-9. The error at each time step due to neglecting the last term in equation 3-35 is given by the vertical height of the shaded areas. If the calculation were carried out in a single time step the error at each horizontal position would be given by the height of the triangle ABC. Adapted from /Mitrovica and Milne 2003/.

3.5.2 Treatment of floating and marine-grounded ice

Further modifications to the extent of the ice- and ocean-loading functions arise in the presence of floating and marine-grounded ice. In previous versions of the sea-level equation, ocean-loading is assumed to apply wherever sea-level is positive (i.e. the geoid surface lies above the solid surface: $G-R>0$), with the height of the ocean column that contributes to ocean-loading equivalent to ocean height, $S(\theta,t)$. However in the presence of floating or marine-grounded ice, water will be displaced by ice even when $G-R>0$, and loading at this location will depend upon ice thickness instead of ocean height in the case of floating ice, or just ice thickness in the case of marine-grounded ice.

Special care must be taken when calculating local changes in relative sea-level following the inundation of water into regions uncovered by retreating marine-grounded ice, or the advance of marine-grounded ice into locations with non-zero ocean depth. Ice- and ocean-loading functions must also take into account the position of the transition from grounded to floating ice, which is assumed to take place when the mass of water displaced by the ice is greater than the mass of the ice.

Marine-grounded ice

An ice sheet is marine-grounded if the mass of ice is greater than the mass of water in the ocean column, i.e. if $\rho_I h_I > \rho_W S$, where h_I is the thickness of ice and S is the height of the ocean column. As grounded ice retreats, ocean water will migrate into the region vacated by the ice, resulting in an instantaneous step in sea-level, and hence ocean-loading, at this location. The influx of water into the region vacated by the ice results in a global fall in the sea surface due to the conservation of mass. /Milne 1998/ and /Milne et al. 1999/ refer to this process where water replaces ice as 'water dumping', while /Peltier 1998ab/ describes a similar method for dealing with ice retreat using a method that employs 'implicit ice'.

As grounded ice melts, changes in the accommodation space of the ocean basins due to ice retreat, as well as changes in basin capacity due to solid surface deformation, must be taken into account when calculating the redistribution of meltwater throughout the ocean. Ignoring such effects may lead to an underestimate of ice-equivalent eustatic sea-level change since the LGM by ~10% /Milne et al. 1999/.

A complete treatment of sea-level change in the presence of retreating marine-grounded ice should consider the details of local ice- and water-loading, perturbations to the gravitational potential due to water mass influx, and the implications of mass conservation /e.g. Milne 1998/. In order to deal with temporal variations in the configuration of marine-grounded ice, /Mitrovica and Milne 2003/ include an extra term in the sea-level equation:

$$S(\theta,t) = SL(\theta,t)C(\theta,t)\beta(\theta,t) \qquad \text{3-36}$$

where $C(\theta,t)$ is the ocean function, as defined above, and $\beta(\theta,t)$ takes the value 1 where there is no grounded ice and 0 where there is grounded ice (see Figure 3-10). Therefore ocean height is only non-zero where $G>R$ *and* there is no grounded ice, while it will be zero where $G<R$ *or* there is grounded ice (see Table 3-1).

The expression for the change in ocean height across a time step $t_{j-1} \rightarrow t_j$ becomes:

$$\delta S(\theta,t_j) = S(\theta,t_j) - S(\theta,t_{j-1})$$
$$= SL(\theta,t_j)C(\theta,t_j)\beta(\theta,t_j) - SL(\theta,t_{j-1})C(\theta,t_{j-1})\beta(\theta,t_{j-1})$$
$$= [SL(\theta,t_0) + \Delta SL(\theta,t_j)]C(\theta,t_j)\beta(\theta,t_j) \qquad\qquad 3\text{-}37$$
$$- [SL(\theta,t_0) + \Delta SL(\theta,t_{j-1})]C(\theta,t_{j-1})\beta(\theta,t_{j-1})$$

Note that this expression collapses to yield $\delta S(\theta,t_j)=SL(\theta,t_j)$ when either $C(\theta,t_{j-1})$ or $\beta(\theta,t_{j-1})$ are zero and $C(\theta,t_j)$ and $\beta(\theta,t_j)$ are both 1. This implies that the change in ocean height when water inundates a region evacuated by retreating ice is equivalent to instantaneously introducing the total height of the new sea-level, as required (Figure 3-10).

Table 3-1.

	Relation between geoid height (G) and solid surface (R)	Ocean function (C)	Ice function (β)	Ocean height (S)
On land, no ice	R > G	0	1	0
On land, ice	R > G	0	0	0
In ocean, grounded ice	G > R	1	0	0
In ocean, no grounded ice (can be floating)	G > R	1	1	SL
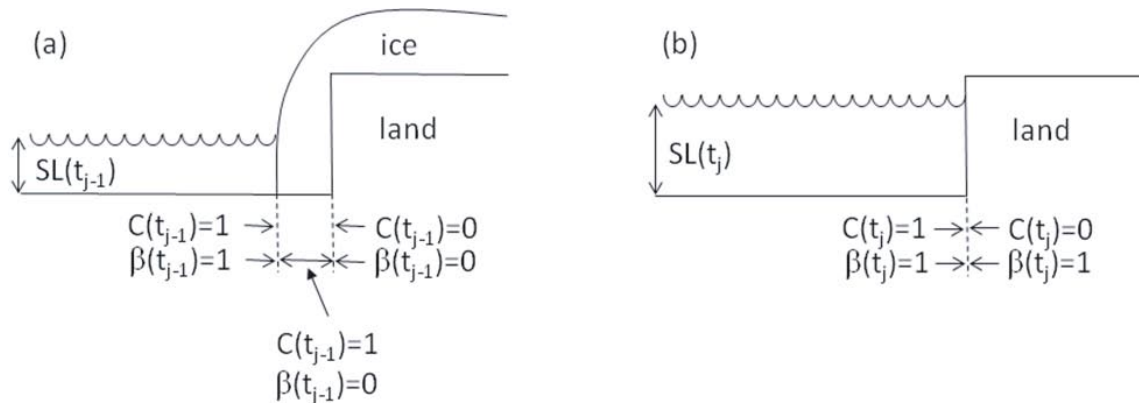
Figure 3-10. *(a) Time t_{j-1}. The ice function, β, is non-zero where there is no grounded ice and zero where there is grounded ice. The ocean function (C) is defined as in section 3.5.1; it is zero when $G<R$ and non-zero when $G>R$. Ocean height is only non-zero where both the ocean and ice functions are non-zero. (b) Time t_j. Following ice melting sea-level increases by $(SL(t_j)-SL(t_{j-1}))$ away from former ice-covered regions, and by $SL(t_j)$ in former regions of marine-grounded ice. Adapted from /Mitrovica and Milne 2003/.*

Equation 3-37 may be rewritten in a form that lends itself to solution by a numerical algorithm. First recall that topography is defined to be the inverse of sea-level:

$$T(\theta,t) = -SL(\theta,t) \tag{3-38}$$

and that

$$T(\theta,t_j) = T(\theta,t_0) + \Delta T(\theta,t_j)$$
$$SL(\theta,t_j) = SL(\theta,t_0) + \Delta SL(\theta,t_j) \tag{3-39}$$

where $\Delta T(\theta,t)$ refers to the change in topography between time t_0 and time t_j. This yields the identity

$$T(\theta,t_j) = T(\theta,t_{j-1}) + \Delta SL(\theta,t_{j-1}) - \Delta SL(\theta,t_j) \tag{3-40}$$

and hence, setting $j=1$ in equation 3-40, noting that $\Delta SL(\theta,t_0)=0$, and using recursion, equation 3-37 becomes

$$\delta S(\theta,t_j) = [-T(\theta,t_0) + \Delta SL(\theta,t_j)]C(\theta,t_j)\beta(\theta,t_j)$$
$$- [-T(\theta,t_0) + \Delta SL(\theta,t_{j-1})]C(\theta,t_{j-1})\beta(\theta,t_{j-1})$$

$$= [-T(\theta,t_{j-1}) - \Delta SL(\theta,t_{j-1}) + \Delta SL(\theta,t_j)]C(\theta,t_j)\beta(\theta,t_j)$$
$$- [-T(\theta,t_{j-1}) - \Delta SL(\theta,t_{j-1}) + \Delta SL(\theta,t_{j-1})]C(\theta,t_{j-1})\beta(\theta,t_{j-1})$$

$$= C(\theta,t_j)\beta(\theta,t_j)[\Delta SL(\theta,t_j) - \Delta SL(\theta,t_{j-1})]$$
$$+ T(\theta,t_{j-1})[C(\theta,t_{j-1})\beta(\theta,t_{j-1}) - C(\theta,t_j)\beta(\theta,t_j)] \tag{3-41}$$

Equation 3-41 must be solved by iterative methods; first the distribution of $T(\theta,t_0)$ must be determined (see below), then the integral form of the sea-level equation must be solved, and finally the distribution of C from the time-varying topography must be determined before the incremental change in sea-level can be calculated. Note that β is defined *a priori* by the ice sheet history.

$T(\theta,t_0)$ is the topography distribution at some time t_0 prior to glaciation. Present-day topography $T(\theta,t_p)$ is commonly used as an initial guess for $T(\theta,t_0)$. There is no similar obvious *a priori* guess for $SL(\theta,t_0)$, hence the recasting of the equation in terms of topography. Adopting this guess for $T(\theta,t_0)$ in the sea-level equation yields a prediction for the present-day change in sea-level $\Delta SL(\theta,t_p)$, which in turn is used in a re-written version of equation 3-39;

$$T(\theta,t_p) = T(\theta,t_0) - \Delta SL(\theta,t_p) \tag{3-42}$$

to yield a second guess for $T(\theta,t_0)$, and so on.

Floating ice

If ice thickness is non-zero in a location defined to lie within the ocean (i.e. $h_I(\theta,t)>0$ and $C(\theta,t)=1$), but $\rho_I h_I < \rho_W S$, then the ice will float. The height of the water column that contributes to ocean-loading is reduced due to the displacement of water by floating ice (see Figure 3-11).

Isostasy implies that

$$\rho_W S(\theta,t) = \rho_W S^*(\theta,t) + \rho_I h_I(\theta,t) \tag{3-43}$$

where S^* is the actual water depth (see Figure 3-11):

$$S^*(\theta,t) = \max\{0, S(\theta,t) - \rho_I h_I(\theta,t)/\rho_W\} \tag{3-44}$$
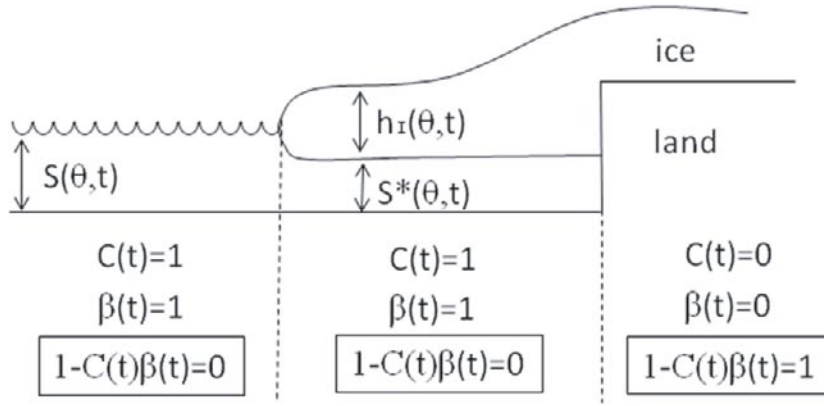
Figure 3-11. *Ocean height change in the presence of floating ice. Actual water depth (S*) is dependent upon the thickness of the ice, $h_I(\theta,t)$, the density of the ice, ρ_I, and the density of sea-water, ρ_w. (See equation 3-43).*

Therefore the loading function becomes

$$L(\theta,t) = \rho_W S^*(\theta,t) + \rho_I h_I(\theta,t)$$
$$= \rho_W S(\theta,t) + \rho_I h_I(\theta,t)[1 - C(\theta,t)\beta(\theta,t)]$$

3-45

When $C(\theta,t)=0$ the point is above sea-level, and when $\beta(\theta,t)=0$ there is grounded ice. In either case ocean height will be zero and equation 3-45 reduces to $L(\theta,t)=\rho_I h_I(\theta,t)$. If $C(\theta,t)= \beta(\theta,t)=1$ the point is in the ocean, either with floating ice or no ice. In this case equation 3-45 reduces to $L(\theta,t)=\rho_W S(\theta,t)$: By Archimedes' principle the mass of a column of water in the open ocean is the same as the mass of a column of floating ice plus the mass of the undisplaced water (equation 3-43), thus it is clear that any floating ice contributes to the load applied upon the surface of the Earth within the oceans. The total contribution to the ocean-load from floating ice is given by the expression.

$$M_{floating}(t) = \rho_I \int_\Omega h_I(\theta,t)C(\theta,t)\beta(\theta,t)d\Omega$$

3-46

Given that ice history is defined *a priori*, total ice volume can be determined for any time t, and therefore the mass of (grounded) ice that directly acts as a load upon the surface of the Earth is

$$M_{grounded}(t) = M_{total}(t) - M_{floating}(t)$$

3-47

3.5.3 Rotational effects

The theory presented by /Farrell and Clark 1976/ is valid for a non-rotating Earth. Several studies have extended the theory to include rotational effects /e.g. Han and Wahr 1989, Bills and James 1996, Milne and Mitrovica 1996, 1998a, Milne 1998, Mitrovica and Milne 1998, Peltier 1998a, Mitrovica et al. 2001a, Kendall et al. 2005/.

Changes in the configuration of the Earth's surface mass load (ice and ocean) perturb the Earth's rotation vector. A change in the rotational state of the Earth deforms both the geoid and the solid surface, and hence affects relative sea-level, thus further reconfiguring the Earth's surface mass load. This feedback process must be incorporated into the sea-level equation, and will require iterative methods to solve.

The effect of the time-varying 'rotation potential', $\Lambda(\theta,t)$, can be determined in a similar manner to the effect of surface loading. Expressions for the solid surface and geoid heights may therefore be rewritten to account for rotation-induced changes in relative sea-level:

$$R(\theta,t) = L(\theta,t) * GF^R(\theta,t) + \Lambda(\theta,t) * GF^R(t)$$

3-48

$$\Phi(\theta,t) = L(\theta,t) * GF^\Phi(\theta,t) + \Lambda(\theta,t) * GF^\Phi(t)$$

3-49

Note that the rotational potential is only convolved with the Green's function over time. The theory for computing GIA-induced variations to the magnitude and orientation of the Earth's rotation vector on a spherically symmetric, viscoelastic Earth is presented in /Mitrovica et al. 2005/. The Earth's ellipticity is accounted for in this theory, but this is a factor that is neglected in most GIA models. Details of the relationship between these load-induced perturbations to the Earth's rotation vector and the rotation potential, $\Lambda(\theta,t)$, are given in /Lambeck 1980/ and /Milne and Mitrovica 1996, 1998a/.

3.5.4   3-D Earth structure

Early formulations of the sea-level equation only allowed for the use of a 1-D, depth-varying Earth model consisting of an elastic lithosphere of constant thickness and a radial mantle viscosity profile /e.g. Farrell and Clark 1976, Mitrovica and Peltier 1991a/. However, surface geology and seismic tomography clearly indicate that the Earth exhibits complex lateral structure in terms of composition, layer thickness, density, temperature, elastic properties, and viscosity. Lateral variations in the elastic and viscous properties of the Earth affect the response of the solid Earth to loading /Nakada and Lambeck 1991/, hence recent work has focused on the use a modified version of the original sea-level equation that can account for the effect of lateral Earth structure /e.g. Kaufmann et al. 2000, Martinec 2000, Kaufmann and Wu 2002, Zhong et al. 2003, Wu and van der Wal 2003, Wu et al. 2005, Paulson et al. 2005, Martinec and Wolf 2005, Latychev et al. 2005a, Steffen and Kaufmann 2005, Whitehouse et al. 2006, Kendall et al. 2006/.

The modification to the sea-level equation itself principally involves redefining Earth properties to vary with lateral position as well as with depth. This complication necessitates more advanced solution methods which permit additional mode coupling, and use a fully 3-D, spherical, solution domain. Further details are given in chapter 4.

One of the primary goals of GIA modelling has been to infer ice history and radial mantle viscosity profiles, using the fit between observed and predicted surface deformation rates and relative sea-level curves to determine the best-fitting input models /e.g. Fjeldskaar and Cathles 1991, Mitrovica 1996, Mitrovica and Forte 1997, Lambeck et al. 1998a, Milne et al. 2001, Kaufmann and Lambeck 2002, Milne et al. 2004/. All of the principle ice and viscosity models currently used as inputs to GIA models (e.g. ICE-3G /Tushingham and Peltier 1991/, RSES /Kaufmann and Lambeck 2002/, ICE-5G /Peltier 2004/, and their accompanying viscosity profiles) have been inferred from 1-D GIA studies. However, recent work has shown that the inclusion of 3-D structure can perturb predictions of GIA-related surface velocities by amounts greater than current observational uncertainties /Zhong et al. 2003, Wu et al. 2005, Wang and Wu 2006, Whitehouse et al. 2006/. If these perturbations can be mimicked by a change in the underlying 1-D Earth model then previous inferences of ice history and mantle viscosity may be biased. Future attempts to quantify details of these input models by inverting GIA observables must take lateral Earth structure into account.

3.5.5   Relative importance of modifications to the sea-level equation

Neglecting any of the processes described above introduces errors into the GIA calculations. The largest errors arise due to the neglect of shoreline migration; relative sea-level change since the LGM will be over/under-estimated by up to 125 m (i.e. the same as the eustatic change since the LGM) within the region of shoreline migration. The errors peak close to the present-day shoreline, but errors of over 10% may also be incurred in regions with broad continental shelves, and late Holocene far-field sea-level highstand predictions may contain errors of over 2 m /Milne and Mitrovica 1998b/. The errors will be smaller in regions with steep topography at the shoreline, since this limits the spatial extent of shoreline migration. The errors can be reduced to ~1% using the solution algorithms developed by /Johnston 1993, Milne et al. 1999, Kendall et al. 2005/, and will be a function of the time-step used.

The incorrect treatment of marine-based ice introduces the second largest error into the GIA calculations. Within regions that contained marine-grounded ice at the LGM, such as Hudson Bay or the Gulf of Bothnia, predictions of relative sea-level change may be wrong by up to 100 m if the inundation of ocean water following ice melting is not handled correctly /Kendall et al. 2005/. This water acts as a load upon the Earth, and slows the rate of rebound. Neglecting this effect will lead to the overestimation of relative sea-level change in the near-field, and the underestimation of LGM ice volumes by ~10% /Milne et al. 1999/.

Away from shorelines and regions of former ice-loading, the neglect of the two processes described above has a negligible effect upon relative sea-level predictions. However, the neglect of rotational feedback in the GIA calculations has a much broader spatial effect. If rotation is not included, errors in predictions of relative sea-level change since the LGM peak at 7–8 m in the four quadrants of the Earth centred upon eastern North America, the tip of South America, northern China, and the southern Indian Ocean /Milne and Mitrovica 1998a/. The error decreases to zero at the equator and between these quadrants. Neglecting rotational feedback also introduces an error of up to 0.15 mm/yr in predictions of present-day sea-level change.

Errors due to the neglect of lateral Earth structure have the most complicated spatial signature. /Whitehouse et al. 2006/ find that neglecting lateral heterogeneities in lithosphere thickness and mantle viscosity can introduce a bias of up to 3 mm/yr into predictions of present-day uplift rates in Fennoscandia, 1 mm/yr for horizontal rates, or 70 m for predictions of relative sea-level at 10 ka BP. All of these biases peak at the centre of former loading. The magnitude and distribution of errors away from the formerly-loaded regions is poorly understood, and will be dependent upon the 3-D Earth model used in the GIA calculations.

All of the errors discussed above are greater than the current resolution of available data sets.

3.6   Outputs of the sea-level equation

The sea-level equation may be used to solve for relative sea-level change, and rates of relative sea-level change, at any time and any position on the surface of the Earth. The calculation of terms relating to solid Earth deformation also allow for the prediction of remaining solid Earth uplift/subsidence, the state of stress, and the 3-D kinematics of present-day solid Earth deformation. Relative sea-level change is a result of perturbations to the gravitational potential, hence present-day gravity anomalies, and the rate of change of gravity anomalies may also be predicted. The inclusion of rotational effects in the calculations allows changes in the Earth's rotation rate to be predicted. All of these outputs may be compared to observations.

4   State-of-the-art GIA models

4.1   Introduction

In this chapter the methods used to solve the sea-level equation, and more recent modifications to the sea-level equation, are described. A brief discussion on the methods used to model the inputs to the sea-level equation is included. The work of various key research groups are discussed and compared. The accuracy of the principal methods is assessed, and potential errors and shortcomings are discussed. Many of the methods are calibrated against data sets and therefore these data sets are a briefly described. Finally, the uses of GIA modelling are briefly discussed, including the use of GIA modelling as a tool to constrain the rates and causes of present-day sea-level change, Earth rheology and structure, and ice-loading history.

4.2   Modelling inputs to the sea-level equation

The principle inputs to the GIA system are described in chapter 2. A brief description of how these inputs are formulated within state-of-the-art GIA models is given below.

The first input to a GIA model is the ice-loading history (Figure 4-1). Methods for defining the ice-loading history are described in sections 4.2.2 and 4.2.3. The ice-loading history determines the ocean-loading history via the sea-level equation, assuming mass conservation and the gravitationally-consistent redistribution of water over the surface of the Earth. The combined surface mass distribution (ice and water) is then applied as a load to the chosen Earth model – the second input to the GIA model (Figure 4-1) – the details of which determine the response of the Earth to loading. The methods used to model Earth structure are given in section 4.2.1. Once the solid Earth deformation is calculated the resulting change in relative sea-level can be determined.
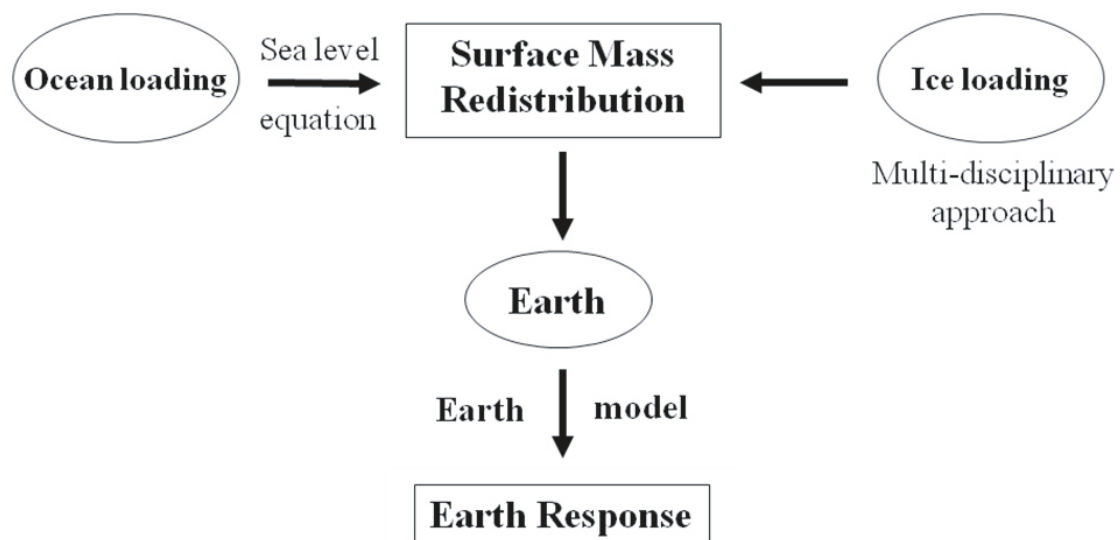

Figure 4-1. *Flow chart showing the principle inputs and outputs of a GIA model. Surface loading (ice and ocean) is applied to an Earth model. The details of the ice and Earth models determine the solid Earth response to loading.*

4.2.1   Earth structure and rheology

A description of the Earth structure used in GIA modelling, including details of the parameter space for lithosphere thickness and mantle viscosity, is given in section 2.2.3. The way in which the chosen Earth structure is implemented depends upon the method used to solve the sea-level equation (see section 4.3). In simple half space and finite element models Earth parameters are defined for each element. However, a different method is required when the sea-level equation is solved using spectral, i.e. spherical harmonic, methods.

When spectral methods are used, the spectral response equations incorporate frequency dependent Love numbers which are related to the rheological structure of the Earth /Mitrovica et al. 1994a/. Love numbers /Love 1909/ govern the response of a spherically-symmetric, self-gravitating Earth, with an elastic mantle and fluid core, to gravitational and surface mass load forcing. The original form of the elastic Love numbers has been extended to the general linear viscoelastic case by /Peltier 1974, 1976/ using the correspondence principle, to yield the viscoelastic surface load Love numbers. These are dimensionless numbers which define the response of the Earth to an applied point impulse load. In the time domain they have the normal mode form:

$$h_l^L(t) = h_l^{L,E}\delta(t) + \sum_{k=1}^{K(l)} r1_k^{L,l} \exp(-s_k^l t) \qquad \text{4-1}$$

$$l_l^L(t) = l_l^{L,E}\delta(t) + \sum_{k=1}^{K(l)} r2_k^{L,l} \exp(-s_k^l t) \qquad \text{4-2}$$

$$k_l^L(t) = k_l^{L,E}\delta(t) + \sum_{k=1}^{K(l)} r3_k^{L,l} \exp(-s_k^l t) \qquad \text{4-3}$$

E denotes a coefficient related to a purely elastic mantle, l is the spherical harmonic degree, L refers to the surface load (described in terms of spherical harmonics), t is time, and $\delta(t)$ is the Kronecker delta function used to apply an instantaneous load at time t. Hence the first term in equations 4-1–4-3 represents the instantaneous elastic response to an applied point mass load. The second term is the non-elastic response, which is represented by the superposition of $K(l)$ modes of pure exponential decay. $r1_k^{L,l}$, $r2_k^{L,l}$, and $r3_k^{L,l}$ are the normal mode amplitudes of the non-elastic response, and s_k^l are the inverse decay times of these normal modes. h_l^L, l_l^L, and k_l^L represent the coefficients of degree l in the Legendre polynomial expansion of Green's functions for the radial (U) and tangential (V) displacement, and the potential perturbation (ϕ), due to the redistribution of mass, respectively:

$$G_U^L(\gamma,t) = \frac{a}{M_e} \sum_{l=0}^{\infty} h_l^L(t) P_l(\cos\gamma) \qquad \text{4-4}$$

$$\vec{G}_V^L(\gamma,t) = \frac{a}{M_e} \sum_{l=0}^{\infty} l_l^L(t) \frac{\partial}{\partial\gamma} P_l(\cos\gamma)\hat{\gamma} \qquad \text{4-5}$$

$$G_\phi^L(\gamma,t) = \frac{ag}{M_e} \sum_{l=0}^{\infty} k_l^L(t) P_l(\cos\gamma) \qquad \text{4-6}$$

In the above equations a is the mean radius of the Earth, M_e is the mass of the Earth, $\hat{\gamma}$ is a unit vector tangent to the surface of the Earth, and γ is the angular distance between the load point (θ',ψ',t') and the observation point (θ,ψ,t).

The response of a spherically symmetric, self-gravitating, viscoelastic Earth to an arbitrary surface mass load $L(\theta,\psi,t)$ is therefore computed by convolving the load with the appropriate Green's function. Denoting a general Green's function as $G^L(\gamma,t)$, the response, R is given by

$$R(\theta,\psi,t) = \int_{-\infty}^{t} \iint_{\Omega} a^2 L(\theta',\psi',t') G^L(\gamma,t-t') d\Omega' dt' \qquad \text{4-7}$$

where the spatial integral, $d\Omega$, is taken over the surface of the Earth. This equation is of the same form as the first term in equation 3-48, where the perturbation to the gravitational potential is calculated in order to determine a change in sea-level.

GIA model output is less sensitive to differences in Earth model parameters than differences in ice thickness history /SKB 2006/. However, differences of up to 30% of the maximum signal are found between uplift rate predictions for Fennoscandia generated using the same loading model but different Earth models /Whitehouse et al. 2006/ (see also section 4.5.4). This study and others, e.g. /Paulson et al. 2005/, that investigate the sensitivity of GIA observables to variations in lithospheric thickness and mantle viscosity, highlight the importance of using an Earth model that is representative of the region of interest. Earth model parameters vary laterally; therefore using a spherically symmetric Earth model will lead to errors in GIA predictions in regions whose rheology deviate strongly from the mean. Note that even if regional Earth models are used the sea-level equation must still be solved in the global domain to ensure the correct redistribution of meltwater in the oceans.

4.2.2   Ice-loading

In GIA modelling, ice-loading history is defined using temporal step functions; ice thicknesses at each location are specified at a series of discrete times. Early models used parabolic 'disks' of ice whose thickness, but not area, vary with time. The axisymmetry of the disks enable the viscoelastic response to such a load to be determined analytically for a spherically symmetric Maxwell Earth (see /James and Ivins 1998/ for a thorough analysis). More recent models specify ice thicknesses for a given time at a set of discrete points on the surface of the Earth. The ice thickness distribution is converted into a spherical harmonic loading function (see /Spada and Stocchi 2007/ for a complete explanation of the method) if the sea-level equation is to be solved using spectral methods (see section 4.3.2). It is commonly assumed that ice thicknesses vary linearly between time steps.

4.2.3   Ice sheet modelling

As previously mentioned, the accuracy of a GIA model is strongly dependent upon the accuracy of the input ice model. Ice models may be constrained geomorphologically, and/or thermomechanically. Early attempts to reconstruct ice sheet history relied upon the collection of extensive geomorphological data, such as dated moraine deposits. More recently, cosmogenic dating has been used to reveal the time which has elapsed since a surface was exposed, for example, due to the melting of an ice sheet (see /Dyke et al. 2002/ for an overview of results in North America). Such observations are able to place constraints upon the timing and areal extent of an ice sheet in some locations, but the labour-intensive nature of this approach means that there are still vast regions and time spans where the ice history is poorly constrained.

Another major drawback to using geomorphological data is that it does not provide any information about the thickness of the ice. Occasionally, glacial 'trimlines' may be used to determine the thickness of ice in an enclosed valley /Ballantyne 1997, Johnston and Lambeck 2000/, but the majority of ice sheets completely covered vast, flat areas, rendering this approach redundant. Once an ice sheet's extent was established for a given time, early modellers typically assumed a parabolic steady-state ice profile to determine the thickness of the ice /e.g. Denton and Hughes 1981/. As acknowledged by the authors, this is a coarse first approximation, and a reasonable fit to GIA observables has been achieved using such models. However, ice sheets rarely adopt a steady-state configuration, and modern ice sheet models are capable of handling the non-steady-state nature of realistic ice sheets.

GIA modellers used two other ways of constraining these early ice models. The first made use of the understanding of relative sea-level history. Observations of relative sea-level at locations far from the LGM ice sheets are a good proxy for eustatic sea-level. This allows constraints to be placed on the total volume of ice locked up in ice sheets at any given time during the last deglaciation. The second tool used by GIA modellers was the use of an iterative method when solving the sea-level equation /e.g. Lambeck et al. 1998a/. A first estimate of the ice-loading history would be used to calculate the change in relative sea-level at each time step, which would then be compared to observations throughout Fennoscandia. Any misfit would then be used to adjust the ice-loading history in an attempt to improve the fit between predictions and observations.

In addition to tuning the ice-loading history, adjustments to the earth model are sometimes carried out in parallel, in order to better fit the observations /e.g. Lambeck et al. 1998a, Peltier 2004/. When using a given ice model, it is important to use the appropriate radial viscosity profile if the two were developed in parallel, otherwise the output will not fit the observations, and predictions of other variables that were not used in the tuning procedure will be invalid.

Modern ice sheet models use inputs such as geothermal heat flux (in order to determine whether an ice sheet is frozen to its base, or if the presence of meltwater enables it to slide), basal sliding coefficients (related to e.g. basal water pressure, basal relief, the type of material at the base of the ice sheet, e.g. sediment or bedrock), albedo, climatic parameters (e.g. temperature, precipitation), mass balance calculations, and the physics of ice flow to determine how an ice sheet grows, flows, and melts.

Ice sheet model simulations need to be constrained by geological markers, and produce ice histories that are consistent with observations, before they can be used in conjunction with GIA modelling. Some model simulations have been developed in parallel with glacial geologists, resulting in simulations that fit both geological observations and dynamical laws. Such models will be able to be refined further following collaborations with GIA modellers, who will be able to feedback with vital information about ice thicknesses. A brief description of ice-loading models currently used within GIA modelling follows.

The most widely-used global ice models are the ICE-3G /Tushingham and Peltier 1991/ and ICE-5G /Peltier 2004/ models. These are constrained by geological data, and have been developed in conjunction with GIA modelling. ICE-5G is an updated version of ICE-3G, and was developed following the introduction of improved ice-dynamic modelling and the availability of new data, including new far-field sea-level histories from equatorial regions /Hanebuth et al. 2000, Yokoyama et al. 2000/, ice margin data from Siberia /Svendsen et al. 1999/, GIA data from the British Isles /Peltier et al. 2002/ and North America /Dyke et al. 2002/, and geodetic and gravity data from North America /Argus et al. 1999, Lambert et al. 2001/ and Greenland. ICE-5G should be used in conjunction with the VM2 Earth model /Peltier 2004/. /Tarasov and Peltier 2004/ have also developed a deglaciation history for North America using a three-dimensional thermo-mechanically coupled ice-sheet model constrained by ice margin chronology, relative sea-level histories, geodetically-derived uplift rates, and absolute gravity measurements.

A second global model has been developed by Kurt Lambeck. It is available for use in GIA models (Lambeck, pers. comm.) but has not been published as a single data set. The Fennoscandian part of this model, which also covers the Barents Sea, is known as FBK8 and is detailed in /Lambeck et al. 1998a/. It has been combined with the Laurentide and Greenland parts of ICE-1 /Peltier and Andrews 1976/, the BK4 British Isles ice model /Lambeck 1993b/, and the ANT3 Antarctic model /Nakada and Lambeck 1988/ to form a global model known as the RSES model /Kaufmann and Lambeck 2002/.

There are a considerable number of other ice sheet models available at present, including a northern hemisphere ice model developed by /Zweck and Huybrechts 2005/ which awaits testing by the GIA community, a Fennoscandian model developed by Näslund et al. (see /SKB 2006/), Greenland and Antarctic models reviewed in /Huybrechts 2002/ and an Antarctic model developed by /Ivins and James 2005/.

The two principal ice models used to represent the Fennoscandian ice sheet are ICE-5G /Peltier 2004/ and FBK8 /Lambeck et al. 1998a/. The /SKB 2006/ model has also been used to investigate GIA in this region. The spatial extent of these three models at the LGM is similar over north-western Europe, but the /SKB 2006/ model predicts continuous ice across the North Sea to the UK, whereas the other two models predict negligible ice thicknesses here. To the north, ICE-5G contains the most extensive ice cover, with ice thicknesses at the LGM predicted to have been greater than 1,500 m over Svalbard and in the central Barents Sea, with thinner ice (~500 m thick) extending across to Severnaya Zemlya. FBK8 also contains ~1,500 m of ice over the Barents Sea at the LGM, but the ice sheet is thinner over Svalbard, and is only predicted to have extended as far as Novaya Zemlya. The /SKB 2006/ model does not extend into the Barents Sea. None of the models include any significant ice cover over Siberia (a feature that was present in ICE-3G /Tushingham and Peltier 1991/). All three models predict ice thicknesses of > 2,400 m over central Fennoscandia, but the /SKB 2006/ and FBK8 model ice sheet maxima are centred over the Gulf of Bothnia, whereas ICE-5G maximum thicknesses are found in central Sweden. The models will therefore produce different patterns of rebound when implemented within a GIA model.

4.3 Methods for solving the sea-level equation

The principle methods used to solve the sea-level equation are described, along with a description of how GIA models are used to constrain the input ice history and Earth structure. Table 4-1 details how GIA models may be categorised according to a range of properties; not all are discussed in detail in this section.

4.3.1 Solution domain and geometry

Several authors /James and Lambert 1993, Amelung and Wolf 1994/ have shown that flat Earth models may be used to describe the solid Earth component of GIA in small regions such as Fennoscandia, but since a global approach is required to solve for sea-level change (see below) state-of-the-art GIA models should employ spherical geometry. /Wu and Johnston 1998/ and /Wu and van der Wal 2003/ also show that spherical effects become important beyond the ice margin, thus decreasing the accuracy of flat Earth models in these regions.

In order to accurately solve the sea-level equation, the solution domain must include the whole Earth /e.g. Milne et al. 1999, Wu and van der Wal 2003, Paulson et al. 2005/. This ensures that water produced by the melting of ice sheets is gravitationally-consistently redistributed throughout the oceans; a calculation that is impossible with a non-global solution.

Using a global domain also permits the calculation of surface deformation due to mass changes in far-field ice sheets: Large ice loads, such as the Laurentide, had a long wavelength effect, and solid surface deformation will have occurred both in the region of former loading and throughout the peripheral bulge of the deformation /Mitrovica et al. 1994b/, which may extend across several thousands of kilometres /e.g. Whitehouse et al. 2007/.

Table 4-1.

Property	Options				
Geometry	Flat Earth	Spherical axisymmetric		Full spherical	
Solution method	Analytical solution of idealised problem	Finite Element Methods	Spectral Methods	Perturbation Methods	
Solves sea-level equation?	Yes, gravitationally-consistent redistribution of meltwater		No, solves for solid Earth GIA effects only		
Global or Regional	Global study		Regional study		
Radial Earth model	VM2 (to be used with ICE-5G)	Earth model developed in conjunction with Lambeck's 1998 ice model	Earth model iterated during the solution process	Other test Earth models defining lithospheric thickness and mantle viscosity	
Ice model	Global ice models developed from GIA studies. E.g. Peltier, Lambeck	Global and regional geomorphologically constrained ice models	Climate-driven, thermo-mechanical ice models, e.g. Tarasov, Huybrechts	Idealised ice-loads, e.g. circular disc with a parabolic profile	
Compressibility	Compressible		Incompressible		
Self-gravitating?	Yes		No		
Shoreline migration	Yes, accurate treatment of time-varying shoreline migration		No, fixed shorelines		
Rotation	No rotation effects included		Rotation effects included	Calculations allow for polar wander	
3-D Earth structure	No lateral Earth structure included	Realistic Earth structure included at all depths	Realistic lithospheric thickness variations included	Realistic 3-D mantle viscosity variations included	Plate boundary effects included	Idealised 3-D structure for sensitivity tests
Rheology	Purely viscous model		Elastic lithosphere, viscous mantle		Full viscoelastic rheology. Earth modelled as a Maxwell solid
Treatment of marine-based ice	Accurate treatment of shoreline migration and meltwater redistribution in the presence of marine-based ice		No special treatment of marine-based ice		

The effect of Laurentide loading is predicted to have caused ~5 m of uplift across Fennoscandia at the LGM /Lambeck et al. 1998a/; around 1% of the magnitude of the local subsidence signal. Tangential motion is also perturbed by both far-field loading and far-field Earth structure /Wang and Wu 2006/. Horizontal deformation rates are predicted to have been perturbed by ~5 mm/yr in an easterly direction as a result of peripheral bulge collapse during deglaciation /SKB 2006/. This figure is an upper bound; actual rates may be lower due to the presence of the Atlantic plate boundary between the load and bulge region /Latychev et al. 2005b/. Due to the long-wavelength nature of these effects, the signal is likely to be homogenous across north-western Europe.

4.3.2 Normal mode and spectral methods

Solutions to the full sea-level equation build on work relating to the response of the Earth to loading. Most methods are based upon the normal-mode formalism developed by /Peltier 1974/ and /Wu 1978/. In this approach Love numbers are derived, and hence the Green's functions for displacement and gravity anomalies.

Solutions have been obtained via analytical /Wolf 1984, Amelung and Wolf 1994, Vermeersen and Sabadini 1997/, semi-analytical /Peltier 1974, Wu 1978, Wu and Peltier 1982, Sabadini et al. 1982, Tromp and Mitrovica 1999a/, and numerical methods /Clark et al. 1978/. Numerical solutions for the relaxation may be determined in the time domain /e.g. Cathles 1975/ or, more efficiently, in the Laplace-transform domain /e.g. Peltier 1974/, where the correspondence principle /Fung 1965/ reduces the stress-strain relationship for a viscoelastic material to the same form as the elastic case in the time domain.

The calculations relating to solid Earth deformation have been extended to solve the full sea-level equation by accounting for the gravitationally-consistent redistribution of meltwater throughout the oceans and the perturbation to the geoid at each loading time step /e.g. Milne et al. 1999/. The integral form of the sea-level equation, and the fact that ΔSL appears on both sides of the equation, means that solutions must be obtained using an iterative method.

The original Green's function method of discretizing loading using the Heaviside function is computationally inefficient when combined with iterative methods, especially when ice history is complex or a change in resolution is required. As a consequence, the majority of current state-of-the-art GIA models use a pseudospectral approach, based on the method derived by /Mitrovica and Peltier 1991a/, to solve the sea-level equation. In this method sea-level change is projected onto the ocean function:

$$\Delta S(\theta,t) = C(\theta,t)\Delta SL(\theta,t)$$ 4-8

where

$$\Delta SL(\theta,t) = \frac{\rho_I}{g}\Phi * \Delta I(\theta,t) + \frac{\rho_W}{g}\Phi * \Delta S(\theta,t) + c_{SL}(t)$$ 4-9

and

$$c_{SL}(t) = -\frac{M_I(t)}{A_O \rho_W} - \frac{1}{A_O}\left\langle \frac{\rho_I}{g}\Phi * \Delta I(\theta,t) + \frac{\rho_W}{g}\Phi * \Delta S(\theta,t) \right\rangle_O$$ 4-10

$\Delta S(\theta,t)$ is the change in ocean height and $\Delta SL(\theta,t)$ is the change in relative sea-level as defined in equation 3-22. $C(\theta,t)$ is the ocean function, which takes the value 1 over the oceans and 0 elsewhere, thus ensuring that ocean height is zero outside the oceans. $c_{SL}(t)$ is the spatially-independent (eustatic) change in sea-level at time t. The * symbol represents the spatial convolution of the loading functions ($\Delta S, \Delta I$) with the Green's functions (Φ) (see section 4.2.1), and the notation $<x>_O$ is used to denote the mean of variable x over the oceans. The use of the ocean function in equation 4-8 negates the need for the convolution integrals to be spatially restricted. Note also that equation 4-9 is no longer an integral equation (as it was in section 3.3.3) since $\Delta SL(\theta,t)$ does not appear in a convolution integral on the right-hand side. This re-casting of the sea-level equation enables it to be solved by spectral methods.

Spectral methods refer to a method whereby the governing equations are Fourier transformed, and hence partial differential equations are reduced to ordinary differential equations, which may easily be solved by numerical methods. When solving the sea-level equation by spectral methods, the ocean and ice loads are also expressed as spherical harmonic expansions, and the Fast Fourier Transform is used to compute the coefficients /e.g. Dilts 1985/. Transforming the sea-level equation enables the spatial convolutions to be calculated analytically in the spectral domain.

A simple algorithm is then used to solve the sea-level equation:

(i) Using an initial guess for the global distribution of the change in ocean height for a given time step ($\Delta S(\theta,t)$), the resulting global distribution of the change in sea-level ($\Delta SL(\theta,t)$) in the spectral domain is calculated using equation 4-9.

(ii) This solution is transformed into the spatial domain (hence the name 'pseudospectral'), and equation 4-8 is used to project the calculated sea-level change distribution on to the ocean function.

(iii) The solution is transformed back into the spectral domain to yield a next estimate for ocean height change ($\Delta S(\theta,t)$). The process is repeated until convergence is achieved for ocean height change for that time step.

This method is computationally efficient because it is able to make use of fast transform methods when moving between the spatial and the spectral domain. Additionally, spatial resolution may be increased by simply increasing the truncation level of the harmonic expansions, given sufficient computational power.

The spectral method approach has been further developed in recent years, and incorporated into finite difference /Martinec 1999/ and finite element methods /Martinec 2000/, in order to allow the sea-level equation to be solved in the presence of 3-D mantle viscosity variations. In order to solve the coupled partial differential equations governing viscous relaxation in the presence of 3-D Earth structure, /Martinec 1999, 2000/ converts the partial differential equations into a series of simultaneous ordinary differential equations, which may then be solved by numerical integration.

Spectral methods have been used by the research groups led by Mitrovica and Milne (e.g. /Mitrovica and Milne 2003/), Kaufmann (e.g. /Nakada and Lambeck 1987, Kaufmann and Lambeck 2002/), Zhong (e.g. /Paulson et al. 2005/, to verify the results of their finite element calculations), and Spada /Spada and Stocchi 2007/. This last group has developed a publically-available sea-level equation solver called SELEN2 (see http://flocolleoni.free.fr/Welcome.html) which solves the original sea-level equation on a self-gravitating Maxwell Earth /Farrell and Clark 1976/, but does not account for shoreline migration or rotational feedback. Their model incorporates a semi-analytical loading solver called TABOO /Spada et al. 2004/.

4.3.3 Finite element/finite volume methods

The second principle method of solving the sea-level equation employs a finite element, or finite volume, approach. The principle difference between this method and the spectral method is that the governing equations are integrated numerically in the time domain rather than the Laplace domain in the finite element method. Finite element packages, such as Abaqus /Hibbit et al. 2005/, Tecton /Melosh and Raefsky 1980/ and Marc /MSC Marc 2003/, are commonly used, but must be adapted to deal with viscoelasticity, compressibility, pre-stress advection and self-gravitation. It has been shown that there is close agreement between solutions derived using finite element (FE) methods and the spectral approach /Wu 1992b, 2004/.

/Peltier et al. 1978/ realised the importance of developing a global finite element model to solve the sea-level equation. However early GIA models were principally interested in studying the solid Earth response to regional ice-loading, and hence just used a 2-D, viscoelastic half space model /e.g. Wu 1992a/ which did not attempt to solve the sea-level equation /Gasperini and Sabadini 1989, 1990/. Axisymmetric test loads were typically used, and the Earth was assumed to be flat /Wu 1993, Kaufmann et al. 1997/. Later models incorporate realistic ice-loading but still just redistribute meltwater eustatically due to the neglect of self-gravitation in the calculations /Wu 1999, 2001, 2002b/. Lateral Earth structure has also been included into these flat Earth models to give a regional 3-D model /Kaufmann and Wu 1998, Kaufmann et al. 2000, Kaufmann and Wu 2002, Kaufmann et al. 2005, Steffen et al. 2006/ but still they do not solve the full sea-level equation, which requires a global solution domain.

/Zhong et al. 2003/ developed the CitcomSVE code /Zhong et al. 2000/ to give a global 3-D, spherical, viscoelastic finite element model which is used to study the dynamic response of the Earth to surface loading. It includes self-gravitation and permits lateral variations in Earth structure. /Paulson et al. 2005/ extended the model to include solutions to the sea-level equation, and benchmarked their results against solutions obtained using the spectral method. This GIA model does not account for shoreline migration, but does account for the retreat of marine-grounded ice, and rotational effects.

At the same time, /Wu 2002b/ developed the Coupled Laplace Finite Element method (CLFE) to solve for Earth deformation in the spherical domain, and /Wu and van der Wal 2003/ coupled it to the sea-level equation. This method is used by /Wu et al. 2005/ and /Wang and Wu 2006/ to solve the gravitationally self-consistent sea-level equation on an incompressible Maxwell Earth in the spherical domain. The model uses realistic ice- and ocean-loading, but does not account for shoreline migration or rotational effects.

Most recently, /Latychev et al. 2005a/ developed a finite volume method for calculating the Maxwell viscoelastic response of a 3-D, self-gravitating, elastically compressible Earth to surface loading. It has been used in conjunction with realistic ice-loading and lateral Earth structure /Whitehouse et al. 2006/, but just assumes a complementary, eustatic ocean load; it has not yet been fully coupled to the sea-level equation.

/Spada et al. 2006/ have also developed a 3-D finite element model to investigate the deformation of an incompressible, non-self-gravitating spherical Earth in response to realistic ice-loading. They carry out global calculations but do not solve the sea-level equation as they neglect the self-consistent ocean load. This group, and others, have also used finite element methods to investigate the effect of non-Newtonian rheology upon GIA predictions /e.g. Wu 1992b, 1995, 2002a, Giunchi and Spada 2000, Gasperini et al. 2004, Wu and Wang 2008/.

4.3.4   Other solution methods

The need to include lateral Earth structure in GIA models has led several authors to use perturbation methods when investigating the response of the Earth to ice-loading, although it should be noted that the full sea-level equation has not been solved using this method.

/Kaufmann and Wolf 1999/ present analytical solutions for the deformation of a viscoelastic material in Cartesian ('flat Earth') geometry due to a simplified loading history, and they model lateral variations in mantle viscosity as small perturbations.

/Tromp and Mitrovica 1999a/ update the Peltier-Wu normal mode formalism for the response of a self-gravitating, linear viscoelastic Earth to an arbitrary surface load. They use an eigenfunction expansion method instead of the traditional Love number approach, but still determine the response to the load in the form of a Green's function. When the density or viscosity structure of the Earth is perturbed away from the spherically-symmetric case this leads to a non-linear eigenvalue problem, which they overcome by using perturbation theory to linearize the problem.

The drawback of using perturbation methods to account for lateral variations in Earth structure is that convergence problems limit the magnitude and geometry of the perturbations for which the theory is valid. Mantle viscosity may vary over several orders of magnitude; this could not be represented by perturbation theory.

4.3.5   Solutions with a time-dependent ocean function

If a time-dependent ocean function is used, an additional iterative loop must be carried out when solving the sea-level equation in order to determine the change in the distribution of the ocean function, $C(\theta,t)$, at each time step.

First the sea-level equation is solved, using the iterative method described in section 4.3.2 to determine sea-level at each position θ, for each loading time step t_j ($j=1,N$, where N is the number of loading time steps). For this first solution fixed ocean geometry is assumed, e.g. present-day geometry. Using this solution, the change in relative sea-level between the present-day (t_p) and each past time, t_j, is calculated for each position, θ:

$$\Delta SL(\theta, t_j) = SL(\theta, t_j) - SL(\theta, t_p) \qquad (j=1,N) \qquad\qquad \text{4-11}$$

The palaeotopography distribution may then be calculated at each position, for each time step:

$$T(\theta, t_j) = T(\theta, t_p) - \Delta SL(\theta, t_j) \qquad (j=1,N) \qquad\qquad \text{4-12}$$

$T(\theta, t_p)$ is the present-day topography distribution. The coastline at time t_j will follow the zero height contour of the palaeotopography distribution, thus the sign of $T(\theta, t_j)$ may be used to define a new ocean function distribution at each time step: $C(\theta, t_j)$ ($j=1,N$) takes the value 1 over the oceans (where $T(\theta, t_j) < 0$), and the value 0 over land (where $T(\theta, t_j) > 0$):

$$C(\theta, t_j) = \begin{array}{ll} 1 & where \quad T(\theta, t_j) < 0 \\ 0 & where \quad T(\theta, t_j) > 0 \end{array} \qquad (j=1,N) \qquad\qquad \text{4-13}$$

The ocean function is now uniquely defined for each time step. The sea-level equation is re-solved for the whole glacial cycle, using the newly-defined time-dependent ocean function. This process is repeated until the ocean function distribution converges for all time steps. Reasonable accuracy can be achieved in 3–4 iterations.

4.3.6   Using GIA modelling to refine model inputs

Once a solution to the sea-level equation has been obtained a second iterative process is often carried out in an attempt to improve the accuracy of the input ice and Earth models (see Figure 4-2). GIA observables, such as relative sea-level histories or present-day deformation rates, are output from the sea-level calculations and compared to real world observations. The input models are then 'tuned' in an attempt to improve agreement between predictions and observations. Care must be taken when attempting to tune the input models, due to the potential non-unique nature of the solutions.

This method was used by /Lambeck et al. 1998a/; relative sea-level data from Fennoscandia were used to calibrate the input ice-loading history and Earth model parameters. Recently, /Lambeck et al. 2006/ have used a similar procedure to estimate ice thickness across northern Eurasia at the end of the Saalian glaciation (~140 ka BP) using observations of solid Earth rebound and shoreline locations.
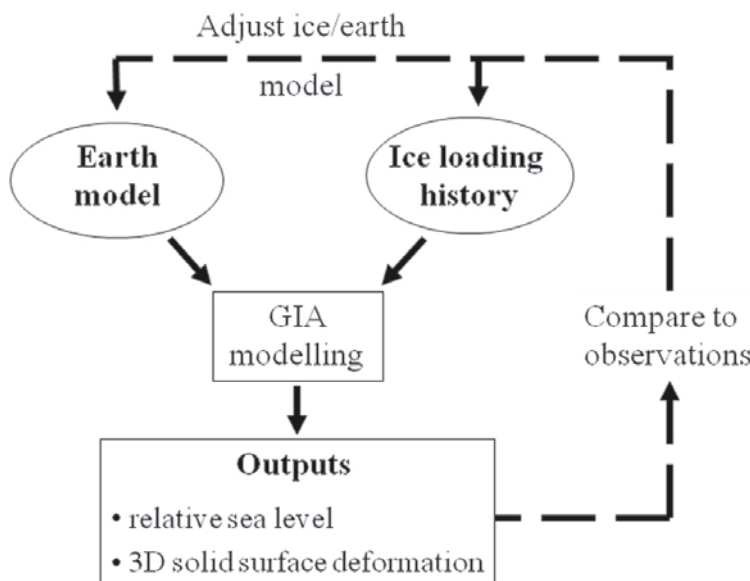

Figure 4-2. Iterative procedure used to tune the GIA input models.

Several authors have used a more formal inversion procedure to invert for ice-loading history or rheological parameters. /Mitrovica and Peltier 1993a/ invert the relaxation-time spectrum for Fennoscandia to yield a 1-D viscosity profile for that region. /Davis et al. 1999/ invert tide gauge data from the same region to refine the local ice history and Earth model. /Milne et al. 2004/ use a Bayesian inversion method to invert the BIFROST GPS data and yield a detailed radial viscosity profile for the region. And /Steffen and Kaufmann 2005/ use a global inverse procedure to investigate the likelihood of there being a low viscosity zone in the Fennoscandian upper mantle using palaeo-shoreline data and the BIFROST uplift rate data.

/Mitrovica and Forte 2004/ seek to constrain the mantle viscosity profile and present a joint inversion of data relating to both GIA and mantle convection. /Kaufmann and Lambeck 2000/ also combine information from mantle convection models with GIA modelling, while in /Kaufmann and Lambeck 2002/ they formally invert for the radial mantle viscosity profile using a range of data: relative sea-level data, observations relating to the Earth's rotational state, changes in the gravitational field, and present-day uplift rates.

As discussed in section 4.5.4, it is unlikely that it will be possible to use GIA models to invert for complex lateral Earth structure at a given depth. However, future inversions should investigate the potential of the Laurentide ice sheet; this larger ice sheet will have excited deformation at greater depths, and at greater distances from the loading region, and may be used to place tighter bounds on lower mantle viscosities.

4.4   State-of-the-art GIA models

State-of-the-art GIA models, developed by the leading researchers in this field, are described, and the principle results discussed. At the end of the chapter, the principle implications for ice history and Earth rheology are briefly listed.

4.4.1   Peltier

Richard Peltier was at the forefront of developing the theory of GIA in the late '70's and early '80's. He applied his work on solving for the impulsive response of a viscoelastic Earth to loading /Peltier 1974/ to the forward and inverse problems of GIA /Peltier and Andrews 1976, Peltier 1976/. He pioneered both numerical /Clark et al. 1978/ and finite element solutions to the sea-level equation /Peltier et al. 1978/, and, with Jerry Mitrovica, went on to develop a formal inverse theory for mantle viscosity /Mitrovica and Peltier 1991b/ and the pseudo-spectral method for solving the sea-level equation /Mitrovica and Peltier 1991a, Mitrovica and Peltier 1992a/. The pseudo-spectral method generates high-degree solutions for the deformation of a viscoelastic Earth and the redistribution of meltwater in the oceans, and is still the most widely-used method for solving the full sea-level equation. The paper /Mitrovica and Peltier 1991a/ was also the first to identify the process of 'ocean syphoning' as an explanation for ongoing changes in relative sea-level.

Peltier's original modelling methods have been updated to include the effects of shoreline migration /Peltier 1994/, and the accuracy of this method has been further improved by the inclusion of a 'broad-shelf effect' /Peltier and Drummond 2002/. Peltier has also studied the feedback between deglaciation and the rotational state of the Earth /Peltier 1988, 1999/, and used observations of the rate of polar wander and the acceleration of the rate of rotation to show that mantle viscosities likely increase by one order of magnitude across the lower mantle /Peltier and Jiang 1996a/.

Peltier has also inferred deep mantle viscosities from rebound data /Peltier 1985/ and free-air gravity anomalies /Mitrovica and Peltier 1991c/. However, in the latter case, the authors caution that such inferences are also dependent upon the extent and timing of ice sheet coverage.

A large portion of Peltier's contribution to the field of GIA has been the simultaneous development of global ice history and radial Earth models. He has published a series of global deglaciation models that are tuned to fit the observational data, and identified the accompanying radial viscosity profiles that give the best fit to these data. The most recent model is the ICE-5G ice model, which should be combined with his VM2 viscosity model /Peltier 2004/, but ICE-3G /Tushingham and Peltier 1991/ and

ICE-4G /Peltier 1994/ are still widely used, often in combination with alternative local ice models, e.g. for Fennoscandia. The ice and Earth models are commonly tuned to fit relative sea-level, geomorphological, and geoid data, but recently Peltier has worked with Lev Tarasov to pioneer the use of dynamic ice models as a starting point for GIA modelling, in an attempt to improve constraints upon both Earth and ice models /Tarasov and Peltier 2002, 2004, 2006/.

GIA predictions made using Peltier's ice models have been repeatedly tested, and the models retuned, using a range of data, including geodetic data /Peltier 1995, Argus et al. 1999, Peltier 2002a, Tarasov and Peltier 2002, 2004/, relative sea-level data /Tushingham and Peltier 1992, Rostami et al. 2000, Nunn and Peltier 2001, Peltier et al. 2002, Shennan et al. 2002/, and absolute gravity data /Peltier 2002a, Tarasov and Peltier 2004/.

Many of these studies have allowed inferences to be made about local Earth structure, for example, in North America /Tushingham and Peltier 1992/ and the British Isles /Peltier et al. 2002/. Inversions of the relative sea-level relaxation spectrum /Mitrovica and Peltier 1993a, 1995, Peltier and Jiang 1996b, Peltier 1996a/ also permit inferences of Earth structure to be made: /Mitrovica and Peltier 1993a/ invert the Fennoscandian spectrum to yield a preferred Earth model with upper and lower mantle viscosities of $0.37–0.45 \times 10^{21}$ Pa s and $2.2–1.9 \times 10^{21}$ Pa s, respectively. While /Mitrovica and Peltier 1995/ infer an Earth model with a lithospheric thickness of 120 km, and upper and lower mantle viscosities of $0.5–1 \times 10^{21}$ Pa s and $0.5–3 \times 10^{21}$ Pa s for Hudson Bay. In such studies the authors highlight the importance of understanding the resolving power of the data and their sensitivity to depth-dependent viscosity variations, in order to determine the accuracy of the inversions /Mitrovica and Peltier 1992b, Mitrovica and Peltier 1993a/, and determine which data should be used to determine structure at a given depth /Mitrovica and Peltier 1991b, Mitrovica and Peltier 1995, Peltier 1998c/.

Peltier has used the output from his GIA modelling to address several important questions, including determining the volume of ice at the LGM from far-field relative sea-level data /Peltier 1994, 2002b/, identifying the magnitude and source of meltwater pulse 1A /Peltier 2005/, and refining the detailed glacial history of the Laurentide ice sheet. Peltier's original estimates for the LGM ice volume were low in comparison to other estimates, but his most recent work yields a eustatic change of ~120 m since the LGM /Peltier and Fairbanks 2006/, in line with other values determined from GIA modelling. In the course of studying the relative contribution of different ice sheets to this eustatic change, Peltier's work on the Laurentide ice sheet has led him to conclude that this was a multi-domed ice sheet /Tarasov and Peltier 2004/ which had a large contribution to meltwater pulse 1A /Tarasov and Peltier 2006/.

Finally, Peltier has addressed the problem of determining the magnitude and source of present-day sea-level change. In several studies, tide gauge records have been corrected for GIA relative sea-level effects in order to determine the eustatic rate of sea-level change /Peltier and Tushingham 1991, Peltier 1996b/, while /Douglas and Peltier 2002/ point out that a ~0.3 mm/yr correction must be applied to present-day sea-level rates determined using satellite altimetry over the oceans in order to account for the ongoing effect of ocean syphoning.

4.4.2   Mitrovica and Milne

Over the past decade Jerry Mitrovica and Glenn Milne have continued to develop highly accurate methods for solving the sea-level equation, and have used their modelling to investigate and explain a range of geophysical phenomena. Much of Mitrovica's early work was carried out in collaboration with Peltier, in particular the development of the pseudo-spectral method for solving the sea-level equation, inversions of the relaxation spectrum in order to infer mantle viscosities, and an understanding of the sensitivity of GIA data to structure at different depths; this work is covered in the previous section.

Mitrovica continued to develop his spectral and pseudo-spectral methods for solving the sea-level equation using spherical harmonics /Mitrovica et al. 1994ab/, and also pioneered several new methods for tackling the problem, often using a cross-disciplinary approach. For example, /Mitrovica and Forte 1997/ combined observations relating to mantle convection with GIA data in order to infer the radial profile of mantle viscosity. This study was recently updated /Mitrovica and Forte 2004/ as the availability of additional data has enabled the accuracy of the joint inversion to be improved. The most recent solution /Mitrovica and Forte 2004/ consists of a 25-layer radial viscosity profile which ranges from 0.4×10^{21} Pa s in the upper mantle to 10^{23} Pa s in the mid-lower mantle, beneath an 80 km lithosphere. Mitrovica has also obtained solutions for the deformation of a viscoelastic Earth to surface loading using a normal mode formalism /Tromp and Mitrovica 1999ab, 2000/.

In much of their work, Mitrovica and Milne highlight the potential errors that have been introduced into models of ice history, inferences of mantle viscosity, and estimates of present-day melting, by neglecting key physical features and processes when modelling GIA. Having identified errors in earlier GIA models /e.g. Mitrovica et al. 1993/, Mitrovica and Milne have updated the theory behind the sea-level equation itself to include shoreline migration /Milne and Mitrovica 1998a/ (section 3.5.1), rotation /Milne and Mitrovica 1996/ (section 3.5.3), the effect of marine-based ice /Milne et al. 1999/ (section 3.5.2), and lateral Earth structure /Latychev et al. 2005a/ (section 3.5.4) into their models. Seminal papers on the updated sea-level equation, along with comparisons with earlier versions, are /Mitrovica and Milne 2003/ and /Kendall et al. 2005/.

Early studies into the influence of including time-dependent ocean geometry showed that assuming fixed shorelines can lead to errors of > 2 m when predicting the amplitude of late Holocene far-field sea-level highstands /Milne and Mitrovica 1998b/. Subsequently time-dependent ocean geometry is included in the gravitationally-self-consistent GIA model of /Milne and Mitrovica 1998a/.

Following initial sensitivity studies into the affect of Late Pleistocene glacial cycles upon the Earth's orbital dynamics /e.g. Mitrovica and Forte 1995, Mitrovica and Milne 1998/, /Milne and Mitrovica 1996/ include the effect of perturbations to the rotation vector in the sea-level equation. The most up-to-date theory is presented in /Mitrovica et al. 2005/. /Milne and Mitrovica 1998a/ demonstrate that neglecting perturbations to the rotation vector can bias relative sea-level predictions by up to ~8 m and present-day sea-level rates by up to 0.2 mm/yr, indicating that previous inferences of LGM ice volumes will be biased, and that the rotational effect must be taken into account when correcting tide gauge data. Most recently, /Mitrovica et al. 2001a/ consider the rotational signatures due to present-day melting scenarios and conclude that rotational feedback due to Greenland ice sheet melting is capable of significantly perturbing GIA observables.

As previously mentioned, marine-based ice occupies space that would otherwise be taken up by the ocean. Neglecting this effect leads to inaccuracies when applying ocean-loading in the sea-level equation, and can lead to bias in inferences of ice history and mantle viscosity. In particular, /Milne et al. 1999/ note that ignoring loading perturbations due to the presence of marine-based ice leads to an underestimate of LGM ice volumes by ~10%.

Other important conclusions presented in Mitrovica's early work include the observation that the melting of a large ice sheet, such as the Laurentide, can considerably perturb horizontal velocities several thousand kilometres from the margin of the former ice sheet /Mitrovica et al. 1994b/. In the same study /Mitrovica et al. 1994b/ are among the first to note that the sensitivity of deformation rates to rheology is strongly dependent upon the location of the observation site relative to the former ice sheet. The question of the resolving power and sensitivity of GIA data to Earth structure at different depths is further studied in /Mitrovica and Forte 1995/, and is discussed in subsequent cases where GIA models are used to place constraints upon mantle viscosity profiles /e.g. Mitrovica 1996, Forte and Mitrovica 1996, Mitrovica and Forte 1997, Mitrovica and Forte 2004, Milne et al. 2004/.

More detailed work into the structure of the Earth includes sensitivity studies into the effect of shallow low viscosity zones in the mantle upon GIA predictions /Milne et al. 1998, Di Donato et al. 2000a, Kendall et al. 2003/, and the effect of lateral Earth structure upon GIA predictions /Latychev et al. 2005a/. /Latychev et al. 2005b/ demonstrate that the inclusion of weak zones at plate boundaries can have a significant effect upon predictions of present-day tangential rates of deformation, on the order of 1–2 mm/yr, over horizontal distances of several thousand kilometres, while /Latychev et al. 2005c/ demonstrate a significant perturbation to GIA-induced variations of the Earth's long wavelength gravity field when 3-D structure is included in the modelling. /Kendall et al. 2006/ note that tide gauge corrections will be biased if 3-D structure is neglected, leading to errors in predictions of present-day rates of sea-level change. /Whitehouse et al. 2006/ quantify the bias introduced to uplift rates by neglecting 3-D structure in Fennoscandia, and note that this can be reduced by using a 1-D global model that approximates the local depth-dependent mean of the 3-D model (see section 4.5.4).

Work has also been carried out to investigate the sensitivity of GIA predictions to variations in ice history. It is well known that the timing of deglaciation is the principal factor that determines the pattern of present-day uplift rates, but /Mitrovica and Davis 1995a/ show that altering the glaciation phase of ice build-up can also perturb predictions of present-day deformation by detectable amounts. More recently, /Tamisiea et al. 2007/ isolate the GIA trend from the GRACE gravity data in order to constrain the geometry of the Laurentide ice sheet. On a global scale, /Milne et al. 2002/ use GIA-corrected far-field relative sea-level curves to estimate the LGM ice volume. Their estimates map onto a eustatic sea-level rise of 115–135 m since the LGM.

Recent work has focussed upon understanding the causes and rates of sea-level change. /Mitrovica and Davis 1995b/ determine the present-day rate of eustatic sea-level change, using far-field relative sea-level data corrected for the effects of GIA, to be 1.1–1.6 m/yr. Holocene rates of sea-level rise have been predicted using predictions of rotational parameters from a joint inversion of GIA and mantle convection parameters /Mitrovica and Forte 1997/, and relative sea-level data from the Caribbean and South America /Milne et al. 2005/. /Mitrovica and Milne 2002/ demonstrate that the late Holocene global sea-level high-stand may be explained by appealing to the processes of ocean syphoning and continental levering (see section 3.4.3). Ongoing spatial variations in sea-level change associated with peripheral bulge subsidence are documented in /Gehrels et al. 2004, Milne et al. 2005, Whitehouse et al. 2007/.

Spatial variations in sea-level change are predominantly due to GIA effects. The data must be corrected for this signal before eustatic estimates may be obtained. The spatially-varying signal can also provide important information about the geometry of past ice-loading /Davis et al. 1999/, or the source of present-day sea-level rise /Mitrovica et al. 2001b, Tamisiea et al. 2001, 2003/. This 'fingerprinting' method is developed by /Clark et al. 2002/ in an attempt to determine the source of meltwater pulse 1A.

Geodetic methods have also been used to constrain and verify the results of GIA modelling (see Figure 4-3). The BIFROST GPS network in Fennoscandia beautifully identifies the pattern of uplift in this region due to the lack of significant tectonic deformation which would otherwise contaminate the signal /Scherneck et al. 2001/, and a formal inversion of the data has been carried out to yield a mantle viscosity profile, and investigate the radial resolving power of the data set /Milne et al. 2004/. The best fitting Earth models have a lithospheric thickness greater than 100 km and upper and lower mantle viscosities in the ranges 0.5–1.0×10^{21} Pa s and 5–50×10^{21} Pa s, respectively.
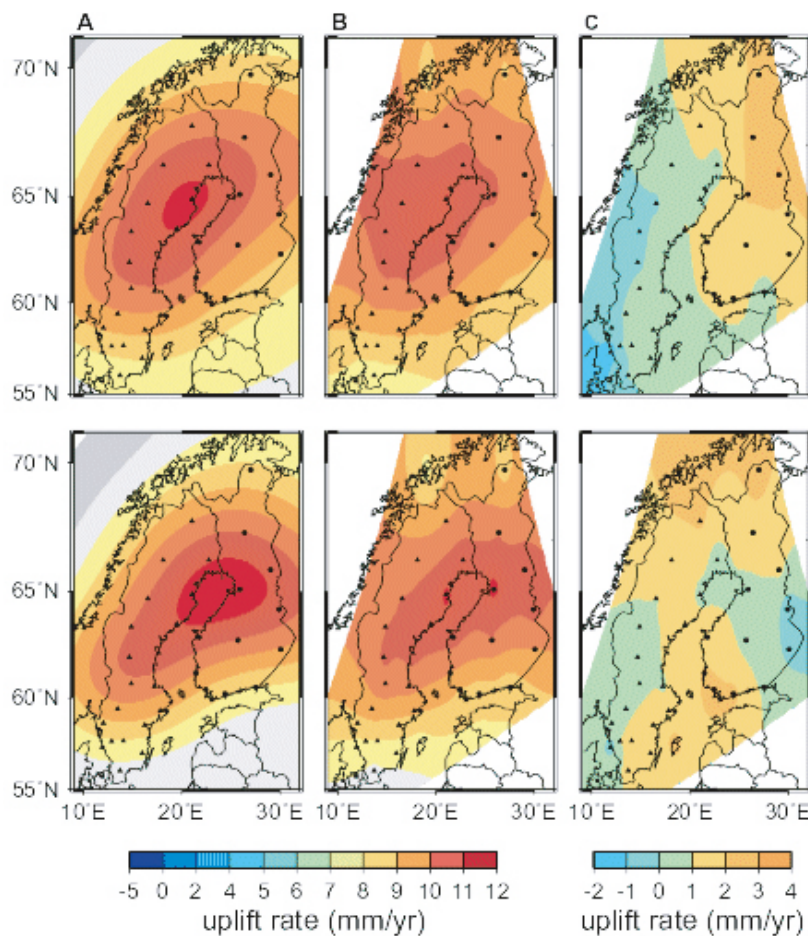
Figure 4-3. *GPS data verifies the results of GIA modelling. Present-day uplift rates predicted using Lambeck's Fennoscandian ice model (top row), and ICE-3G (bottom row). Column A is the model-predicted uplift pattern. Column B shows the model predictions interpolated at the BIFROST GPS sites (black triangles/ squares). Column C shows the difference between the GPS observations and the interpolated uplift pattern. Adapted from /Milne et al. 2004/.*

The GPS data have also been used to correct local tide gauge measurements thus yielding a local rate of present-day sea-level rise of 2.1 ± 0.3 mm/yr /Milne et al. 2001/. This method is reversed by /Kuo et al. 2004/; sea-level changes detected by satellite altimetry are used to correct tide gauge data in order to determine the GIA uplift component in Fennoscandia. The robustness of the method is confirmed following comparison with the GPS data. GPS data have also been used in conjunction with GIA modelling in North America /Park et al. 2002/ and the UK /Milne et al. 2006/.

4.4.3   Lambeck

Kurt Lambeck has been at the forefront of GIA research for the past two decades. His work includes the development of a model that solves the full sea-level equation, accounting for both ice- and ocean-loading, as well as more complex processes such as shoreline migration /Lambeck 1993a/ and sea-level change in the presence of marine-grounded ice /Lambeck et al. 2003/. Lambeck highlights the importance of using a global model in order to correctly account for the redistribution of meltwater in the oceans /Lambeck 1993a, Lambeck 1996a, Fleming and Lambeck 2004/. The theory behind the model is discussed in /Lambeck 1990, Lambeck 1993c/, and the computational details are clearly presented in /Lambeck et al. 2003/, along with a comparison to results output from the model of /Milne et al. 2002/. Lambeck's work is complete in its consideration of all inputs into GIA modelling, including ice sheet history, Earth structure, and the feedbacks between climate, glacial cycles, and sea-level change /Lambeck et al. 2002a/. He has not carried out extensive work into the effect of lateral Earth structure upon GIA observables, but was among the first to infer lateral variations in mantle viscosity from sea-level studies /Nakada and Lambeck 1991/, and has acknowledged its necessity in the light of regional studies /Lambeck and Chappell 2001/.

Lambeck's early work consisted of sensitivity studies into the effect of deglaciation upon Earth's rate of rotation, true polar wander, and Earth's gravity field /Nakiboglu and Lambeck 1980, 1981, Johnston and Lambeck 1999/. More recently he has used data inversions to further our understanding of ice history and Earth structure. /Lambeck et al. 1998a/ invert relative sea-level data via an iterative method in order to simultaneously constrain both the Fennoscandian ice history, and radial Earth structure. The results are verified using tide gauge data /Lambeck et al. 1998b/, and the dependence of the predictions upon the input parameters is investigated /Johnston and Lambeck 1999/. /Kaufmann and Lambeck 2002/ use a combination of global sea-level data, observed changes to the Earth's rotational and gravitational fields, and present-day uplift rates in Fennoscandia in their inversion for a radial viscosity profile. More recently, /Lambeck et al. 2006/ invert crustal rebound data and palaeoshoreline positions to determine palaeotopography and ice thicknesses from Late Saalian and Eemian times. Other data used by Lambeck to constrain past sea-levels includes sill elevations and lake levels /Lambeck 1999/, lake tilting data /Lambeck et al. 1998b/, glacial trimlines /Johnston and Lambeck 2000/, isolation basins /e.g. Lambeck 1999/, coral growth depths /e.g. Yokoyama et al. 2001a/, and archaeological evidence /e.g. Lambeck et al. 2004a/.

Grouping the data into regions allows local constraints to be placed upon Earth parameters. Inversions yield lithospheric thicknesses for Fennoscandia and the British Isles in the range 65–100 km, with the thinner values relating to the British Isles /Lambeck 1993ab, Lambeck et al. 1996, 1998ab, Lambeck 1999/. Upper and lower mantle viscosities are found to lie in the range $3–5 \times 10^{20}$ Pa s and $1–2 \times 10^{22}$ Pa s, respectively, in good agreement with other studies. /Kaufmann and Lambeck 2002/ note that the results are strongly dependent upon the ice model used, while /Lambeck et al. 1996/ highlight the non-uniqueness of the solutions by demonstrating that similar results can be obtained with a thin lithosphere and low upper mantle viscosity as can be obtained with a thick lithosphere and high upper mantle viscosity.

Lambeck has also used the inversions to constrain ice sheet history and global sea-level rates. Far-field sea-level observations, e.g. from Australia, allow constraints to be placed upon LGM global ice volumes and subsequent rates of sea-level change /e.g. Fleming et al. 1998, Lambeck et al. 2000, Yokoyama et al. 2001b, 2006/, including present-day eustatic rates /Lambeck et al. 1998b, Fleming et al. 1998/. Lambeck's estimates for the LGM land-based ice volume lie in the range $46–52.5 \times 10^6$ km³, with the ice-equivalent eustatic sea-level being 125 ± 5 m lower than present-day levels /Fleming et al. 1998, Yokoyama et al. 2001b, Lambeck et al. 2002a/. He predicts maximum sea-level fall to have taken place between 16–12.5 ka BP and 11.5–9 ka BP at rates of up to 15 mm/yr /Fleming et al. 1998, Lambeck et al. 2002a/.

The data also indicate a continued, slow rise in sea-level on the order of 3–5 m since the cessation of melting at ~7 ka BP, and Lambeck attributes this to continued isostatic relaxation as a result of ocean-loading /Lambeck 2002/; a process that is included within his modelling.

Lambeck notes that the spatial and temporal pattern of sea-level data are key to isolating Earth and ice history parameters; a good data set is able to constrain the volume of ice in individual ice sheets /e.g. Lambeck 1993ab, Lambeck et al. 1996, 2000, Lambeck and Purcell 2005/. /Yokoyama et al. 2001c/ and /Lambeck et al. 2006/ also suggest sites where it would be useful to have sea-level data in order to constrain GIA model parameters.

Lambeck's studies into individual ice sheets include work upon the Fennoscandian, Barents, British and Greenland ice sheets. As expected, /Lambeck et al. 1998a/ iterate to yield a much thinner ice sheet than the maximum thick steady-state Fennoscandian ice sheet of /Denton and Hughes 1981/, while /Lambeck 1995a, 1996b/ concludes that a 2–3 km-thick ice sheet centred on the Barents Sea during the LGM is required to explain the local relative sea-level observations. Ice volumes for the Kara Sea are predicted to have been much smaller. A combination of forward modelling, data inversions, and geomorphological observations are use to constrain the history of the British and Irish ice sheets /Johnston and Lambeck 2000, Lambeck and Purcell 2001/. Ice thicknesses were found to be < 1,500 m, and the ice sheet is not predicted to have joined the Fennoscandian ice sheet /Lambeck 1991, 1993a/. Finally, inferences about Greenland ice sheet history are made using isolation basin dating to construct sea-level curves /Bennike et al. 2002, Fleming and Lambeck 2004/. Sea-level curves for Greenland contain a complex signal that reflects both local and far-field (Laurentian and Fennoscandian) ice mass changes, highlighting the importance of solving the full, global sea-level equation.

Applications of Lambeck's GIA modelling include the prediction of palaeoshorelines and palaeotopography, primarily in the region of the Fennoscandian ice sheet. Modelling in the Barents Sea region /Lambeck 1995a/ reveals that much of the area was sub-aerially exposed during the last sea-level lowstand, thus creating a suitable environment for ice sheet inception and growth. Reconstructions of palaeotopography around the Baltic Sea have allowed constraints to be placed upon the timing, depth and extent of the Baltic Ice Lake, which formed when the Baltic was cut off from the North Sea by a land or ice barrier /Lambeck 1999/, thus allowing palaeoshoreline data to be correlated to either sea-level or lake-levels. Palaeotopography predictions have also been used in conjunction with reconstructions of the British ice sheet /Lambeck 1995b/ to study the emergence of the North Sea, the land bridge between mainland Britain and Ireland, and whether an ice-dammed lake formed in southern Britain. These events have important anthropological implications and the study highlights locations which could yield constraining data.

/Johnston et al. 1998/ investigate the role of ice-unloading in triggering seismicity, and find that small ice sheets are more likely to result in fault instability, with thrust faulting predicted in the region of the former ice sheet and normal faulting outside. Lambeck has also used GIA modelling to place constraints upon tectonic rates outside formerly glaciated regions by correcting the sea-level data for the eustatic and isostatic GIA signals. For example, in Greece and western Turkey uplift rates predicted using GIA-corrected sea-level data agree with estimates obtained by alternative methods /Lambeck 1995c/. Conversely, if tectonic rates are independently well constrained, sea-level data can be corrected for non-GIA effects and hence used to constrain GIA model parameters /e.g. Lambeck et al. 2004b, Lambeck and Purcell 2005/.

Lambeck's contribution to GIA modelling includes the development of accurate solutions to the sea-level equation, the refinement of GIA input parameters related to both ice and Earth models, and the application of GIA modelling in a series of case studies that include Fennoscandia, the British Isles, the Barents Sea and northern Russia, the Mediterranean, Greenland and Australia.

4.4.4   Wu

Patrick Wu used finite element (FE) methods to produce some of the first solutions for isostatic deformation and relative sea-level change related to GIA /Wu and Peltier 1978/. He has developed this work over the last ten years, focussing on studying the structure and rheology of the Earth, and the implications upon GIA observables.

Wu has used analytical solutions to investigate the deformation of the Earth under loading /Wu and Ni 1996/, but in the majority of his work he has employed commercial FE methods (principally the ABAQUS package from Hibbit, Karlsson and Sorrensen Inc.), adapted to solve the sea-level equation /Wu 2004/. Early studies used the flat Earth approximation /Wu 1992a, 1993, 1999, 2001, Kaufmann and Wu 2002/ and did not account for self-gravitation. Therefore, the calculations just consider a uniform complementary ocean load following melting as opposed to one that is distributed according to the full sea-level equation. More recently, Wu has used a Coupled Laplace-Finite Element (CLFE) method and spherical geometry to study the deformation of a Maxwell solid under loading, both with radially-varying and laterally-varying Earth structure /Wu and van der Wal 2003, Wu et al. 2005, Wu 2006/. The CLFE method allows non-negligible lateral variations in viscosity to be included, and has been benchmarked against flat Earth models and solutions obtained using spectral methods /Wang and Wu 2006/. Shoreline migration and rotational effects are often neglected in the CLFE studies, but self-gravitation is included, allowing for the gravitationally-consistent redistribution of meltwater in the oceans /Wu et al. 2005, Wang and Wu 2006/. Wu has carried out both sensitivity studies, using axisymmetric ice and Earth models /Wu and van der Wal 2003, Wu, 2006/, and studies that include realistic ice history and Earth structure /Wu 1999, Kaufmann and Wu 2002, Wu 2005, Wu et al. 2005/.

In his early work, Wu predicted that GIA-related free-air gravity anomalies and changes in the rotational state of the Earth could constrain parameters relating to mantle viscosity and lithospheric thickness /Wu and Peltier 1983, 1984/. He went on to investigate the suitability of using different rheologies to explain the behaviour of the mantle under loading, including using linear and non-linear power law creep, and low viscosity channel flow in 2-D finite element models that used the flat Earth approximation /Wu 1992a, 1993, 1995, 1999, 2001, 2002a/. Synthetic relative sea-level data generated using both simplified /Wu 1992a, 1993, 1995/ and realistic /Wu 1999, 2001, 2002a/ ice histories is used to distinguish between rheologies. /Wu 1995/ demonstrates that data from the margin of the former ice sheet is most sensitive to rheological changes, but in general the non-uniqueness of solutions prevents firm conclusions to be drawn /Wu 1999, 2002a/.

Wu has also used his modelling to investigate the relationship between surface loading and seismicity. /Wu and Hasegawa 1996ab/ calculate the stress due to glacial loading and predict the timing, location, and mode of fault failure for a range of different scenarios. The results of this sensitivity study were used to explain the post-glacial distribution of earthquakes in eastern Canada /Wu and Hasegawa 1996b, Wu 1997, Wu and Johnston 2000/, at the same time placing bounds on the viscosity structure of the mantle. Extending this study to Fennoscandia, /Wu et al. 1999/ find that information relating to the location of pre-existing faults is required to explain the present-day pattern or seismicity.

Recently, Wu has focussed upon the effect of lateral heterogeneities in Earth structure upon GIA pre-dictions. Axisymmetric sensitivity studies reinforce the observation that fully 3-D models are required in any attempt to infer lateral variations in lithospheric thickness or mantle viscosity /Kaufmann et al. 1997/, and that GIA observables have the greatest sensitivity to lateral Earth structure at the margin of the former load /Kaufmann et al. 1997, Wu and van der Wal 2003, Wu et al. 2005/. The introduction of lateral structure introduces perturbations that are large enough to be detected by GPS, with the strongest effect coming from viscosity perturbations in the upper mantle. In general, the underlying pattern of present-day deformation is found to be governed by ice history, but the magnitude of deformation rates is governed by Earth model parameters.

To generate realistic 3-D Earth models, the VM2 mantle viscosity model /Peltier 2002a/ is perturbed using the S20A shear velocity model of /Ekström and Dziewonski 1998/, where mantle velocity perturbations are converted to viscosity perturbations using the scaling laws of /Ivins and Sammis 1995/. In such studies /e.g. Wu 2005, Wang and Wu 2006/, the ICE-4G ice history of /Peltier 1994/ is used. Variations in lithospheric thickness are also sometimes also included.

Several studies focus on North America, where it is shown that a reverse viscosity contrast in the upper mantle (a thick, high viscosity continental root lies above a low viscosity upper mantle in the region of Hudson Bay) can mask the effect of lateral viscosity contrasts in the lower mantle /Wu and van der Wal 2003, Wu 2005, Wang and Wu 2006/. This highlights the non-uniqueness of inferring lateral Earth structure from GIA observables.

/Wu 2006/ develops this idea and investigates the sensitivity of GIA observables to viscosity variations at different depths, and at different relative positions to the location of the data site, in an attempt to determine optimal locations for geodetic sites which could potentially be used to infer lateral Earth structure. The sensitivity also changes with time; relative sea-level data of different ages are sensitive to structure at different depths. Understanding the sensitivity of different data to various parameters allows the proper weight to be assigned in an inversion. As an example, radial velocities are found to be influenced by their position relative to both the former ice load and a region of anomalous viscosity, whilst tangential velocities are found to be predominantly sensitive to Earth structure beneath the former ice load, even when that site is in the far-field. In all cases, GIA data from the centre of rebound seem to have a limited sensitivity to Earth structure, and only provide information relating to structure directly beneath an observation site.

4.4.5 Kaufmann

During the last ten years Georg Kaufmann has made important contributions to GIA studies, both working alone, and with co-workers Wu, Lambeck and Steffen. His research has focussed on inverting GIA observables to constrain mantle viscosities, and studying the effects of laterally-varying Earth structure.

When solving for a 1-D radially-varying viscosity structure, Kaufmann uses the pseudo-spectral approach to solve the sea-level equation in the spherical domain /e.g. Kaufmann 1997, Kaufmann and Lambeck 2000, 2002, Steffen and Kaufmann 2005/. However, when studying the effect of lateral Earth structure upon GIA observables, he uses the finite element method /e.g. Kaufmann et al. 1997, Kaufmann and Wu 1998, Kaufmann et al. 2000, Kaufmann and Wu 2002, Kaufmann et al. 2005, Steffen et al. 2006, 2007/. This latter method is limited to the flat Earth case, where calculations are carried out for a regional model represented by a viscoelastic half space, and the global redistribution of meltwater is not accurately accounted for. /Kaufmann et al. 2005/ note that for this case results far outside the former region of loading should be treated with caution /Kaufmann et al. 2005/.

Kaufmann has also used perturbation theory to determine analytical solutions to the sea-level equation in the presence of sinusoidally-varying lateral Earth structure in the presence of a test load /Kaufmann and Wolf 1999/. However, the limited model complexity permitted by this method limits the usefulness of this approach.

Kaufmann's lateral Earth studies have developed from early models that use a simplified loading history and Earth structure, through to the use of realistic ice histories constrained by glaciological and climatological models, and Earth structure inferred from surface geology and seismic tomography /Ekström and Dziewonski 1998/. Kaufmann has used a range of ice models, including the global ICE-3G model /Tushingham and Peltier 1991/, BARENTS-2 (Barents Sea /Kaufmann and Wolf 1996/), FBK8 (Fennoscandia /Lambeck et al. 1998a/), BK4 (British Isles /Lambeck 1993b/), and various Antarctic models from /James and Ivins 1997, Nakada and Lambeck 1988, Huybrechts 1990/.

A key result of Kaufmann's early work is that the greatest sensitivity to lateral structure is found at the margins of the former ice load /Kaufmann et al. 1997/. Using realistic ice-loading, calculations demonstrate that the introduction of lateral Earth structure can perturb relative sea-level histories by 10–20 m at the LGM, present-day uplift rates by 0.5–3 mm/yr, and present-day free-air gravity anomalies by 0.5–4 mGal across Fennoscandia and the Barents Sea /Kaufmann and Wu 1998, Kaufmann et al. 2000/. All of these perturbations lie within the observational uncertainty of modern geophysical observation techniques, therefore inferences of ice history and Earth structure based on 1-D radially-varying models are likely to be biased. Indeed, /Kaufmann et al. 2005/ show that strong lateral variations in mantle structure beneath Antarctica can result in a pattern of horizontal motion that completely overprints the GIA signal predicted for a 1-D radially-varying Earth model. The authors also note the importance of distinguishing between the GIA signal from the LGM and the signal due to present-day mass changes in this region.

Further sensitivity studies into the affect of lateral variations in Earth structure /Steffen et al. 2006, 2007/ lead to the following conclusions: (1) Fennoscandian GIA observables are relatively insensitive to lower mantle structure due to the small spatial scale of the ice sheet. (2) Within the former ice-covered region, observables are sensitive to structure beneath the observation site. (3) Horizontal velocities reflect lateral variations in Earth structure outside the formerly-loaded region. The better fit to the GPS-derived surface velocity field by the 1-D radially-varying Earth model is attributed to the fact that the ice model used (Lambeck's FBKS8 model /Lambeck et al. 1998a/) was tuned using a 1-D Earth model.

By comparing model output with observations, Kaufmann's work has yielded constraints upon ice history /Kaufmann 1997/ and radial profiles of mantle viscosity /Kaufmann and Lambeck 2000, 2002, Steffen and Kaufmann 2005/. In the latter case the results are strongly dependent upon the ice history used, and are in the range 2.5–7 × 10²⁰ Pa s and 1–3 × 10²² Pa s for upper and lower mantle viscosity respectively. /Steffen and Kaufmann 2005/ note that the data have poor resolving power when trying to solve for Earth parameters in more than three layers. The data used include relative sea-level histories, palaeoshoreline data, present-day surface rates, long wavelength geoid data, free-air gravity anomalies, and observations of true polar wander. Similar to other authors,/ Kaufmann and Wu 2002/ find that inversion results have some dependence upon the spatial distribution of these data.

Using 3-D GIA models, the data reveal evidence for a low viscosity layer beneath the Barents Sea /Steffen and Kaufmann 2005/, but not Fennoscandia /Kaufmann et al. 1997/. When the data are grouped into regions, different radial viscosity profiles are obtained for different regions, again indicating the importance of accounting for lateral variations in Earth structure when inverting GIA data /Kaufmann and Lambeck 2002, Kaufmann and Wu 2002, Steffen and Kaufmann 2005/. Finally, /Kaufmann and Lambeck 2002/ caution against using GIA models to invert for lateral Earth structure until ice history models can be tightly constrained, due to the stronger dependence of GIA observables upon ice history than Earth structure.

4.4.6   German Research Centre for Geosciences

At the German Research Centre for Geosciences (GFZ) in Potsdam Zdeněk Martinec has pioneered the development of spectral finite difference /Martinec 1999/ and finite element /Martinec 2000/ methods to investigate the viscoelastic response of a spherical Earth with 3-D viscosity structure to surface loading. In the finite difference version /Martinec 1999/ an initial value approach is used to carry out forward modelling. Spherical harmonics are used to parameterize the problem and solve the governing equations for viscoelastic deformation; the momentum equation, Poisson's equation and the constitutive equation. Spectral methods are used to transform these partial differential equations into ordinary differential equations which are solved by numerical integration. The time dependence of the problem is dealt with in the time domain, unlike earlier numerical viscoelastic studies, thus reducing computation time. The complication of including lateral Earth structure places some limitations upon the problems that can be solved.

The spectral finite element method /Martinec 2000/ calculates the deformation of a spherical viscoelastic body with 3-D viscosity variations. The solution domain is divided into a series of finite elements in the radial direction. This leads to the derivation of a series of linear algebraic equations that are solved using the Galerkin method /Brenner and Scott 2005/. This model is more efficient than the finite difference model, and requires less complex boundary conditions. Once again time dependence is dealt with in the time domain. The method is tested using a series of 2-D axisymmetric problems, and the results are compared to semi-analytical solutions.

The original spectral methods of /Martinec 1999, 2000/ do not solve the sea-level equation. This is rectified in /Martinec and Hagedoorn 2005/ and /Hagedoorn et al. 2007/, where the spectral finite element method is developed to include self-gravitation and output vertical displacement and geoid height, thus solving the sea-level equation. A time-varying ocean function is used to ensure the correct redistribution of glacial melt and calculate shoreline migration. Water redistribution in the presence of marine-grounded ice is also considered /Hagedoorn et al. 2007/.

Changes in the direction and magnitude of the Earth's rotation vector due to internal and surface mass redistribution are also introduced in /Martinec and Hagedoorn 2005/. Previous studies required Laplace transform methods to solve for these time-dependent quantities, but the formulation of the spectral finite element method in the time domain means that no transformations are needed, thus decreasing computation time. The solutions are verified by comparison with results obtained using the Laplace transform method. Changes due to rotational perturbations are expressed in terms of changes in the gravitational potential, thus allowing the accurate calculation of meltwater redistribution.

The spectral finite element code has been applied in a number of recent studies. /Martinec et al. 2001/ investigate how inferred 1-D viscosity profiles are affected by the presence of shallow lateral structure. Synthetic relative sea-level data are generated via forward calculations carried out in the presence of simple axisymmetric viscosity variations. These data are then inverted to yield the best-fitting 1-D radial viscosity profile. The resulting profile differs from the average of the input 2-D model, implying that there are likely to be systematic errors in viscosity profiles generated by inverting real uplift data.

In the most recent study by this group, /Hagedoorn et al. 2007/ use the spectral finite element method to solve the sea-level equation, and they compare their output to Holocene relative sea-level data in order to determine the optimum radial viscosity model for each of five regions. The fact that they obtain four different optimum viscosity profiles highlights the presence of lateral structure in the Earth. Using the optimum Earth models they correct tide gauge data for GIA effects in order to estimate the rate of eustatic sea-level change.

Within the GFZ group, Volker Klemann and Detlef Wolf have also been involved in the development of GIA models. Much of their work has focussed upon developing rheological models to investigate the roles of e.g. compressibility /Wolf and Kaufmann 2000, Klemann et al. 2003/ or ductile layers /Klemann and Wolf 1999/ within the deformation process. Wolf has also been involved in studies into the effect of lateral viscosity variations upon GIA predictions /Kaufmann et al. 1997, Kaufmann and Wolf 1999/.

In their early work, Klemann and Wolf sought to understand changes in the stress field in Fennoscandia due to GIA /Klemann and Wolf 1998, 1999/. They found the inclusion of a ductile layer in the lithosphere to be key to understanding long-term variations in the stress field in this layer, which is often assumed to be elastic in GIA calculations /Klemann and Wolf 1999/. Latterly, they have used sea-level indicators and shoreline markers to revise the relaxation time spectrum for Fennoscandia /Klemann and Wolf 2005/. They have developed methods to invert this, and a range of other sea-level indicators, for the viscosity stratification in this region /Klemann and Wolf 2005, 2007/, and determine a best-fitting Earth model with a lithospheric thickness of 80 km, and upper and lower mantle viscosities of 5×10^{20} Pa s and 2.4×10^{21} Pa s, respectively.

4.4.7 Zhong, Paulson and Wahr

The US-based group of Shijie Zhong, Archie Paulson and John Wahr have adapted their spherical finite element model, originally developed to study purely viscous mantle convection problems /Zhong et al. 2000/, to investigate postglacial rebound.

/Zhong et al. 2003/ present the governing equations used to describe the time-dependent viscoelastic deformation of a spherical 3-D Earth. Their model is incompressible, self-gravitating, and capable of including 3-D viscoelastic structure. Model output is tested against semi-analytical solutions to spherically symmetric problems.

In their study of postglacial rebound /Zhong et al. 2003/ use the ICE-3G ice-loading model /Tushingham and Peltier 1991/ but do not solve the full sea-level equation explicitly; relative sea-level change is determined by calculating the difference between solid Earth and geoid rates. The conservation of water is not used as a constraint, and the ocean function is not incorporated until the later study of /Paulson et al. 2005/. The effects of lateral variations in lithospheric thickness, for a range of mantle viscosities, are studied in /Zhong et al. 2003/, while the effects of lateral variations in mantle viscosity are studied in /Paulson et al. 2005/.

Lithospheric thickness variations /Zhong et al. 2003/ are derived using assumptions about the thermal structure of oceanic lithosphere and by scaling the elastic thickness of the continents (as estimated from studying long-term loading /Watts 2001/). /Zhong et al. 2003/ do not invert for 3-D lateral structure, but aim to understand the effect of lithospheric variations upon GIA observables, and hence how we can further our understanding using appropriate 1-D Earth models.

They find that the effect of lithospheric thickness variations upon relative sea-level is dependent upon the size of the load, and the location of the relative sea-level observation. Relative sea-level change is most sensitive to lithospheric thickness variations in the region of small ice sheets and at the margins of ice sheets; here GIA is controlled by local lithospheric structure. This result provides insight into how radially-varying GIA models can be used to infer Earth structure. For example, when trying to fit relative sea-level data from the margins of a former ice sheet it is most computationally-economic to use a 1-D Earth model. The resulting best-fitting model will reflect the lithospheric thickness at the location of the data.

The finite element model is updated in /Paulson et al. 2005/ to account for motion of the Earth's centre of mass and the influence of polar wander (see section 4.5.3). The updated model also solves the sea-level equation in a gravitationally-consistent manner: water mass is conserved, and sea-level responds to evolving topography and geoid heights. An ocean function is used to account for shoreline migration, even in the case of marine-grounded ice retreat. The spectral method of /Mitrovica and Peltier 1992a/ is used to iteratively solve for vertical displacement and the gravitational potential. The ICE-3G loading history is used, and 3-D viscosity structure is included, based on the seismic tomography models S20RTS /Ritsema et al. 1999/ and NA00 /van der Lee 2002/.

Once again, the aim of the study is to understand the sensitivity of GIA observables to viscosity per-turbations. The principle observation is that uplift is sensitive to viscosity structure beneath the site of observation *and* beneath the loaded region. This implies that if a 1-D radial viscosity profile is inferred from uplift data it will reflect structure both beneath the point of observation and beneath the load.

Output from realistic 3-D models and related 1-D Earth models are compared in order to determine to what extent 1-D models can be used to study GIA in the presence of 3-D structure. /Paulson et al. 2005/ find that a 1-D Earth model can be used to study loaded regions, but in non-loaded regions struc-ture from both local and loaded regions must be considered, therefore a 3-D model is required. A 1-D Earth model that is weighted to consider viscosity beneath the ice sheets will give the best fit to global GIA data because viscosity beneath loaded regions affects output everywhere. But a good fit to data will only be achieved in formerly-loaded regions; elsewhere the data reflect laterally-varying structure.

In their most recent study, /Paulson et al. 2007/ investigate the resolving power of GIA data in terms of inverting for radial viscosity structure. They attempt to invert for many layers of viscosity, but find that the data are insensitive to strong viscosity contrasts in neighbouring layers. They conclude that GIA observables can only be used to invert for two viscosity layers; the upper and lower mantle.

4.4.8 Sabadini, Spada et al.

The Italian group of Sabadini, Gasperini, Giunchi, Spada and co-workers pioneered work into the effect of lateral Earth structure upon GIA. In early studies they used finite element packages /Melosh and Raefsky 1983/ to carry out axisymmetric flat Earth, plane strain calculations in the presence of simplified lateral structure and ice-loading /Sabadini et al. 1986, Gasperini and Sabadini 1989, Giunchi et al. 1997, Giunchi and Spada 2000/. A linear Maxwell Earth rheology is adopted and a spectral approach is used to analyse the impact of viscosity variations upon solid Earth displacement and quantify to what extent lateral viscosity contrasts influence inferences of mantle viscosity.

Initial studies showed that sites at the edge of the former ice sheet are most sensitive to lithospheric thickness /Sabadini et al. 1986/, while displacement beneath the centre of the load is controlled by the average viscosity beneath the load /Gasperini and Sabadini 1990/. Lateral variations in lithospheric thickness are found to perturb predictions of horizontal deformation rates, but have little effect upon uplift rates /D'Agostino et al. 1997/. The introduction of lateral viscosity variations is also found to perturb rates of horizontal deformation /Giunchi et al. 1997/.

Radial viscosity variations are also investigated. /Di Donato et al. 2000a/ find that the inclusion of a low viscosity layer within the lithosphere can perturb crustal velocities by ~0.5 mm/yr, and postulate that the presence of such a layer can explain the residual pattern from GIA-corrected tide gauge data along the US East Coast. The effect of introducing power law rheology into the GIA models is also investigated /Giunchi and Spada 2000, Dal Forno et al. 2005/, but the question of whether such a complexity is required to accurately model GIA remains inconclusive.

In their most recent work, /Spada et al. 2006/ use realistic ice histories (ICE-1 and ICE-3G) and Earth structure (from the 3SMAC model of /Nataf and Ricard 1996/) within a spherical, viscoelastic finite element model. The full sea-level equation is not solved; ocean-loading and self-gravitation are neglected. They note that small ice sheets are less sensitive to deeper lateral heterogeneities, and find that sea-level change is more sensitive to load history than lateral Earth structure. They conclude therefore that relative sea-level data cannot be used to constrain 3-D Earth structure until ice models can be more accurately constrained.

4.4.9   Vermeersen

/Vermeersen et al. 1996/ and /Vermeersen and Sabadini 1997/ develop an analytical normal mode method for solving for viscoelastic relaxation due to surface loading on a spherically-symmetric, self-gravitating, incompressible Earth with Maxwell rheology. A continuous elastic and rheological stratification can effectively be modelled due to the many layers permitted in the model.

Using this method /Vermeersen et al. 1997/ investigate the rotational response of the Earth to deglaciation. They place constraints upon upper and lower mantle viscosities by assuming that true polar wander is solely due to GIA.

/Di Donato et al. 2000b/ adapt the method to solve the sea-level equation and predict GIA-induced free-air gravity anomalies. They demonstrate that the magnitude of the predicted signal is large enough to be resolved by the GOCE satellite mission (see http://www.esa.int/esaLP/LPgoce.html). /Vermeersen 2003/ and /van der Wal et al. 2004/ extend this work and investigate the pattern of geoid anomalies predicted by the model in the presence of shallow low viscosity zones (SLVZs). They find that geoid perturbations in the presence of such zones may be significant, especially at the margins of former ice-loading, and hence may be used to identify the location of SLVZs.

Finally, the method has been used to investigate the sensitivity of geoid height to ice-loading history /Schotman and Vermeersen 2005/. This study indicates that it should potentially be possible to distinguish between ice-loading histories using gravity data from GRACE and GOCE, but in practice the method will be complicated by the fact that gravity data are insensitive to the source of mass variations, which may arise due to atmospheric and hydrological processes as well as GIA. In all of these studies, the limitation of the model in not considering lateral heterogeneities is acknowledged.

4.4.10   Fjeldskaar

/Fjeldskaar 1994/ uses a simple half space model consisting of a viscous mantle overlain by an elastic lithosphere and considers the response to loading by a realistic deglaciation model using Fourier transform methods. Output is compared to uplift rates and the tilting of palaeoshorelines, implying that a low viscosity asthenosphere is required to fit the data, and that the asthenosphere cannot be more than 150 km thick. The work is extended /Fjeldskaar 1997/ to include estimates of flexural rigidity and elastic thickness throughout Fennoscandia. It should be noted that these studies use a simplified Earth model and a relatively crude ice model /Denton and Hughes 1981/, and seek to fit data sets with large error bars.

4.4.11   Implications of GIA modelling for ice sheet history, global ice volumes and eustatic sea-level change

The GIA models discussed above have enabled tighter constraints to be placed upon parameters of ice history, including the volume of ice in individual ice sheets, the timing of their deglaciation, and the eustatic sea-level history.

Global ice history models have been developed via GIA modelling by /Tushingham and Peltier 1991/ (ICE-3G) and /Peltier 1994, 2004/ (ICE-4G and ICE-5G). In addition, the individual ice sheets that have been refined by GIA modelling include the Fennoscandian ice sheet /Lambeck et al. 1998a, 2006/, including the British ice sheet /Lambeck 1993b, 1995b, Johnston and Lambeck 2000, Shennan et al. 2002/ and the Barents Sea ice sheet /Lambeck 1995a, 1996b, Kaufmann 1997/, the Laurentide ice sheet /Tarasov and Peltier 2004, 2006/, the Greenland ice sheet /Tarasov and Peltier 2002, Fleming and Lambeck 2004/, and the Antarctic sheet /Ivins and James 2005/. Measurements of GIA observables in Greenland and Antarctic will contain signals relating to both post-LGM and present-day melting; these signals must be separated in order to learn about the LGM ice configuration /Velicogna and Wahr 2002, Ivins and James 2005, Sasgen et al. 2007/.

Estimates for the global ice volume at the LGM range from 43.5×10^6 km³ to 51×10^6 km³ /Milne et al. 2002/, equivalent to a eustatic sea-level change of 115–135 m. /Fleming et al. 1998/ reach an estimate of $46–49 \times 10^6$ km³, representing 125 ± 5 m eustatic sea-level change between the LGM and present, while /Lambeck et al. 2000/ reach an estimate of 52×10^6 km³. /Lambeck et al. 2002b/ conclude that ice volumes were almost constant between 30 ka BP and 19 ka BP, during which time the eustatic sea-level was 120–130 m lower than the present-day. /Peltier 2002b/ also analyses eustatic sea-level history and estimates an ice-equivalent sea-level change of ~120 m since the LGM.

Combining global ice volumes with estimates of mass contained within the individual ice sheets allows tighter constraints to be placed upon the mass of poorly constrained LGM ice sheets, such as Antarctica, which, by this method, is estimated to have contained extra ice equating to 25–30 m equivalent sea-level at the LGM /Lambeck and Chappell 2001/.

GIA models have also been used to reconstruct rates of eustatic sea-level change /Fleming et al. 1998, Lambeck et al. 2002b/, and investigate the source of rapid deglacial events such as meltwater pulse 1A /Peltier 2005/. /Lambeck et al. 2002b/ predict maximum rates of eustatic sea-level change up to 15 mm/yr either side of the Younger Dryas, and that the eustatic sea-level stabilised at present-day levels around 7000 years BP.

4.4.12 Implications of GIA modelling for Earth structure

The principal aim of many GIA model studies is to constrain mantle viscosities. Many studies invert for three Earth layers: the lithosphere, upper mantle, and lower mantle /e.g. Lambeck et al. 1998a, Fleming et al. 2002/. Several attempts have been made to invert for a greater number of mantle layers /e.g. Milne et al. 2004/ but it has been shown that, with the current observational data set, the limit of resolution is approximately the size of the upper mantle /Paulson et al. 2007/.

Values for lithospheric thickness used in global GIA models lie in the range 70–170 km /Milne and Mitrovica 1998a/; however recent studies have demonstrated the importance of using a value of lithospheric thickness that is representative of local values in order to accurately fit the data. Regional thicknesses obtained via GIA modelling include 120 km for central Fennoscandia, 60 km for the British Isles, and 70 km for the Barents Sea /Steffen and Kaufmann 2005/.

Similarly, values for upper and lower mantle viscosities cover a range of values. Best-fitting upper mantle viscosities are typically found to lie in the range 10^{20}–10^{21} Pa s, and lower mantle viscosities in the range 5×10^{21}–10^{23} Pa s /e.g. Kaufmann et al. 2000, Kaufmann and Lambeck 2002, Mitrovica and Forte 2002, Milne et al. 2004/. These values have been further refined to fit regional data sets, although some dependence upon the data used has been found. For example, /Steffen and Kaufmann 2005/ found that an upper mantle viscosity of 4×10^{21} Pa s best fits the Fennoscandian relative sea-level data, whereas a value of 7×10^{21} Pa s best fits the BIFROST GPS data. At present it is not feasible to invert for lateral structure using GIA models.

This is a very brief summary of the results obtained by inverting GIA observables in order to further constrain Earth structure. Other attempts to solve the inverse problem are numerous, and further details may be found in the literature review in sections 4.4.1–4.4.10.

4.5 Modelling advanced GIA processes

The modelling of second-order GIA processes, including shoreline migration, the presence of marine-grounded ice, and rotational effects are briefly discussed below. The affect of lateral Earth structure upon GIA is discussed in greater detail. For further details relating to the modelling of the other processes see section 3.5.

4.5.1 Shoreline migration

Shoreline migration is accommodated in GIA models via the use of a time-dependent ocean function /e.g. Lambeck and Nakada 1990, Johnston 1993, Peltier 1994, Milne 1998, Milne et al. 1999, Lambeck et al. 2000, Lambeck et al. 2003, Mitrovica 2003, Mitrovica and Milne 2003, Kendall et al. 2005/. In models that does not account for shoreline migration, the ocean function may still be used to discriminate between regions which receive meltwater and are subject to ocean-loading, and those which are not. But in this case the ocean function is only dependent upon position; shorelines are fixed in time. Models which do include a time-varying ocean function calculate the position of the zero topography contour for each time step, and hence uniquely define the value of the ocean function for each position at time step. See sections 3.5.1 and 4.3.5 for details of how the time-varying ocean function is implemented within the sea-level equation.

If a time-dependent ocean function is used, or the outputs of the sea-level equation are used to predict palaeotopography or shoreline migration, the calculations must be combined with a topographical data set. The most accurate, freely-available, global topography data set is currently ETOPO2v2 (National Geophysical Data Center, www.ngdc.noaa.gov), but higher resolution data sets are likely to be available on a regional basis.

4.5.2   Floating and marine-grounded ice

The contribution of floating and marine-grounded ice to ocean and surface loading was first considered by /Milne 1998/ and /Lambeck et al. 1998a/, and in some regions it has been shown to have a greater impact upon relative sea-level than shoreline migration /Kendall et al. 2005/. Milne uses a revised ocean function to ensure the correct geometry of ice- and ocean-loading, and meltwater redistribution. The function takes the value one where the geoid lies above the solid surface *and* there is no ice present, and it takes the value zero elsewhere /Milne et al. 1999, Mitrovica and Milne 2003, Kendall et al. 2005/. An alternative method for dealing with retreating marine-based ice is used by /Peltier 1998ab/ in his 'implicit ice' method, where the volume of water that fills each 'hole' left by melting marine-grounded ice is computed *a posteriori*.

Lambeck and co-workers employ a similar method /Lambeck et al. 2000/ and extend the method to account for floating ice /Lambeck et al. 2003/: At each time step ice thickness is compared to water depth and Archimedes' principle is used to determine whether the ice is floating (in which case it forms part of the ocean load) or not (in which case it forms part of the surface load).

Finally, /Paulson et al. 2005/ also account for changes in the geometry of marine-grounded ice when defining the ocean function: The ocean function is allowed to vary smoothly from 0 to 1 between time steps in locations where the retreat of ice is replaced by the inundation of ocean water during that time step. See section 3.5.2 for further details of how floating and marine-grounded ice are implemented within the sea-level equation.

4.5.3   Rotational effects

The theory of GIA-induced rotational perturbations was developed by /Wu and Peltier 1984/, but the effect of polar wander upon sea-level was hypothesized as early as the 1950's /Gold 1955/. Several other early studies also investigated the effect of time-varying ice-loading upon the rotational state of the Earth /Nakiboglu and Lambeck 1980, Sabadini and Peltier 1981, Ricard et al. 1993, Mitrovica and Peltier 1993b, Peltier and Jiang 1996a, Vermeersen et al. 1997/ but did not initially exploit the link between rotational perturbations and relative sea-level height.

/Wu and Peltier 1984/ demonstrate that a change in surface loading can cause a change in the rate of rotation of the Earth and a drift in the orientation of the pole of rotation (known as 'polar wander') by up to a degree. The change in the rotational state alters the centrifugal force, which causes the equatorial bulge of the Earth to be displaced. This results in deformation of the solid surface and geoid, and hence perturbs sea-level /Peltier 1988/. The polar motion will continue until the Earth's rotation axis coincides with the axis of maximum moment of inertia. A change in the Earth's rotation axis will also alter the angle of insolation, thus affecting the ice mass balance /Vermeersen and Sabadini 1999/.

Early studies investigated this rotation-induced sea-level change using simplified ice-loading models and a eustatic ocean load /Han and Wahr 1989, Sabadini et al. 1990/ or a rigid Earth model /Bills and James 1996/. /Milne and Mitrovica 1996/ were the first to couple the theory with a realistic ice-loading model and a gravitationally self-consistent ocean load (i.e. solve the full sea-level equation). /Vermeersen et al. 1997/ adopt a similar model within an analytic method which is based on normal mode theory, as do /Johnston and Lambeck 1999/, who investigate the sensitivity of the rotational parameters to the ice and Earth models, and use observations of polar wander to infer the source of present-day melting. Several authors do however make the important observation that GIA may not be the sole source of polar wander /e.g. Vermeersen and Sabadini 1999, Johnston and Lambeck 1999, Sabadini and Vermeersen 2002, Sabadini et al. 2002/. Additional forcing may arise from the subduction of oceanic lithosphere /Ricard et al. 1992/, mountain building /Vermeersen et al. 1994/, mantle convection /Steinberger and O'Connell 1997/, and present-day ice mass changes /Gasperini et al. 1986/.

When including rotational feedback into GIA theory, additional 'tidal' Love numbers are included in the forcing equations (see equations 3-48 and 3-49) to determine the response to a varying rotational potential as well as surface loading /Milne and Mitrovica 1998a, Peltier 1998a, 1999, Mitrovica et al. 2001a/. The theory is updated in /Mitrovica et al. 2005/ to account for errors introduced following the use of an approximate value for the fluid Love number /Munk and MacDonald 1960/. /Paulson et al. 2005/ also follow this theory when solving the sea-level equation using spectral methods, but use a slightly simpler method of updating the centrifugal potential at each time step within their finite element method.

Rotational feedback only affects the harmonic degree two, order one component in the spherical expansion of sea-level variations, thus a rise/fall in sea-level occurs in opposite quadrants of the Earth, with the quadrants defined by two axes, perpendicular and parallel to the rotation axis (see Figure 4-4). This pattern of sea-level change leaves a unique signature in the sedimentary record, and peaks at ~5 m /Vermeersen and Sabadini 1999/, and hence must be included in GIA analysis.

4.5.4   3-D Earth structure

In many cases uplift data cannot be explained using radially-symmetric Earth models /e.g. Kaufmann and Wolf 1996/, therefore models that incorporate 3-D Earth structure have become a recent focus of research. State-of-the-art GIA models that account for 3-D Earth structure use a range of geophysical observables to infer lateral variations in lithospheric thickness and mantle viscosity. Recall that the lithosphere may be defined in terms of its seismic, thermal, mechanical, or effective elastic thickness (see section 2.2.2). A few of these methods are discussed below.

Rayleigh wave dispersion data have been used to indicate variations in the thickness of the seismic lithosphere in Fennoscandia /Calcagnile 1982/, while coherence studies have been used in the same region to study gradients of flexural rigidity and elastic thickness /Poudjom Djomani et al. 1999, Watts 2001, Pérez-Gussinyé et al. 2004/. Globally, the study of long-term geological loading by sediment, seamounts, mountain chains etc has been used to determine the elastic thickness of the lithosphere /Watts and Zhong 2000, Watts 2001/, which is generally taken to be ~2/3 the thickness of the mechanical lithosphere. Elastic thicknesses range from ~150 km in cratonic regions to ~10 km in young, tectonically active regions (see Figure 4-5). Lithospheric structure has also been inferred from shear wave tomography /e.g. Wu et al. 2005/ and by tracing the 750°C geotherm in oceanic lithosphere /Zhong et al. 2003/, while plate boundaries have been modelled as linear low viscosity zones /Latychev et al. 2005b/. Fennoscandian lithospheric thickness variations, derived from elastic thickness estimates, are shown in Figure 4-5.
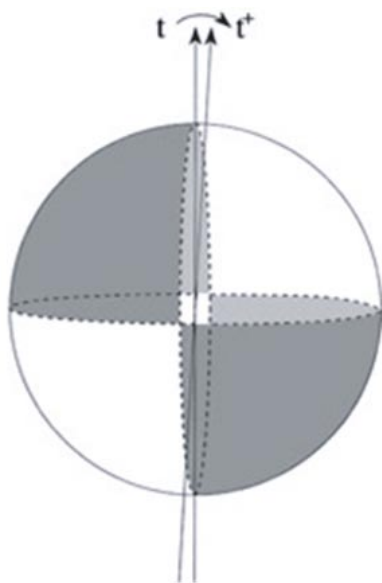

Figure 4-4. *The spatial distribution of sea-level change due to a change in the orientation of the Earth's rotation vector from time t to t+. The perturbation to sea-level has the same sign in the shaded regions. Adapted from /Mitrovica et al. 2001a/.*
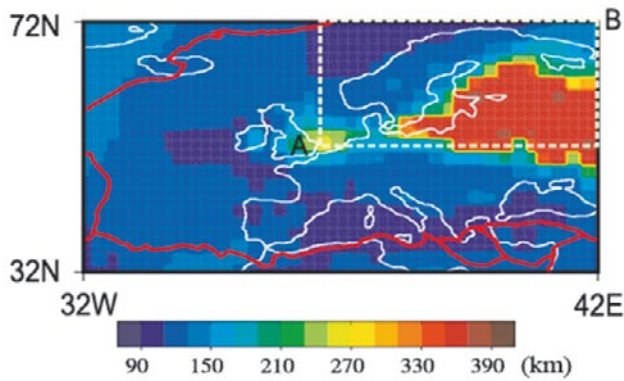
Figure 4-5. Lithospheric thickness derived from the elastic thickness model of /Watts 2001/ and /Pérez-Gussinyé et al. 2004/. This is part of a global model where the thicknesses have been scaled to ensure a global mean lithospheric thickness of 120 km. The red lines define plate boundaries. The dashed area is used to define a Fennoscandian regional mode (see text). The letters A and B define the location of the profile shown in Figure 4-6. Adapted from /Whitehouse et al. 2006/.

Global body-wave tomography probes deeper, and lateral velocity variations of several orders of magnitude have been observed in the upper and lower mantle /Ritsema et al. 2004/. Seismic velocity anomalies have been correlated with lateral viscosity variations within the mantle via a three-step procedure: Firstly, a velocity-to-density scaling is applied /e.g. Forte and Woodward 1997/; secondly, these density perturbations are converted into temperature variations; finally, an exponential relationship is used to map temperature variations onto viscosity variations /Latychev et al. 2005a/. This method assumes that all velocity anomalies are due to viscosity variations, however, velocity perturbations may also be due to lateral variations in chemical composition and non-isotropic pre-stress (which results in the mantle exhibiting 'fast' and 'slow' directions for seismic waves). Hence, laterally-varying viscosity models derived using this method represent the possible extremes of the Earth's lateral viscosity structure (see Figure 4-6).
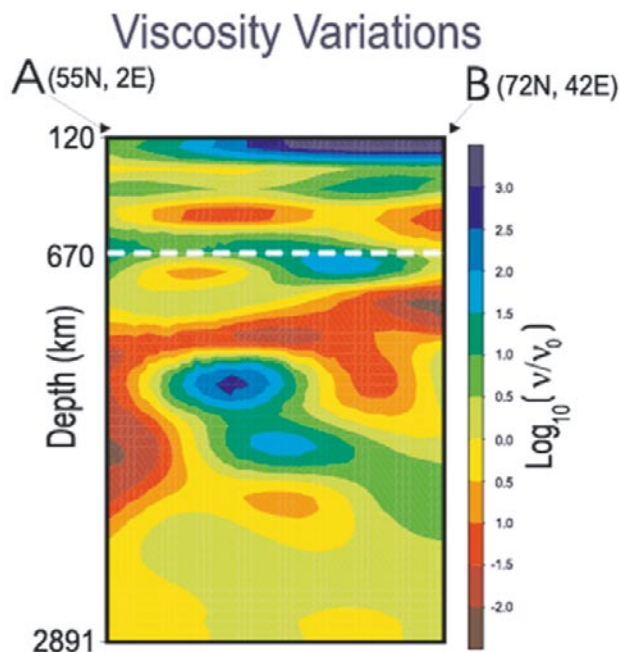
Figure 4-6. Profile of mantle viscosity perturbations from the base of the lithosphere (assumed to be 120 km) to the core-mantle boundary along profile AB (see Figure 4-5). The viscosity perturbations are derived from the global seismic shear wave velocity model of /Ritsema et al. 2004/ using the method described in the text. The white dashed line marks the transition from the upper mantle to the lower mantle. Adapted from /Whitehouse et al. 2006/.

Early GIA studies consisted of a series of sensitivity tests that incorporated 3-D Earth structure within a flat Earth or axisymmetric formulation, upon which plane strain calculations were carried out. Only simple, axisymmetric geometries of lateral structure and ice-loading were used /e.g. Sabadini et al. 1986, Gasperini and Sabadini 1989, Wu 1992a, 1993, Kaufmann et al. 1997, Giunchi et al. 1997, Kaufmann and Wu 1998, Wu et al. 1998, Giunchi and Spada 2000/. These early models often made use of finite element packages, and hence did not explicitly solve the sea-level equation since many did not account for the self-gravitation of the oceans when considering the redistribution of meltwater.

The principle finding of these early studies was that lateral variations in mantle viscosity, on the order of 1 to 2 orders of magnitude, have a non-negligible effect upon rebound rates in the region of the former ice load /Gasperini and Sabadini 1989, Kaufmann et al. 1997, Kaufmann and Wu 1998, Wu et al. 1998, Kaufmann et al. 2000/.

The realisation that 3-D structure can have a significant impact upon GIA processes led to the development of increasingly complex spherical models. The solution to the sea-level equation is often expanded as a sum of spherical harmonics. In the 1-D case, the coefficients of the spherical harmonics are determined by solving a series of decoupled ordinary differential equations /e.g. Wu and Peltier 1982, Mitrovica and Peltier 1991a/. However, in the presence of lateral structure extra harmonics appear in the solution, and the ordinary differential equations are coupled. Simple analytical methods are therefore redundant, and more advanced methods have been developed to solve the sea-level equation in the presence of 3-D structure. Spectral methods /e.g. Martinec 1999, 2000/, finite element/volume methods /e.g. Wu et al. 2005, Latychev et al. 2005a/, and perturbation methods /e.g. Tromp and Mitrovica 2000/ have been used to tackle the problem. Where possible, the results from the different models have been benchmarked against each other /Paulson et al. 2005, Latychev et al. 2005a/. Realistic lateral Earth structure and ice-loading histories are included in the most recent models /Martinec et al. 2001, Zhong et al. 2003, Wu 2004, Latychev et al. 2005b/, and the redistribution of ocean- and meltwater is calculated in a gravitationally self-consistent manner /e.g. Wu and van der Wal 2003, Wu et al. 2005, Paulson et al. 2005/.

In an early 'real world' study, /Kaufmann et al. 2000/ tentatively quantified the magnitude of perturbations to GIA observables due to the inclusion of realistic 3-D Earth structure to be 10–20 m for relative sea-level, 1–3 mm/yr for uplift rates, and 2–4 mGal for free-air gravity anomaly predictions. However, when trying to invert synthetic GIA data (generated using a 3-D Earth model) for the best-fitting 1-D viscosity profile, /Kaufmann and Wu 2002/ found that solutions are dependent upon the spatial distribution of the data set; a point later confirmed by several other authors.

Case study: The effect of lateral Earth structure upon GIA in Fennoscandia

A first order observation from GIA studies that include 3-D Earth structure is that lateral variations in mantle viscosity affect the magnitude, but not the pattern, of GIA-related *uplift* rates, however they affect both the magnitude and direction of *tangential* velocity rates /Kaufmann and Wu 1998, Kaufmann et al. 2000, Kaufmann and Wu 2002, Latychev et al. 2005b, Whitehouse et al. 2006/. A case study into the effect of including realistic Earth structure in Fennoscandian GIA models is presented below.

The sea-level theory presented in /Mitrovica and Milne 2003/ is implemented using the 3-D finite volume model of /Latychev et al. 2005a/ to solve the sea-level equation on a spherical, rotating Earth. Even though this study focuses upon Fennoscandia, global calculations are carried out to ensure the correct redistribution of meltwater throughout the oceans.

The ICE-3G global ice model of /Tushingham and Peltier 1991/ is substituted with the ice model of /Lambeck et al. 1998a/ in Fennoscandia (see Figure 4-7) to give a global ice-loading history for the whole of the last glacial cycle that is tuned to fit global ice volumes as determined using far-field sea-level data /Bassett et al. 2005/.

Calculations are initially carried out using a 1-D Earth model with a lithospheric thickness of 120 km, an upper mantle viscosity of 5×10^{20} Pa s, and a lower mantle viscosity of 5×10^{21} Pa s. The calculations are then repeated using an Earth model which includes lateral variations in lithospheric thickness and mantle viscosity, and attempts to account for the presence of plate boundaries. The 3-D Earth model was derived using estimates of elastic thickness as a proxy for lithospheric thickness, and seismic velocity anomalies as a proxy for mantle viscosity, as described above. Plate boundary zones are defined to be 200 km-wide bands of low (2×10^{20} Pa s) viscosity within the lithosphere. Portions of this model are shown in Figures 4-5 And 4-6.
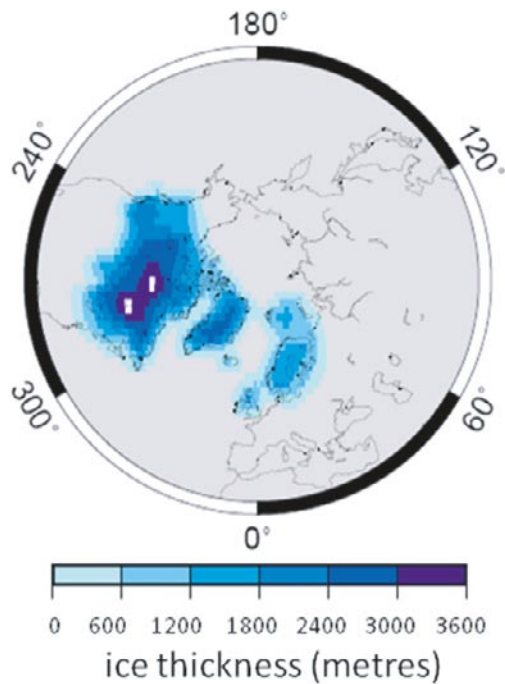
Figure 4-7. *Ice thicknesses in the northern hemisphere at the LGM (20 ka BP). From the model of /Lambeck et al. 1998a/.*

A scaling method is used to ensure that the 1-D and 3-D Earth models have the same depth-averaged mean structure; thus permitting a meaningful comparison of the results. For the lithosphere, this means that the elastic thicknesses of the 3-D model were multiplied by a uniform constant to ensure that the global mean lithospheric thickness is still 120 km. This results in the use of lithospheric thicknesses > 300 km for the Fennoscandian shield: these values are larger than independent estimates /e.g. Calcagnile 1982/, but it should be noted that this study was carried out to explore the sensitivity of GIA calculations to variations in lateral Earth structure, and does not seek to accurately replicate global 3-D Earth structure. For the mantle, the logarithm of the lateral viscosity perturbations at each depth (the calculations are carried out upon a finite volume grid) are multiplied by a uniform constant to ensure the mean (of the logarithm of the viscosity) for that depth is the same as in the 1-D model. For further details of the construction of the Earth model see /Whitehouse et al. 2006/.

Figure 4-8 shows the predicted present-day uplift and horizontal deformation rates for Fennoscandia generated using the 1-D Earth model. Uplift is centred upon the region of maximum ice-loading, and horizontal deformation exhibits a radial pattern of motion away from the centre of uplift.
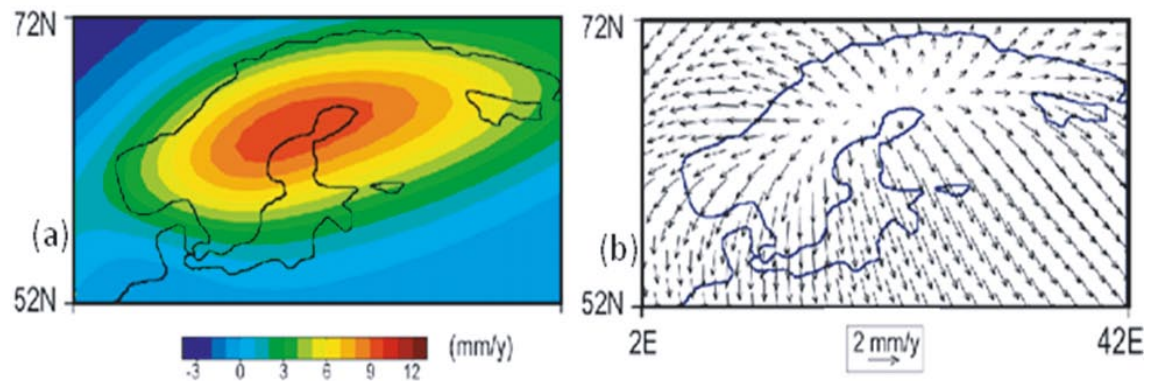

Figure 4-8. *Predicted present-day uplift rates (a) and tangential rates (b) generated using the best-fitting 1-D Earth model for Fennoscandia and the ice model discussed in the text. Tangential rates are given relative to a point on the north coast of the Gulf of Bothnia.*

67

Figure 4-9 shows the misfit in present-day vertical and horizontal deformation rates between the 1-D and 3-D models. Note that the maximum differences of ~3 mm/yr for uplift rates and ~1 mm/yr for horizontal rates are greater than the current limit of observational uncertainty (e.g. GPS), implying that any inferences of Earth structure obtained from the inversion of geodetic data will be biased if a 1-D profile is assumed.

In Figure 4-9 1-D model predictions are subtracted from 3-D model predictions, therefore the blue region surrounded by the orange band in Figure 4-9a indicates that the 1-D model predicts higher maximum uplift rates and lower minimum subsidence rates (more negative) than the 3-D model. The differences are predominantly related to the magnitude of the predictions, and not the pattern, indicating that the introduction of lateral Earth structure has little effect upon the geometry of predicted uplift rates. However, in Figure 4-9b the change in the direction of the arrows indicates that both the magnitude and the pattern of horizontal deformation are perturbed with the introduction of realistic lateral Earth structure.

The question of whether we will be able to constrain 3-D Earth structure via GIA modelling remains open. The large number of degrees of freedom means that it is unlikely to be possible to carry out a unique inversion of 3-D viscosity structure using GIA observables. /Wu et al. 2005/ claim that 3-D Earth structure can be resolved using relative sea-level data from the centre of present-day rebound. However, this is disputed in other studies /e.g. Spada et al. 2006, Whitehouse et al. 2006/, due to the similarity of the effect of lateral structure at different depths upon GIA observables. We investigate this aspect of GIA modelling below.

Figure 4-10 again shows the difference (3-D minus 1-D) between predicted vertical (left) and horizontal (right) deformation rates. A different aspect of the 3-D model is varied in each row. In the first row (Figure 4-10a) lithospheric thickness variations are permitted in the 3-D calculations, but upper and lower mantle viscosities are held at the uniform values of the 1-D model. In the second row (Figure 4-10b) a band of low viscosity is defined within the lithosphere along plate boundaries to replicate the weak stress-coupling across these regions. Other parameters are fixed at the 1-D values. In the third row (Figure 4-10c) upper mantle viscosities are allowed to vary laterally while the lower mantle viscosity and lithospheric thickness are held fixed, while in the fourth row (Figure 4-10d) lower mantle viscosities are allowed to vary while the upper mantle viscosity and lithospheric thickness are fixed. In the first, third and fourth cases weak plate boundary zones are never included.
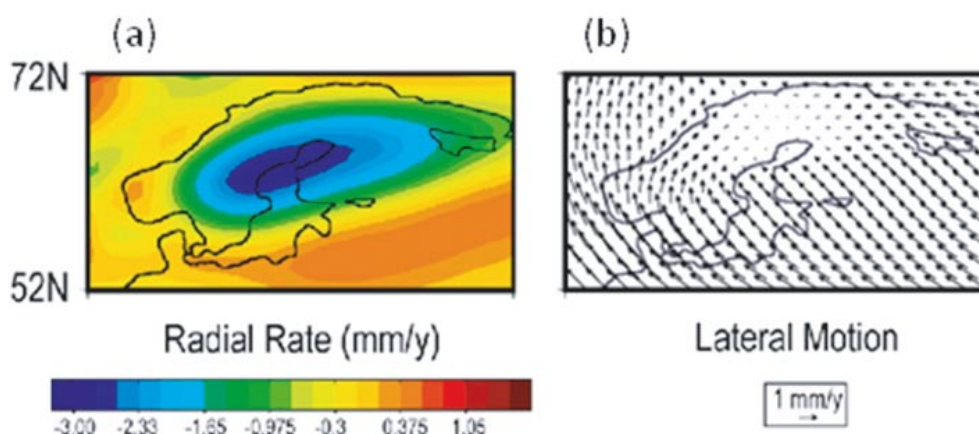

Figure 4-9. *Misfit between (a) uplift rates and (b) tangential rates generated using a 3-D Earth model and a 1-D Earth model. 1-D rates are subtracted from 3-D rates.*
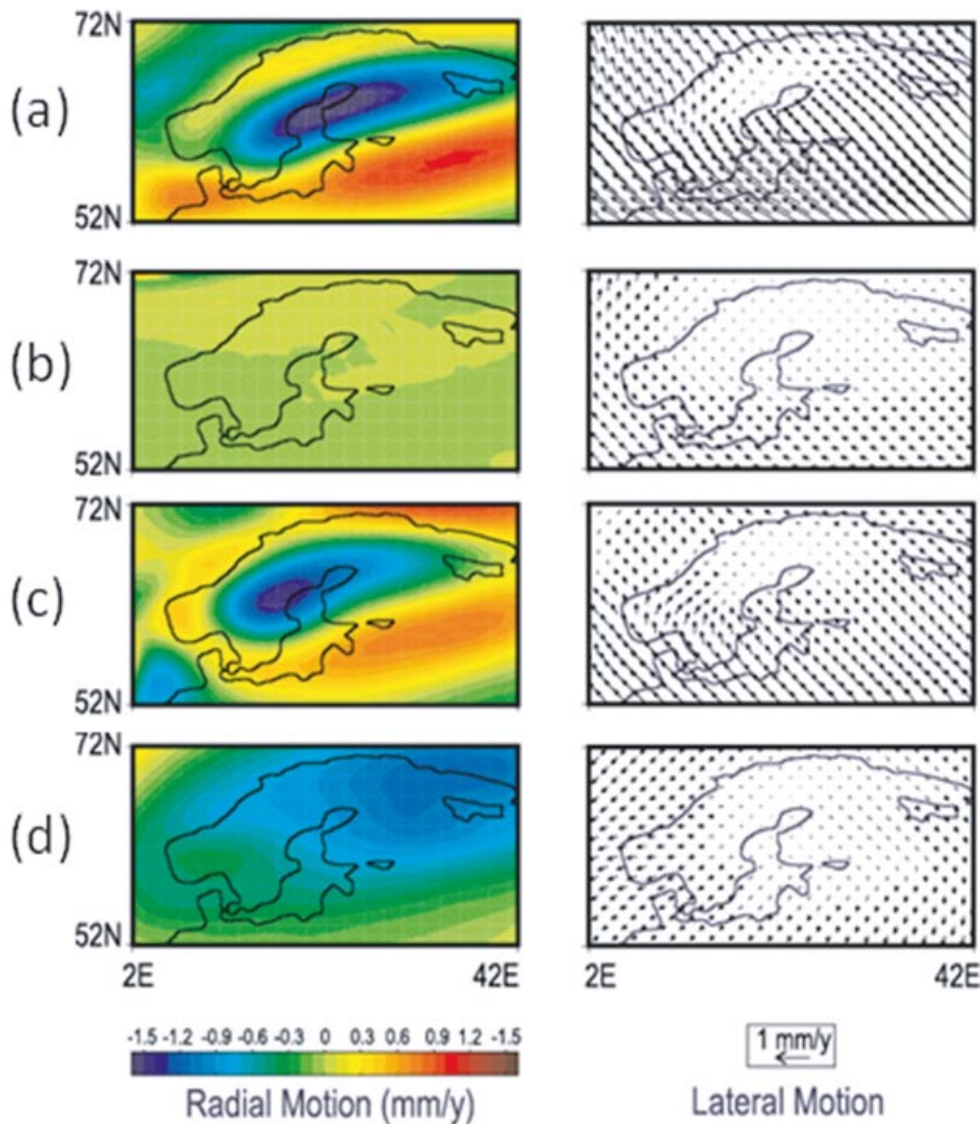
Figure 4-10. *(a) Misfit due to lateral variations in lithospheric thickness. (b) Misfit due to the inclusion of weak plate boundary zones. (c) Misfit due to lateral variations in upper mantle viscosity. (d) Misfit due to lateral variations in lower mantle viscosity. Left column: difference in uplift rates. Right column: difference in horizontal rates. All plots show 3-D predictions minus 1-D predictions.*

The similarity of Figures 4-10a and 4-10c, both in the magnitude of uplift differences and the direction of the horizontal misfit arrows, indicates that lateral Earth structure at different depths can produce similar velocity perturbations in Fennoscandia. Therefore it is unlikely that observations of present-day deformation rates will be able to uniquely infer the underlying Earth structure, or indeed identify the depth of any lateral heterogeneity.

The pattern in Figure 4-10d does not replicate the distribution of LGM ice-loading as in the previous cases, indicating a lesser dependence upon local ice-loading at lower mantle depths. Due to the transmission of stress, the lower mantle in Fennoscandia will play a part in supporting ice-loading in North America as well as Fennoscandia, and the pattern of horizontal perturbations – directed towards North America – reflects this.

The introduction of weak plate boundary zones induces a significant perturbation in horizontal deformation rates, but not vertical rates (Figure 4-10b). The reason for this is that the band of low viscosity decouples the transfer of stress across the plate boundary; the direction of the misfit arrows again reflects the non-negligible effect of North American ice-sheet loading upon surface deformation in Europe. Uplift rates have a strong local dependence upon loading; hence there is no perturbation to these rates when plate boundaries are introduced.

69

The effect of introducing lateral Earth structure at different depths has an approximately linear cumulative effect upon present-day deformation rates. This may be deduced by observing that within the region of uplift the sum of the perturbations in Figure 4-10 approximately equals the cumulative effect (Figure 4-9a).

Predictions of relative sea-level history for the last 10 ka are also compared for the 1-D and 3-D models. This interglacial period, the Holocene, contains the best coverage of relative sea-level estimates for Fennoscandia. Figure 4-11a shows the perturbation to relative sea-level predictions at 10 ka BP due to the inclusion of lateral Earth structure (3-D prediction minus 1-D prediction). There is again a strong correlation between the pattern of ice-loading and the region of maximum perturbations, and there is also a large positive misfit to the east of Fennoscandia in the region of maximum lithospheric thickness (see Figure 4-5). Once again the magnitude of perturbations due to the introduction of lateral Earth structure is greater than the observational uncertainty of relative sea-level data, which can be up to 10 m. Therefore inverting relative sea-level data to yield inferences of Earth parameters or ice-loading history will lead to biased results if lateral structure is neglected.

Along the Norwegian west coast there is very little difference in predictions of relative sea-level by the two models at 10 ka BP. In the top left plot of Figure 4-12 the relative sea-level history for a coastal site with good relative sea-level data (Bjugn: shown by the left-hand star in the bottom plot of Figure 4-12) is plotted for the whole of the Holocene. The black curve is the prediction from the 1-D model and the red curve is the prediction from the 3-D model. The similarity of the curves is characteristic for sites along the length of this coastline, indicating that introducing lateral Earth structure into the GIA model makes little difference to Holocene relative sea-level predictions for this region. Relative sea-level data from the Norwegian west coast may therefore form a data set which is insensitive to the 3-D Earth structure of this region, and hence may be used to tune GIA model inputs such as 1-D Earth structure and ice history. In this case, the poor fit to the data may be rectified by altering either the ice history or the depth-averaged viscosity profile of the Earth model.

The geographical region over which such data would be able to constrain input parameters is limited; it would be useful to also use relative sea-level data from within the Gulf of Bothnia to tune the GIA model. The predicted relative sea-level history for Ångermanälven is shown in the top right plot of Figure 4-12. Ångermanälven is the site of an extensive Holocene relative sea-level data set. It is situated on the east coast of Sweden (right-hand star in the bottom plot of Figure 4-12), in the centre of the region of maximum misfit for both uplift rates and 10 ka BP relative sea-level. The large difference between the two curves during the last 10 ka indicates that using such data to tune GIA model inputs will lead to biased inferences of Earth structure and ice history.
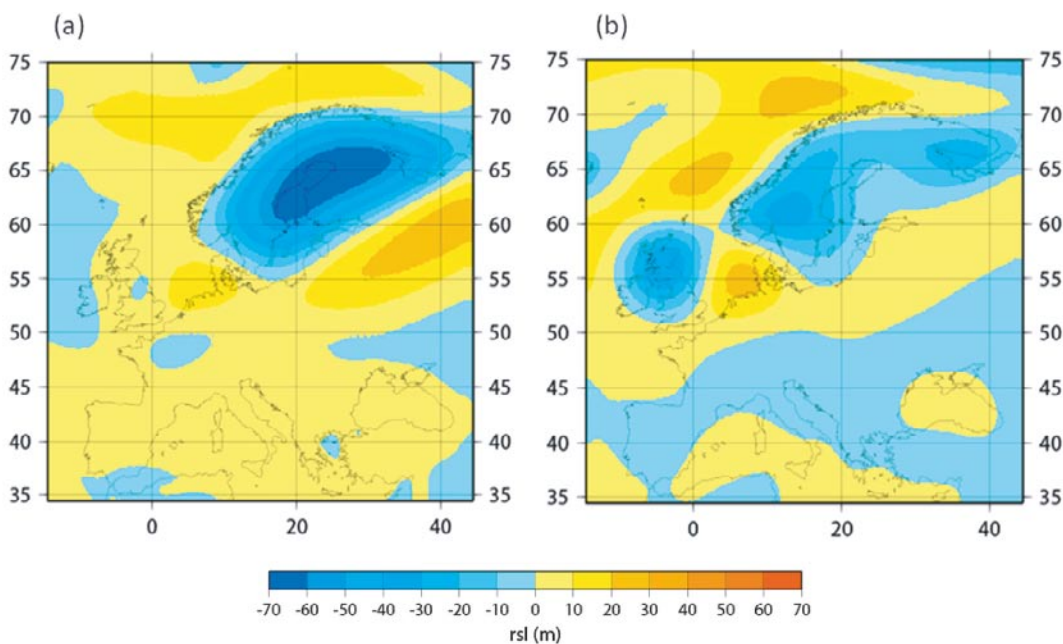

Figure 4-11. *Difference in relative sea-level predictions at 10 ka BP. (a) 3-D model minus 1-D model. (b) 3-D model minus 'regional' 1-D model (see text).*
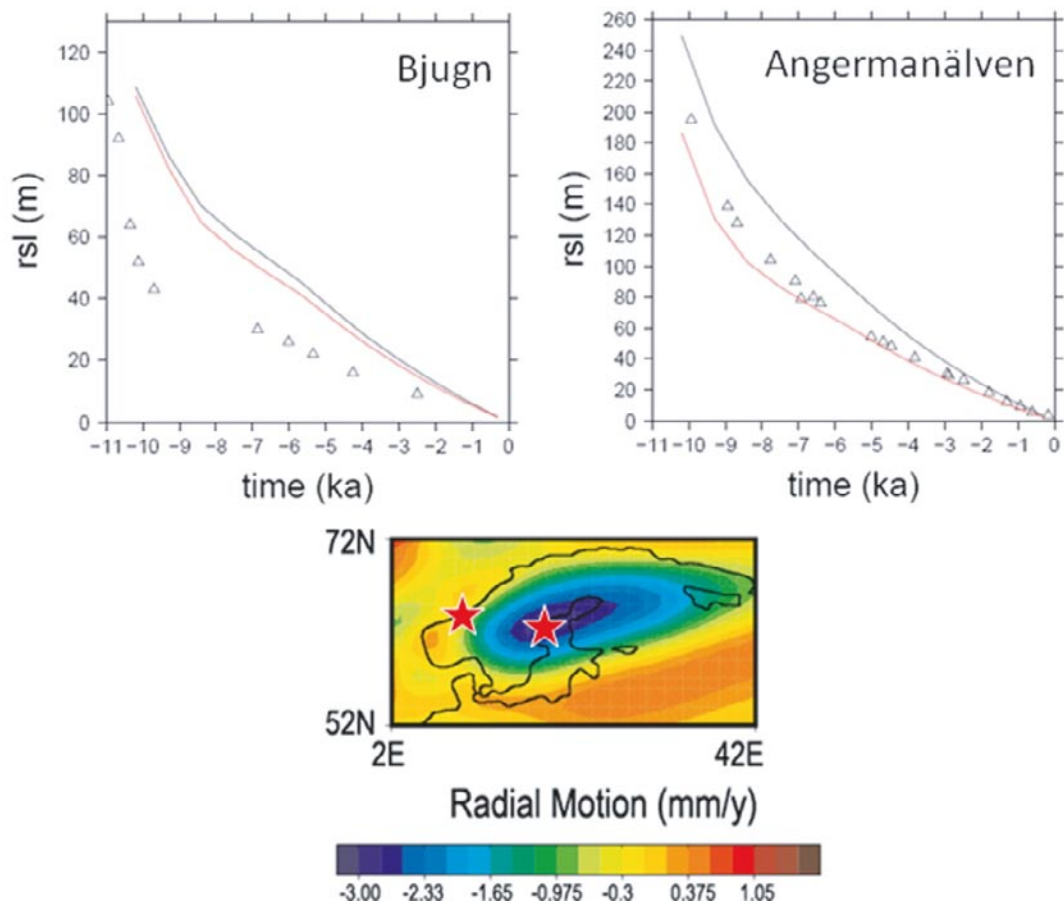
Figure 4-12. *Top left: Predicted relative sea-level history at Bjugn for the last 10 ka. Black line: 1-D model. Red line: 3-D model. Top right: Predicted relative sea-level history at Ångermanälven for the last 10 ka. Line colours are as for Bjugn. Relative sea-level data are shown as triangles; see /Lambeck et al. 1998a/ for references. Bottom plot: Location map for Bjugn (west coast of Norway) and Ångermanälven (east coast of Sweden) overlaid upon the misfit in uplift rates (as for Figure 4-9a).*

The difference in relative sea-level predictions for the 1-D and 3-D models is also plotted for Oskarshamn and Forsmark in Figure 4-13. The magnitude of the error introduced by using a 1-D Earth model instead of a 3-D Earth model to predict relative sea-level at 10 ka BP is ~60 m at Forsmark and ~30 m at Oskarshamn.

Relative sea-level data for Bjugn and Ångermanälven are also plotted in Figure 4-12. This study aims to investigate the sensitivity of GIA predictions to lateral Earth structure, and does not aim to determine the ice history/Earth model combination that best fits the data. And while it is interesting to note the good fit to the data at Ångermanälven when the 3-D Earth model is used, this solution is non-unique, and such a fit may also be acheived using a different combination of (1-D) Earth and ice models. Only one model geometry has been investigated here, and the relative dependence of uplift rate and relative sea-level residuals upon the geometry of lateral Earth structure and the pattern and timing of ice-loading is still poorly understood. Further work is required to determine the sensitivity of the various data to different components of the GIA system before we can be sure our inferences of lithosphere thickness, mantle viscosity, and ice-loading history are as accurate as possible. /Paulson et al. 2005/ suggest that GIA observables are dependent upon Earth structure beneath the site of observation and beneath the formerly loaded region, therefore care must be taken when interpreting data from ice-marginal sites, such as along the Norwegian west coast.
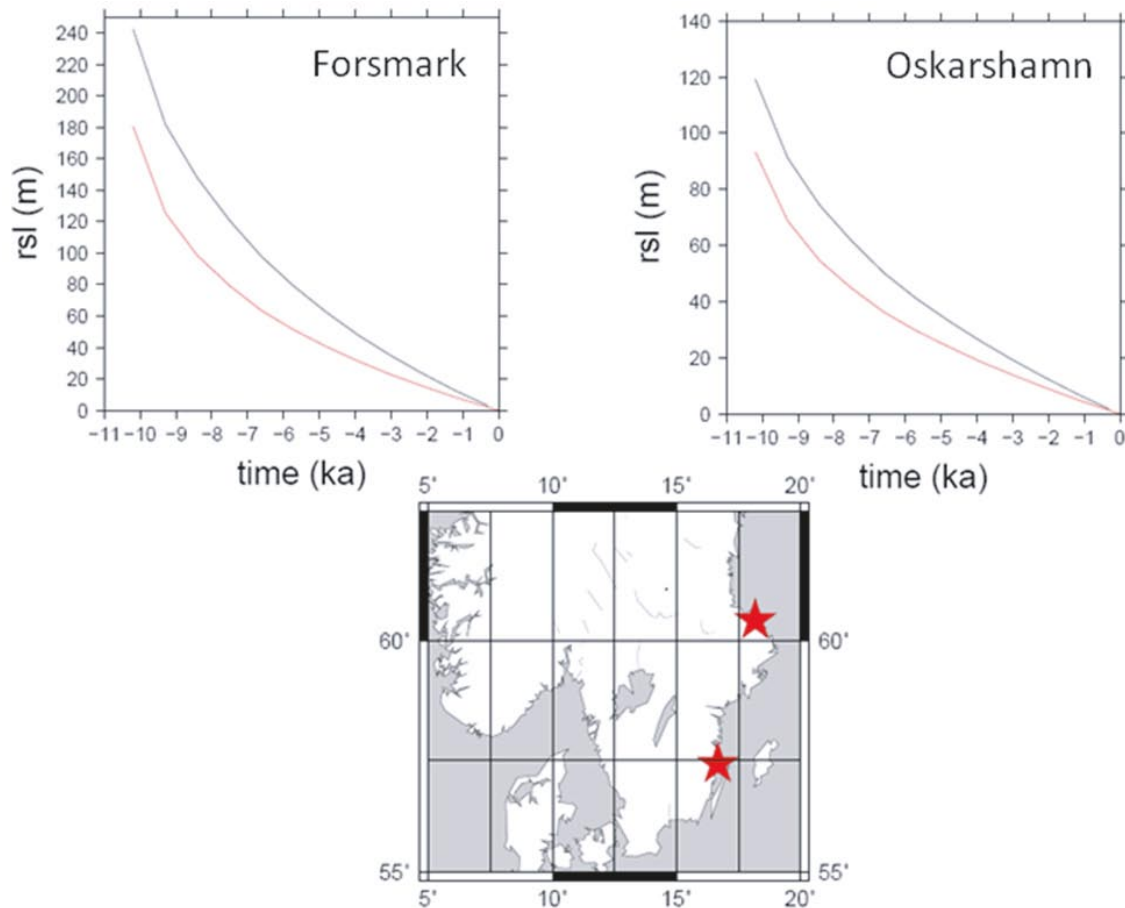
Figure 4-13. *Predicted relative sea-level curves for Forsmark (northern red star) and Oskarshamn (southern red star) calculated using 1-D (black line) and 3-D (red line) Earth models.*

The misfit plots presented here imply that ignoring lateral Earth structure and using a 1-D Earth model in GIA calculations leads to an over prediction of present-day uplift rates and the total amount of relative sea-level change during deglaciation. One simplistic interpretation of these observations is that using a 1-D model will lead to inferred LGM ice thicknesses that are too small. A second interpretation is that the use of a 1-D model will lead to overestimates of mantle viscosity or lithospheric thickness in an attempt to fit the observational GPS and relative sea-level data. In conclusion, it is likely that current estimates of mantle viscosity and ice-loading history will be biased if they were deduced using 1-D Earth structure within a GIA model.

It is computationally demanding to solve the sea-level equation using a full 3-D model; therefore there is ongoing work to determine to what extent we can continue to improve our understanding of GIA using flat Earth models or a suite of spherically-symmetric 1-D models. /Paulson et al. 2005/ suggest that GIA observables within formerly-loaded regions are only sensitive to the local viscosity structure, and a global model which adopts the relevant local viscosity structure should be sufficient to model GIA in that region. The situation becomes more complex away from the centre of the former ice sheets because GIA in these regions seems to be dependent upon both the local viscosity structure and that beneath the ice sheets, which may be different, thus a model that allows for lateral variations in viscosity is required.

The applicability of a 'local' 1-D Earth model to modelling 3-D structure is also investigated. A third set of calculations were carried out using a global 1-D model that adopts the mean structure of the 3-D model beneath Fennoscandia (white box, Figure 4-5). This model, referred to as the 'local 1-D model', has a lithospheric thickness of 195 km, while the mean viscosity at each depth of the 3-D model is used to construct the 'local' 1-D viscosity profile.

The difference in the magnitude of the misfits in Figures 4-14a and 4-14b indicates that using a 1-D Earth model that represents the local 3-D structure as closely as possible will minimise the potential bias introduced into any inferences made using a 1-D model, especially within the region of former loading. A comparison of Figures 4-11a and 4-11b shows that relative sea-level misfits are also reduced when a 'local' 1-D Earth model is used.

Future GIA modelling should concentrate on tuning the (1-D) Earth structure and ice history to fit the observational data on a *regional* basis, making sure to solve the global sea-level equation. In addition, external information relating to total ice volumes and internal Earth structure should be used to constrain the models. This will result a regionalised model of Earth structure rather than a full 3-D inversion, which is currently beyond our computational scope.
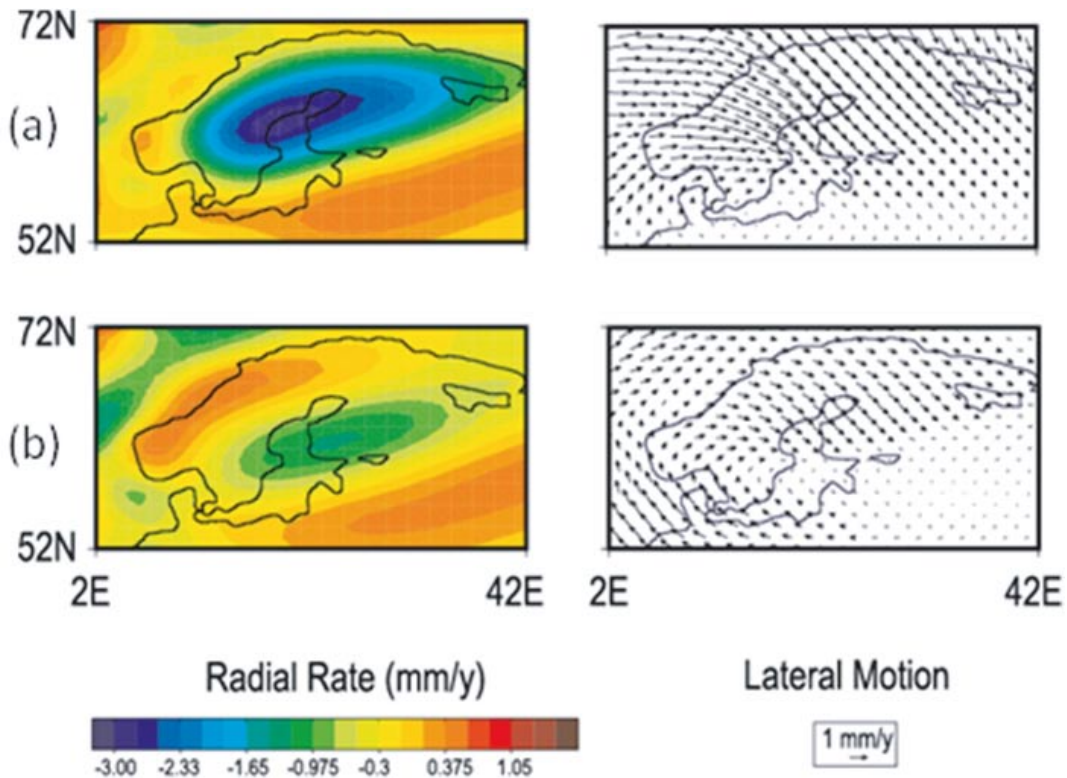

Figure 4-14. *(a) Misfit in uplift rates and horizontal deformation between the 3-D Earth model and the 1-D Earth model (as for Figure 4-9a). (b) As for (a), but predictions from the 'local' 1-D model are subtracted from the 3-D model. Absolute horizontal rates are plotted.*

4.6　Data sets used to constrain GIA models

The data sets used to constrain GIA models cover different time spans and geographical areas; the most tightly constrained models therefore use a combination of data sets. Many GIA effects have a unique geographical signature, therefore the location of data are important in order to distinguish between different Earth and ice models.

4.6.1　Relative sea-level data

Relative sea-level data record the height of the land-sea interface from the start of deglaciation to the present-day. Data relating to ice build-up (rising sea-level in the near-field and falling sea-level in the far-field) have been destroyed by subsequent sea-level changes. In many cases post-LGM far-field data are only preserved where tectonic uplift has elevated the shoreline markers faster than the rate of post-glacial sea-level rise. Sites covered by marine-grounded ice during the LGM provide information from the time of local melting onwards.

Classical relative sea-level data consist of dated palaeoshorelines (see /Lambeck et al. 1998a/ for a comprehensive overview of the Fennoscandian data set). These may be identified as beach formations or wave-cut notches, or simply by the discovery of biological sea-level markers. Such markers are called sea-level indicators, and should be accompanied by four pieces of information: the age of the sea-level indicator, its present height above sea-level, its indicative meaning, and its location. Only closely-spaced data (up to a few kilometres apart) may be combined to form a sea-level curve since the shape of such a curve will vary with location. In the present-day, contemporaneous palaeoshorelines will not lie at the same elevation as the land has been tilted rather than uniformly uplifted, in response to the melting of a greater ice mass inland.

The indicative meaning /Van de Plassche 1986/ of a sea-level indicator refers to the relationship between the environment in which the datum lived/was formed, and the contemporary reference water level. For example, if a certain type of coral only lives between 3 and 5 m below mean tide level then the relative sea-level height implied by this datum must be adjusted accordingly. Many sea-level markers only provide an upper or lower bound on sea-level height; this should be accounted for when using the data to constrain GIA models.

Errors bars must take account of the local tide range, which will be greater along the Norwegian Atlantic coast than in the Gulf of Bothnia. Dating errors should be minimised during periods of rapid sea-level change, and height errors should be minimised during periods of slow sea-level change. Care should be taken when using potentially reworked material, for example shells which may have been deposited high above mean sea-level during a storm event.
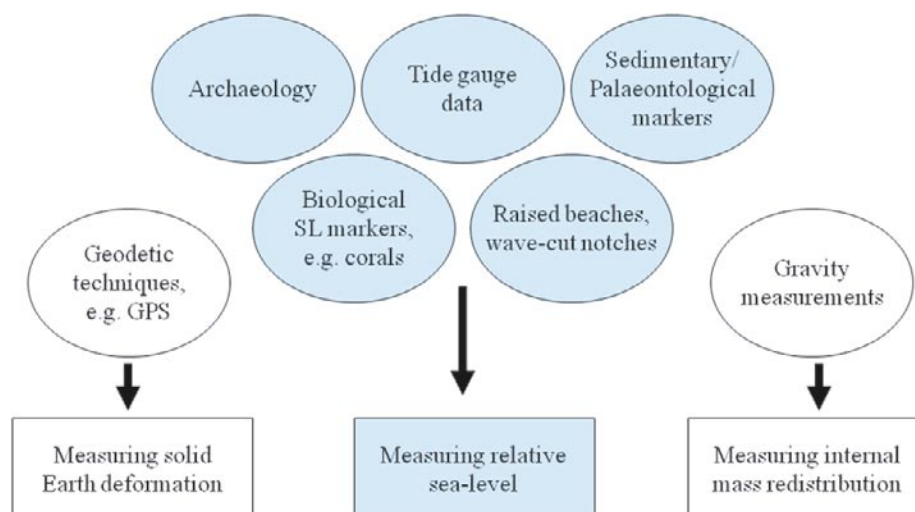

Figure 4-15. *Principal data sets used to constrain GIA models.*

Lake isolation events are commonly used to determine the height of relative sea-level at a specific time in Fennoscandia /e.g. Eronen et al. 2001/. As sea-level drops below the threshold of a lake, the change from marine to freshwater conditions within the lake will be marked by a change in sediment type and diatom population within the stratigraphic sequence. The height of the lake threshold, commonly a bedrock sill, above present-day sea-level determines the change in relative sea-level since the isolation event. Carbon-14 dating and diatom analysis are used to identify the timing of the transition from marine to freshwater conditions. Similarly, if the land-sea interface was defined by the extent of marine-grounded ice at a certain location, then the timing of ice retreat can be identified by dating the transition from sub-glacial conditions to marine conditions within the sedimentary layers.

Salt marshes also provide a control on age and height due to the limited environmental conditions in which they can exist, although care must be taken to identify whether compaction has subsequently taken place /Törnqvist et al. 2006/. Archaeological remains specifically related to the location of the shoreline, e.g. harbours, can also be used to identify past sea-level heights /Lambeck et al. 2004a/. This is an example of 'limiting data': data which are used to imply whether sea-level was above or below a certain height at a given time. For example, submerged tree stumps imply that relative sea-level was below this height at the time the trees were alive.

Care should be taken to determine whether the water-level indicator records the height of relative sea-level, or the height of a former ice-dammed lake. Such a lake existed within the Baltic at several times during the last deglaciation /Björck 1995/, and water levels were likely a few tens of metres above contemporary sea-level.

Far-field relative sea-level data are used to construct post-LGM eustatic sea-level curves /e.g. Fleming et al. 1998, Lambeck and Chappell 2001/. The distance of the data from the principal ice sheets means that far-field sea-level change is relatively insensitive to the source of melting, and isostatic corrections are small. Coral-dating is commonly used to determine past equatorial sea-levels because corals only grow in a narrow depth range. Samples from key sites such as Barbados /Fairbanks 1989/, the Huon Peninsular /Chappell and Polach 1991/, and the Sunda shelf /Hanebuth et al. 2000/ have been dated. In several cases the corals are now found above sea-level due to local tectonic activity. Such activity must always be considered as a potential (non-GIA) cause of relative sea-level change, and corrections made where necessary /Chappell 1974, Bard et al. 1990, Yokoyama et al. 2001a, Lambeck and Purcell 2005/.

Relative sea-level data necessarily occur within close proximity of present-day shorelines. There is a greater density of data within Fennoscandia than anywhere else in the world (Figure 4-16). Care should be taken when using such a spatially-limited data set to constrain ice and Earth models as there may be long wavelength features related to GIA loading that are unidentified in the current relative sea-level data set. Records of sea-level data are scattered throughout the literature, but regional data sets have been compiled by /Lambeck 1993a, 1993b, Tushingham and Peltier 1993, Kaufmann and Wolf 1996, Lambeck et al. 1998a, Dyke et al. 2003, Klemann and Wolf 2005, 2007, Whitehouse 2007/.

Tide gauge and mareograph data provide a historical record of relative sea-level change /Ekman 1988, Douglas 1997, Lambeck et al. 1998b/ and lake-level tilting /Mainville and Craymer 2005/. The longest records exceed 100 years, and there is a relatively good spatial coverage of gauges across the globe. The tide gauge data are archived by the Permanent Service for Mean Sea Level (PSMSL) via the Proudman Oceanographic Laboratory (www.pol.ac.uk/psmsl/). These data provide a record of sea-level change due to ongoing GIA processes related to post-LGM melting, such as ocean syphoning, as well as sea-level change associated with present-day ice mass, temperature, and salinity changes. The data may also be affected by temporal variations in air pressure, dynamic ocean topography, sediment compaction, groundwater extraction, the seasonal water cycle, and tectonics. Tide gauges measure sea-level relative to a solid Earth marker, therefore corrections must be made to account for the vertical displacement of each marker, e.g. by combining tide gauge data with GPS data /Milne et al. 2001/ or satellite altimetry data /Kuo et al. 2004/.
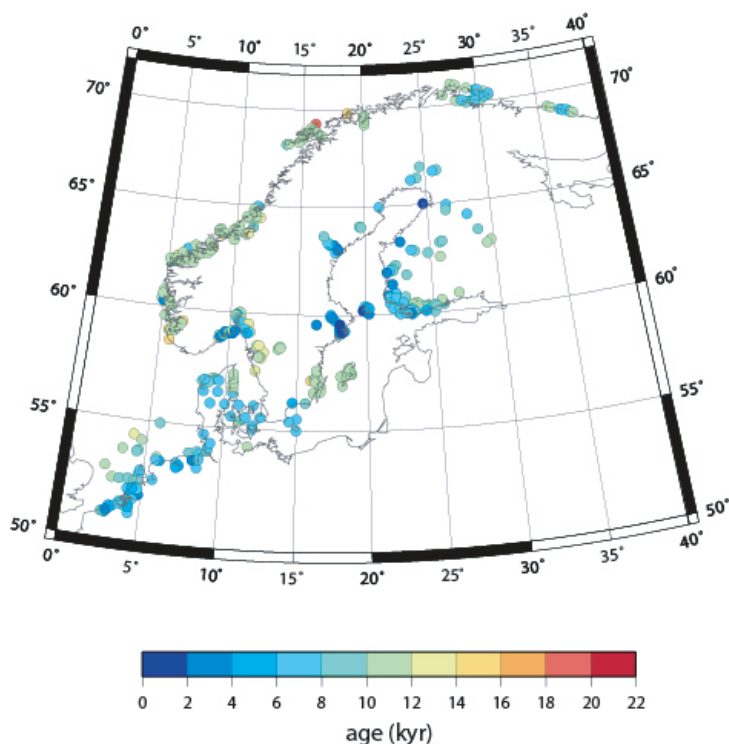
Figure 4-16. *Locations and ages of relative sea-level data across Fennoscandia. Taken from the data base compiled by /Whitehouse 2007/.*

Sea-level height is currently measured by the TOPEX/POSEIDON and JASON-1 satellite altimeters (see http://topex-www.jpl.nasa.gov/mission/topex.html). The data represent the change in the height of the geoid relative to the centre of mass of the Earth. While this does not directly provide a measurement of relative sea-level, it can be used in conjunction with tide gauge data to determine GIA-related solid Earth uplift rates in the absence of GPS data /Nerem and Mitchum 2002/.

4.6.2 Relaxation-time spectrum

When spectral methods are used to solve the sea-level equation, output can be compared to the relaxation-time spectrum for postglacial uplift. The spectrum is constructed from palaeoshoreline data that represent relative sea-level heights at discrete times along a given profile. The spectrum represents an estimate of the decay time of postglacial uplift as a function of spherical harmonic degree /Mitrovica and Forte 2004/.

The relaxation-time spectrum for Fennoscandia was first compiled by /McConnell 1968/, and has recently been updated by /Wieczerkowski et al. 1999/. It has traditionally been used in inversions to yield constraints upon mantle viscosity in the context of GIA modelling /e.g. Parsons 1972, Mitrovica and Peltier 1993a, Wieczerkowski et al. 1999, Mitrovica and Forte 2004, Klemann and Wolf 2005, Martinec and Wolf 2005/. The spectrum has been found to be strongly influenced by the viscosity structure beneath Fennoscandia, but is less sensitive to ice history /Wieczerkowski et al. 1999/.

4.6.3 Geodetic data

Present-day deformation rates are constrained by a variety of geodetic data, including levelling, Very Long Baseline Interferometry (VLBI), Satellite Laser Ranging (SLR), Global Positioning System (GPS), and other satellite data. Geodetic data provide better spatial coverage than relative sea-level data across large continental interiors such as northern Canada; however, they cover a much shorter time period than sea-level data.

Forward modelling of present-day deformation rates reveals that these short time-span data sets can distinguish between ice models /Milne et al. 2004/, but there would be significant non-uniqueness if attempts were made to invert the data for ice history. The data must be combined with longer-period relative sea-level data in order to determine the temporal and spatial details of deglaciation.

However, in terms of inverting for mantle viscosity, geodetic data prove to be very useful. For example, the resolving power of the BIFROST GPS data set may be as accurate as ~200 km at the base of the upper mantle /Milne et al. 2004/.

The geodetic data that cover the longest time span are levelling data, with records on the order of 100 years for Canada and Fennoscandia. However, the acquisition of such data is costly and labour intensive, and limited to more accessible regions. The levelling data base for Canada (maintained by the Geodetic Survey Division, Natural Resource Canada) contains over 46,000 re-levelled segments. These have been used in conjunction with tide gauge data to construct maps of vertical crustal movements /Koohzare et al. 2008/. Programs for precise re-levelling throughout Fennoscandia were initiated in 1978 and completed in 2006; historical data extend back to 1880 /Vestøl 2006/.

Over a shorter timescale, VLBI data have provided highly accurate measurements of baseline length-change rates over distances on the order of 1,000 km. Horizontal motion cannot be detected using relative sea-level data, and these data provided the first accurate test of predictions of GIA-related tangential motion /James and Lambert 1993, Mitrovica et al. 1993/. /Argus et al. 1999/ combine VLBI data with SLR data to constrain motion of the Earth's geocenter (the distance between the centre of mass of the Earth system and the centre of the Earth's geometrical figure) in response to postglacial rebound. The use of both data sets has since been superseded by GPS.

GPS data throughout North America and Fennoscandia now provide the basis for testing predictions of GIA-related solid Earth deformation. The BIFROST GPS network has been measuring rates of horizontal and vertical deformation throughout Fennoscandia since 1993 /Johansson et al. 2002, Lidberg et al. 2007/. The long time span of the data set means that observational accuracy is < 1 mm/yr. The sites are evenly distributed throughout the region of ongoing rebound (Figure 4-17), therefore the data may be easily interpolated to yield the spatial distribution of present-day solid Earth uplift across the region. The data show a concentric pattern of vertical and radial horizontal motion (Figure 4-17), and have been used to place constraints upon regional ice history and mantle viscosity /Milne et al. 2004/. /Milne et al. 2004/ also demonstrate that radial and horizontal velocity estimates provide distinct constraints upon mantle viscosity. /Nocquet et al. 2005/ combine the BIFROST data with more southerly data from the European Permanent GPS Network (EUREF-EPN), and are able to quantify the predicted peripheral subsidence surrounding Fennoscandia.
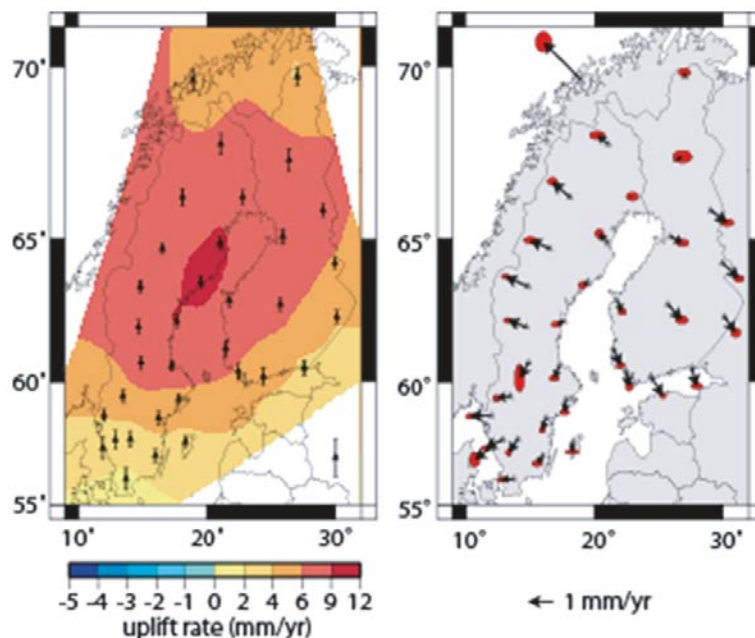

Figure 4-17. Observations of vertical (left) and horizontal (right) rates of present-day deformation in Fennoscandia measured using the BIFROST GPS network /Scherneck et al. 2001/. Vertical rates (left) have been interpolated and errors are shown as vertical bars. Horizontal errors are shown as ellipses (right).

/Park et al. 2002/ were the first to employ North American GPS data to infer mantle viscosities. Recently, /Calais et al. 2006/ and /Sella et al. 2007/ have used data from ~300 continuous GPS sites, installed by a range of groups (see /Calais et al. 2006/), to identify the solid Earth GIA signal in North America. /Sella et al. 2007/ complement the continuous GPS data with campaign-style data to improve the spatial coverage. Both studies find good agreement between model predictions and observations of uplift and subsidence rates, but a poor fit to the smaller magnitude horizontal rates. Horizontal rates are particularly sensitive to lateral variations in mantle viscosity, and are more likely to be contaminated by a long wavelength signal related to plate motion or intra-plate deformation.

In Antarctica and Greenland, present-day deformation is related to both post-LGM ice reduction and present-day ice mass changes. These signals must be separated in order to reconstruct regional ice histories, but the present-day ice coverage makes it difficult to measure solid Earth deformation rates. The ICESat (Ice, Cloud and land Elevation Satellite) measures changes in surface elevation over the ice caps, but surface height changes will be due to a combination of daily or seasonal snow and ice accumulation and melt patterns, horizontal motion of the ice sheet, and bedrock uplift, therefore predictions of solid Earth deformation from this data set contain large error bars. Bedrock-based GPS sites are sparsely located around the edges of the ice sheet, although localised studies with denser GPS networks have been carried out /Capra et al. 2007/.

As mentioned above, satellite altimetry has been used to measure sea surface heights. /Lee et al. 2008/ have also analysed the TOPEX/POSEIDON waveforms over land to determine solid Earth deformation at locations that are seasonally covered by a mixture of snow, ice and vegetation. In the future it should be possible to observe rates of solid Earth deformation in poorly-accessible areas, such as the Canadian Arctic, using satellite-based techniques.

4.6.4 Gravity data

The ongoing process of GIA, relating to both solid Earth rebound and subsurface mass redistribution, results in a signal that is detectable in the secular gravity field.

Land-based gravity measurements have been made throughout Fennoscandia and North America since the 1960's /Pagiatakis and Salib 2003, Mäkinen et al. 2005/, and at 23 sites in Antarctica since the 1990's /Mäkinen et al. 2007/. These data sets provide a reasonably long time span of highly accurate gravity data, but their spatial extent and resolution are limited, and the continued collection of such data is labour intensive. Gravity data are also available commercially from companies such as GETECH (UK).

In addition, measurements of the global gravity field are currently being carried out by the Gravity Recovery and Climate Experiment (GRACE) satellite, which has been in orbit since March 2002. The experiment measures mass movement within the Earth system and monthly solutions can be used to calculate the time-varying gravity trend over the whole Earth. The GIA signal is detectable within this trend /Tamisiea et al. 2007, Sasgen et al. 2007/. However, GRACE cannot determine the height at which mass changes take place; this might be in the atmosphere, on the surface of the Earth, or beneath the surface. The data must therefore be corrected for non-GIA trends, for example due to the present-day melting of ice sheets or mantle convection.

A second gravity mission, the Gravity field and steady-state Ocean Circulation Explorer (GOCE) is scheduled for launch in late 2008. This will measure the static global gravity field to centimetre accuracy at ~100 km resolution. It is hoped that such data will be able to constrain the properties of shallow low viscosity zones by modelling their impact upon GIA-induced geoid anomalies /van der Wal et al. 2004, Schotman and Vermeersen 2005/.

4.6.5 Estimating rotational parameters

Parameters relating to the rotational state of the Earth, such as its dynamic oblateness (J_2) and the rate of true polar wander, are perturbed by GIA. Predictions of such perturbations from GIA modelling have been compared to observations in order to constrain mantle viscosities /Vermeersen et al. 1997, Paulson et al. 2007/.

Estimates of J_2 have been obtained using SLR, and current estimates lie in the range 1.96×10^{-11} yr^{-1} /Cheng and Tapley 2004/ to 2.75×10^{-11} yr^{-1} /Cox and Chao 2002/. The mean path of the rotational pole has been estimated to be 0.925 ± 0.022 degrees Ma^{-1} in the direction 75.0 ± 1.1 degrees West /McCarthy and Luzum 1996/.

4.6.6 Regional stress indicators

Several authors predict how GIA processes affect the local stress field /e.g. Wu 1996, Johnston et al. 1998, Klemann and Wolf 1998/. Such predictions can be tested against stress information from earthquake focal mechanisms /e.g. Gregersen 1992/, well bore breakouts /e.g. Lund and Zoback 1999/, in situ stress measurements, and 'young' geologic data, such as Holocene fault slip. A complete summary of the methods used to determine the global stress field and can be found in /Zoback 1992/.

4.7 Accuracy of solutions to the sea-level equation

The accuracy of solutions to the sea-level equation is dependent upon the size of the time step between ice load configurations, and the spatial resolution; either the maximum spherical harmonic degree if spectral methods are used, or the grid size if finite element/volume methods are used. Solution accuracy can be increased by decreasing the loading time step or increasing spatial resolution. Both these changes increase computation time, and the best gains can be made by increasing spatial resolution during glaciation, and increasing time resolution during deglaciation /Zhong et al. 2003/.

In order to predict palaeotopography or the locations of palaeoshorelines a topography/bathymetry data set is required. The accuracy of such predictions is entirely dependent upon the resolution of the topography/bathymetry data set used. The topography data also determine the location of the zero relative sea-level contour through time; this is used to define the limit of meltwater redistribution and ocean-loading. If a time-varying ocean function is not used, and a constant ocean area is assumed this will introduce large errors into the load distribution (see section 3.5.1).

The input Earth- and ice history models completely determine the output of the sea-level equation, therefore their accuracy influence the accuracy of the output predictions. However, different outputs (e.g. far-field/near-field relative sea-level history, present-day vertical/horizontal deformation rates) are sensitive to different inputs (e.g. upper/lower mantle viscosity, timing of the LGM). At present, the Earth model is known to a higher degree of accuracy than the ice model, and varying mantle viscosity within reasonable bounds has a smaller effect upon relative sea-level predictions than varying ice thicknesses. Future work should therefore focus on improving the accuracy of the ice models, for example using climatologically-driven dynamical models that also include improved treatment of basal processes.

The accuracy of the theory of the sea-level equation, and the numerical methods used to solve it, must also be taken into account, especially since the input models are principally refined using this theory. Current state-of-the-art models that account for shoreline migration, grounded ice, rotational feedback, and lateral variations in Earth structure, show ever-improving agreement with observations, indicating that the theory is robust. Several GIA models, developed by independent groups, have been calibrated against each other, and solutions have been shown to agree to a high level of accuracy /e.g. Lambeck et al. 2003/.

Finally, the accuracy and spatio-temporal distribution of the data used to calibrate the GIA models places limits upon the accuracy of the ice and Earth models that can be deduced via GIA modelling. Future work should focus upon identifying how the current data sets should be expanded to give the greatest returns in increased model accuracy.

4.8 Shortcomings of current GIA models

Several processes are neglected in current state-of-the-art models. They are briefly discussed below, along with an assessment of the implications of neglecting them.

4.8.1 Sediment redistribution

Erosion and deposition by e.g. ice sheets are not accounted for in current GIA models. These processes may produce a non-negligible, long-term isostatic signal that is currently not modelled. Their inclusion may help to explain observations of uplift rates and depositional sequences.

Major northern hemisphere glaciations have occurred throughout the Late Pliocene and Pleistocene and there is evidence that there has been an increase in deposition rates along the shelf related to the glaciation of the Barents Sea and Fennoscandia over the last 2.5 Ma /Riis and Fjeldskaar 1992/. This change is predicted by /Molnar and England 1990/, who argue that major changes in erosion rates, and hence in rates of isostatic rebound due to erosional unloading, are to be expected in response to glacial/interglacial climatic changes.

During each glaciation, grounded ice sheets have transported eroded material away from centres of glaciation to the continental shelf edge, where it will have been deposited in a series of fans. As an example, 1.28 million km^3 of sediment is estimated to have been removed by glacial erosion, and deposited along the western and northern Barents Shelf margins during the Plio-Pleistocene /Rasmussen and Fjeldskaar 1996/, while > 32,000 km^3 of sediment is estimated to have been deposited on the North Sea Fan off the west coast of Norway since ~450 Ma BP /Nygård et al. 2005/. Such processes result in increased offshore loading, decreased onshore loading, and a lowering of the onshore continental surface on the order of several hundred metres /Rasmussen and Fjeldskaar 1996/. However, the isostatic effect will be small in comparison to that induced by ice loading during a glacial cycle, when ~5 million km^3 of ice is loaded upon, and then removed from, Fennoscandia in the course of just ~100,000 years /Lambeck et al. 2000/.

When accounting for sediment redistribution it is important to use applicable rates of erosion: rates principally depend upon bedrock, climate, and tectonic setting. Polar glaciers, or thin glaciers grounded on resistant crystalline bedrock erode ~0.01 mm/yr in the present-day, equivalent to 20 $t/km^2/yr$, while fast-moving temperate valley glaciers grounded on softer bedrock or till can erode > 1 mm/yr, or > 2,000 $t/km^2/yr$ /Hallet et al. 1996/. Erosion is also related to the basal ice sliding rate, and it follows that fast-moving glaciers will transport a greater flux of material than slow-moving glaciers. Sediment yield for Fennoscandia is thought to have peaked at the initiation of the 100 ka glacial cycles in the mid-Pleistocene, and decreased over the last two Fennoscandian glacial cycles /Elverhøi et al. 1998/.

The resulting long-term change in loading will produce an isostatic signal that manifests itself as enhanced uplift on land and subsidence offshore. Simple calculations assuming that erosion is proportional to the basal sliding rate during the last Fennoscandian glaciation lead to the prediction that the resulting isostatic response may perturb present-day uplift rates by up to 1.7 mm/yr /Mohammed 2003/. This is negligible in comparison to peak uplift rates during deglaciation, but neglecting such perturbing effects when tuning the ice history and Earth models to fit observations of present-day uplift rates may lead to overestimations of ice thickness or mantle viscosity. If onshore regions are sufficiently lowered, there are also implications for ice sheet behaviour due to the relationship between altitude and climate. A secondary consequence of sediment redistribution is that the topographic shape of the land will be altered; topography is currently assumed constant in GIA calculations, and changes will have a bearing upon palaeotopography reconstructions.

4.8.2   Ice-dammed lakes

During each deglacial time step of a GIA model, meltwater is assumed to be gravitationally-consistently redistributed throughout the oceans. In reality, substantial amounts of glacial meltwater may be temporarily stored as groundwater or surface water (e.g. in lakes). During the last deglaciation of e.g. the Laurentide and Fennoscandian ice sheets, meltwater was stored in vast lakes for several thousands of years before being released into the ocean.

Meltwater lakes formed as a result of ice-marginal position, topography, and isostatic deformation. During maximum glaciation, the extent of the ice sheets covered potential outlets for large lakes or inland seas, creating ice-dammed lakes. The level of the lakes will have risen rapidly during deglaciation, fuelled by melting. Rapid drainage could only occur when the ice retreated past a topographic low. The lakes may also have been dammed as a result of the isostatic uplift of the lake threshold, for example in ice-peripheral regions. Such lakes will have drained following deglaciation, when the land was isostatically lowered, or eustatic sea-levels rose above the lake threshold.

The existence of two such deglacial lakes is well-documented. In Fennoscandia, an emerging bedrock threshold caused the level of the Baltic to rise above sea-level at ~12 ka BP, thus forming the Baltic Ice Lake /Björck 1995/. The lake was breached at ~11.2 ka BP, but this outlet was blocked again by the re-advance of the ice sheet during the Younger Dryas. The final drainage of the lake took place at ~10.3 ka BP as the ice sheet made its final retreat north. At this time, the water level in the Baltic basin was rapidly lowered by 30 ± 5 m /Lambeck 1999/.

In North America, the principal lake that formed as a result of meltwater-damming by the retreating Laurentide ice sheet was Lake Agassiz. The history of the various North American ice-marginal lakes, controlled by the location of the ice margin and isostasy, is very complex, and a comprehensive review is provided by /Teller 1995/. The Kara Sea and Barents Sea ice sheets are also thought to have supported major ice-marginal lakes during deglaciation.

When meltwater is stored in ice-dammed lakes this results in a non-oceanic water load. Neglecting this load leads to errors in the surface loading function, and errors in the calculation of the volume of water in the ocean. Future models should include the proper hydrological treatment of meltwater. Care must also be taken to determine whether palaeoshoreline markers refer to sea-level or a lake level; the latter may have been several tens of metres above the contemporary sea-level. The sudden drainage of such lakes can have major climatic consequences /e.g. Barber et al. 1999/.

4.8.3   Non-GIA causes of relative sea-level change

GIA models are calibrated using a range of data sets, but if non-GIA causes of relative sea-level change are not corrected for, then fundamental errors may be introduced during the calibration of the GIA models. The principal causes of relative sea-level change are outlined in Figure 4-18 and described below. A comprehensive overview of the causes of sea-level change can be found in /Cazenave and Nerem 2004/.

There are four fundamental reasons for sea-level change: the capacity of the ocean basin may change, the volume of water within the ocean basin may change, the shape of the gravitational potential may be altered, or the land-sea interface may be altered by local effects. Many of the processes outlined in Figure 4-18 are included in the theory of the sea-level equation, including changes to the gravitational potential, ocean syphoning, continental levering, and GIA-related rebound or subsidence.
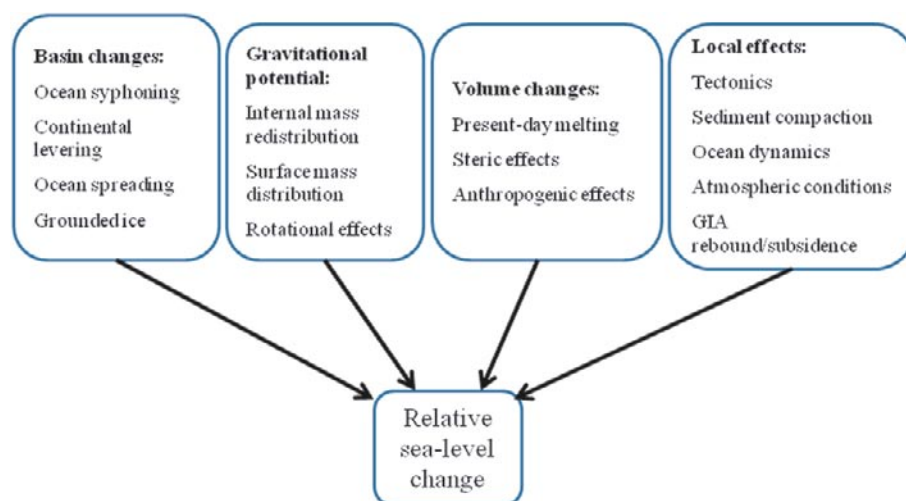

Figure 4-18. *Causes of relative sea-level change.*

Some of the processes that must be corrected for only alter relative sea-level on a daily or seasonal basis. These include the effect of tides, ocean dynamics, atmospheric conditions, and the seasonal water cycle. The local amplitude of these effects may be several times greater than the inter-annual trend of sea-level change. However, it should be noted that such variations, while easily predicted or observed in the present-day, may have exhibited very different patterns of behaviour during past climatic conditions, or during an oceanic low-stand. Some processes, related to decadal climate perturbations, may persist for several years, significantly altering global water storage patterns and hence sea-level /Ramillien et al. 2008/. As data with a high temporal resolution become increasingly available it is important to account for these short term processes, especially when using data with a short time span.

Other processes, such as sea floor spreading, take place over a longer time span than GIA. These processes, along with the effects of local tectonics and sediment compaction, can be independently quantified, and the data corrected. However, several contributions to the sea-level budget are still relatively poorly constrained. These include sea-level changes due to present-day ice mass changes, steric effects, and anthropogenic effects.

Present-day ice mass change will result in a unique pattern of sea-level change depending upon the source of melting /Mitrovica et al. 2001b, Tamisiea et al. 2001/. The resulting distribution of sea-level change will be due to a change in the volume of water in the ocean, and changes to the shape of the gravitational potential as a result of mass redistribution.

Steric sea-level changes arise due to the expansion or contraction of ocean volume due to temperature or salinity changes. In general, thermosteric (temperature) effects are estimated to be an order of magnitude greater than halosteric (salinity) effects /Antonov et al. 2002/. Estimates for the thermosteric contribution derived from ocean temperature data spanning the last 50 years lie in the range 0.42 ± 0.12 mm/yr /IPCC 2007/. However, different rates have been reported for different regions of the world ocean /Antonov et al. 2005/, indicating that spatially-variable corrections must be used. Present-day rates are also observed to be higher than the 50-year mean: /Willis et al. 2004/ combine temperature observations with satellite data to yield an estimate of 1.6 ± 0.3 mm/yr, while /Lombard et al. 2007/ combine altimetry and gravity data to yield an estimate of 1.9 ± 0.2 mm/yr, indicating that estimates must be constantly revised. /Ishii et al. 2006/ independently analyse salinity data and estimate a mean contribution of 0.04 ± 0.01 mm/yr for the past 50 years due to halosteric effects.

Finally, sea-level change takes place due to anthropogenic activity. /Cazenave and Nerem 2004/ tentatively estimate the present-day contribution to sea-level rates to be -0.91 ± 0.45 mm/yr. This estimate has large error bars, indicating the uncertainty in quantifying the range of anthropogenic processes that contribute to both sea-level rise and fall. Processes that cause sea-level rise include urbanization and deforestation (which increase surface runoff), and the extraction of water from aquifers and drainage of wetlands. Processes that cause sea-level fall include the retention of water in reservoirs or for irrigation.

4.9   Applications of GIA modelling

GIA modelling provides insight into many Earth processes, and has been used to quantify Earth parameters and interpret data sets. The principal applications of GIA modelling are shown in Figure 4-19, and briefly discussed below.

4.9.1   Constraining GIA model inputs

GIA modelling can be carried out iteratively to constrain Earth structure and ice history. The results of this work will further our understanding of ice sheet dynamics, and provide tighter constraints upon lithospheric thicknesses, mantle viscosities, and their variation throughout the Earth. This in turn provides feedback into studies of mantle convection, isostasy, continental deformation, etc.

An area of ongoing research is the exploration of the effect of lateral variations in Earth structure upon GIA predictions. This work will help to improve constraints upon GIA input models, in particular 3-D mantle viscosities and variations in lithospheric thickness.
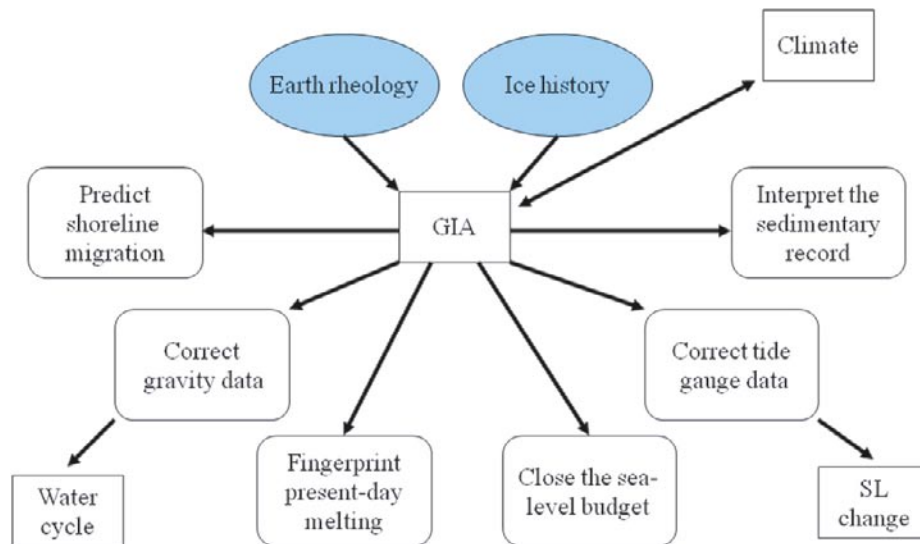
Figure 4.19. *Applications of GIA modelling. Inputs to GIA modelling are shown in blue, outputs are shown in white.*

4.9.2   Climate

Glacial cycles are principally driven by climate changes, which arise for a variety of reasons, and are perpetuated by a complex system of feedbacks. Combining GIA-constrained ice history with insights from dynamic ice modelling helps to further our understanding of the processes driving glacial cycles, and hence climate change. Reconstructing past climatic conditions gives us an insight into the feedbacks that operate in such a system, and will serve as a proxy when predicting future climate change.

4.9.3   Interpretation of the sedimentary record

GIA modelling highlights the fact that sea-level change rarely takes place uniformly over the whole of the ocean, however, in many locations the sedimentary record is interpreted under the assumption that past sea-level change has been uniform. This can lead to errors in reconstructing past global sea-levels, and hence past climatic conditions.

4.9.4   Sea-level change

GIA is a major contributor to sea-level change. The geometry of ice-loading and the timing and source of melting produce a unique pattern of sea-level change following perturbations to the geoid and solid surfaces. GIA models enable us to interpret this pattern, and identify past and present changes in the mass of the global ice sheets via an iterative modelling process. The results provide an independent test for dynamical models of ice sheet behaviour.

Two specific examples are the interpretation of the pattern of present-day sea-level rise, and the pattern of rapid sea-level rise during meltwater pulse 1A at ~14 ka BP /Fairbanks 1989/. The former will enable us to identify current rates and sources of ice sheet melting /Mitrovica et al. 2001b/, whilst the latter will help to identify the source of the meltwater pulse /Clark et al. 2002/, and hence provide a better understanding into how specific ice sheets responded to (independently constrained) climate changes, and how much ice was stored in, and released from, each ice sheet. When identifying the contribution of present-day melting to sea-level change, it is important to first correct for the spatially-varying GIA signal related to the last major deglaciation, before attempting to interpret the remaining signal /Tamisiea et al. 2001/. Predictions of the pattern of sea-level change due to distinct melt sources also identifies locations which may, in future, provide data which will enable us to accept or reject specific hypotheses regarding ice history.

If we wish to quantify the effects of climate change by determining present-day rates of sea-level change and the historical rate of acceleration, historical relative sea-level data, such as tide gauge data, must be corrected for the spatially-varying GIA signal before eustatic estimates may be calculated /e.g. Peltier 2001, Kendall et al. 2006/. Improving the accuracy of the GIA correction will lead to a better understanding of the factors contributing to sea-level change.

The total eustatic rate will be due to a combination of processes (see Figure 4-20). Each of these rates should be determined independently in order to better constrain the individual contributions to the sea-level budget: at present there is significant discrepancy between observed sea-level rise and estimates of individual contributions /Munk 2002/.

The GIA contribution to the present-day sea-level budget arises due to the ongoing deformation of the solid Earth in response to post-glacial ocean-loading. This deformation increases the capacity of the ocean basins; the net effect results in an estimated sea-level fall of 0.3 mm/yr /Douglas and Peltier 2002/. Without this correcting for this effect, estimates of the contribution to sea-level rise due to present-day melting or steric effects will be underestimated.

Sea-level changes are measured by a range of methods, including the measurement of changes in the height of the sea surface by satellite altimetry, the measurement of changes in the position of the land-sea interface by tide gauges, and the measurement of changes in the mass of water within the oceans by satellites measuring the Earth's gravity field. The signal from each of these measurements must be carefully decomposed to determine whether changes are due to a change in the rate of water entering/leaving the ocean, the shape of the solid Earth, or the density of the ocean /Miller and Douglas 2004/. Using GIA modelling, and a combination of these data, we are able to place constraints upon not only changes in the volume and capacity of the oceans, but also spatiotemporal changes to its temperature and salinity.
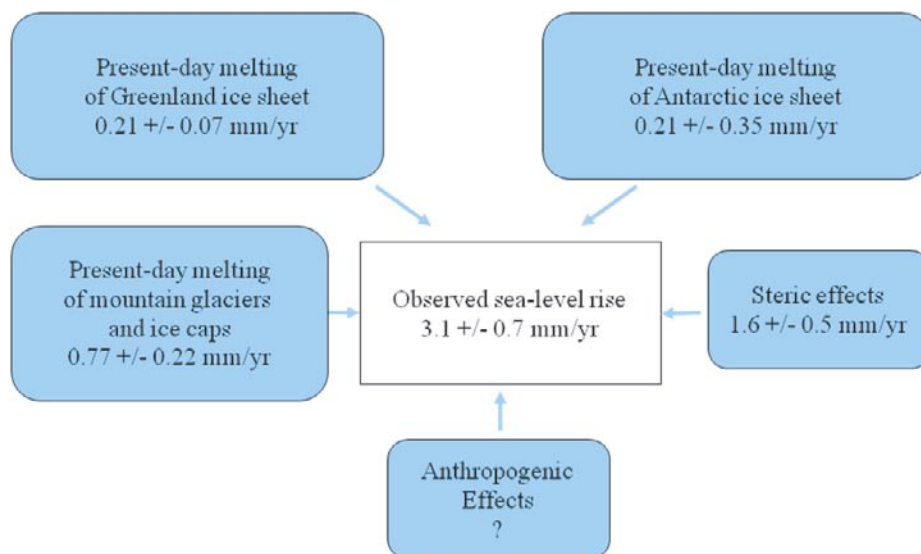

Figure 4-20. *The present-day sea-level budget according to the IPCC Fourth Assessment Report /IPCC 2007/. The misfit between the estimated sum and the observed rate of sea-level rise is 0.3 ± 1.0 mm/yr. No estimate is made for anthropogenic effects.*

4.9.5 Correcting gravity data

Gravity data from the GRACE mission contains information relating to the integral effect of mass movement in the ocean, atmosphere, hydrosphere, and in the Earth's interior. One of the principal aims of the mission is to investigate the Earth's annual and seasonal water cycle. In order to isolate the signal due to the hydrosphere a series of corrections must be made. The data are pre-processed to remove oceanic and atmospheric contributions and tidal effects, but the remaining signal will still contain contributions from internal mass redistribution, relating to GIA, as well as the movement of water on the surface of the Earth. Predictions from GIA modelling of the secular gravity trend due to glacial rebound in areas such as Greenland and Antarctica are vital in order to remove this signal, and hence quantify mass changes within the remaining ice sheets.

4.9.6 Shoreline migration

GIA modelling can be combined with topographic data sets in order to reconstruct past shoreline positions, or predict future changes for a range of predicted sea-level change scenarios. Shoreline reconstructions have implications in the field of anthropology, where the identification of past land bridges helps to understand patterns of human development and migration during the Holocene. The reconstruction of changes in land extent can also help to explain past climatic conditions. For example, the exposure of the Bering Strait during the LGM significantly perturbed the regional climate, thus preventing the extensive glaciation of Alaska. Such reconstructions can also highlight locations of potentially-useful sea-level data. Finally, predictions of future shoreline migration will help to mitigate flooding-related problems brought about by present-day sea-level rise.

4.9.7 Predicting seismic/volcanic activity

GIA models can be used to predict changes in the stress field due to glacial loading and unloading /Lund 2005/. This information can be used to investigate, and perhaps predict, changes in the local level of seismic /e.g. Wu et al. 1999, Stewart et al. 2000, Sauber and Molnia 2004/ or volcanic /e.g. Pagli and Sigmundsson 2008/ activity. GIA predictions can also be used to correct relative sea-level data in tectonically-active regions, such as the Mediterranean, and hence place constraints upon local tectonic rates /Lambeck 1995c/.

4.10 Final remarks

GIA modelling is an evolving subject. As data sets and computing capabilities improve, the subject will continue to grow. The greatest advances will likely be made as a result of cross-disciplinary collaboration. This report provides a summary of the developments that have taken place during the last few decades, as well as highlighting current shortcomings and areas of ongoing research. The information provided here is not exclusive, and the reader is referred to the extensive reference list if further insight is required.

References

Amelung F, Wolf D, 1994. The incremental gravitational force in models of glacial isostasy. Geophysical Journal International, 117 (3): 864-879.

Antonov J I, Levitus S, Boyer T P, 2002. Steric sea level variations during 1957–1994: Importance of salinity. Journal of Geophysical Research, 107 (C12): 8013.

Antonov J I, Levitus S, Boyer T P, 2005. Thermosteric sea level rise, 1955–2003. Geophysical Research Letters, 32 (12): L12602.

Argus D F, Peltier W R, Watkins M M, 1999. Glacial isostatic adjustment observed using very long baseline interferometry and satellite laser ranging geodesy. Journal of Geophysical Research, 104 (B12): 29077–29093.

Ballantyne C K, 1997. Periglacial trimlines in the Scottish Highlands. Quaternary International, 38 (9): 119–136.

Barber D C, Dyke A, Hillaire-Marcel C, Jennings A E, Andrews J T, Kerwin M W, Bilodeau G, McNeely R, Southon J, Morehead M D, Gagnon J M, 1999. Forcing of the cold event of 8,200 years ago by catastrophic drainage of Laurentide lakes. Nature, 400 (6742): 344–348.

Bard E, Hamelin B, Fairbanks R G, 1990. U-Th ages obtained by mass spectrometry in corals from Barbados: sea level during the past 130,000 years. Nature, 346: 456–458.

Bassett S E, Milne G A, Mitrovica J X, Clark P U, 2005. Ice Sheet and Solid Earth Influences on Far-Field Sea-level Histories. Nature, 309: 925–928.

Bennike O, Björck S, Lambeck K, 2002. Estimates of South Greenland late-glacial ice limits from a new relative sea level curve. Earth and Planetary Science Letters, 197 (3–4): 171–186.

Bills B G, James T S, 1996. Late quaternary variations in relative sea level due to glacial cycle polar wander. Geophysical Research Letters, 23 (21): 3023–3026.

Björck S, 1995. A review of the history of the Baltic Sea, 13.0–8.0 ka BP. Quaternary International, 27: 19–40.

Brenner S, Scott R L, 2005. The Mathematical Theory of Finite Element Methods, 2nd edition, Springer.

Calais E, Han J Y, DeMets C, Nocquet J M, 2006. Deformation of the North America plate interior from a decade of continuous GPS measurements. Journal of Geophysical Research, 111 (B6): B06402.

Calcagnile G, 1982. The lithosphere asthenosphere system in Fennoscandia. Tectonophysics, 90 (1–2): 19–35.

Capra A, Mancini F, Negusini M, 2007. GPS as a geodetic tool for geodynamics in northern Victoria Land, Antarctica. Antarctic Science, 19 (1): 107–114.

Cathles L M, 1975. The Viscosity of the Earth's Mantle. Princeton University Press, Princeton, NJ.

Cazenave A, Nerem R S, 2004. Present-day sea level change: Observations and causes. Reviews of Geophysics, 42 (3): RG3001.

Chappell J, 1974. Geology of coral terraces, Huon Peninsular, New Guinea: a study of Quaternary tectonic movements and sea-level changes. Geological Society of America Bulletin, 95: 553–570.

Chappell J, Polach H, 1991. Post-glacial sea-level rise from a coral record at Huon Peninsular, Papua New Guinea. Nature 349: 147–149.

Cheng M, Tapley B D, 2004. Variations in the Earth's oblateness during the past 28 years. Journal of Geophysical Research, 109 (B9): B09402.

Clark J A, Farrell W E, Peltier W R, 1978. Global changes in post-glacial sea-level – A numerical calculation. Quaternary Research, 9 (3): 265–287.

Clark P U, Mitrovica J X, Milne G A, Tamisiea M E, 2002. Sea-level fingerprinting as a direct test for the source of global meltwater pulse 1A. Science, 295 (5564): 2438–2441.

Cox C M, Chao B F, 2002. Detection of large-scale mass redistribution in the terrestrial system since 1998. Science, 297: 831–833.

D'Agostino G, Spada G, Sabadini R, 1997. Postglacial rebound and lateral viscosity variations: A semi-analytical approach based on a spherical model with Maxwell rheology. Geophysical Journal International, 129 (3): F9–F13.

Dal Forno G, Gasperini P, Boschi E, 2005. Linear or nonlinear rheology in the mantle: a 3D finite-element approach to postglacial modelling. Journal of Geodynamics, 39 (2): 183–195.

Davis J L, Mitrovica J X, Scherneck H G, Fan R, 1999. Investigations of Fennoscandian glacial isostatic adjustment using modern sea level records. Journal of Geophysical Research, 104 (B2): 2733–2747.

Denton G H, Hughes T J (editors), 1981. The Last Great Ice Sheets. Wiley, New York, NY.

Di Donato G, Mitrovica J X, Sabadini R, Vermeersen L L A, 2000a. The influence of a ductile crustal zone on glacial isostatic adjustment: Geodetic observables along the US east coast. Geophysical Research Letters, 27 (18): 3017–3020.

Di Donato G, Vermeersen L L A, Sabadini R, 2000b. Sea-level changes, geoid and gravity anomalies due to Pleistocene deglaciation by means of multilayered, analytical Earth models. Tectonophysics, 320 (3–4): 409–418.

Dilts G A, 1985. Computation of spherical harmonic expansion coefficients via FFTs. Journal of Computational Physics, 57 (3): 439–453.

Douglas B C, 1997. Global sea rise: A redetermination. Surveys in Geophysics, 18 (2–3): 279–292.

Douglas B C, Peltier W R, 2002. The puzzle of global sea-level rise. Physics Today, 55 (3): 35–40.

Dyke A S, Andrews J T, Clark P U, England J H, Miller G H, Shaw J, Veillette J J, 2002. The Laurentide and Innuitian ice sheets during the Last Glacial Maximum. Quaternary Science Reviews, 21 (1–3): 9–31.

Dyke A S, Moore A, Robertson L, 2003. Deglaciation of North America. Geological Survey of Canada, Open File 1574.

Dziewonski A M, Anderson D L, 1981. Preliminary Reference Earth Model. Physics of the Earth and Planetary Interiors, 25 (4): 297–356.

Ekman M, 1988. The World's longest continued series of sea-level observations. Pure and Applied Geophysics, 127 (1): 73–77.

Ekström G, Dziewonski A, 1998. The unique anisotropy of the Pacific upper mantle. Nature, 394: 168–172.

Elverhøi A, Hooke R L, Solheim A, 1998. Late Cenozoic erosion and sediment yield from the Svalbard Barents Sea region: Implications for understanding erosion of glacierized basins. Quaternary Science Reviews, 17 (1–3): 209–241.

England P, Houseman G, 1986. Finite strain calculations of continental deformation. 2. Comparison with the India-Asia collision zone. Journal of Geophysical Research, 91 (B3): 3664–3676.

Eronen M, Gluckert G, Hatakka L, Van de Plassche O, Van der Plicht J, Rantala P, 2001. Rates of Holocene isostatic uplift and relative sea-level lowering of the Baltic in SW Finland based on studies of isolation contacts. Boreas, 30 (1): 17–30.

Fairbanks R G, 1989. A 17,000-year glacio-eustatic sea-level record – influence of glacial melting rates on the Younger Dryas event and deep-ocean circulation. Nature, 342 (6250):637–642.

Farrell W E, Clark J A, 1976. Postglacial sea-level. Geophysical Journal of the Royal Astronomical Society, 46 (3): 647–667.

Fjeldskaar W, Cathles L, 1991. The present rate of uplift of Fennoscandia implies a low-viscosity asthenosphere. Terra Nova, 3 (4): 393–400.

Fjeldskaar W, 1994. Viscosity and thickness of the asthenosphere detected from the Fennoscandian uplift. Earth and Planetary Science Letters, 126 (4): 399–410.

Fjeldskaar W, 1997. Flexural rigidity of Fennoscandia inferred from the postglacial uplift. Tectonics, 16 (4): 596–608.

Fleming K, Johnston P, Zwartz D, Yokoyama Y, Lambeck K, Chappell J, 1998. Refining the eustatic sea-level curve since the Last Glacial Maximum using far- and intermediate-field sites. Earth and Planetary Science Letters, 163 (1–4): 327–342.

Fleming K, Martinec Z, Wolf D, 2002. A reinterpretation of the Fennoscandian relaxation-time spectrum for a viscoelastic lithosphere. In: I.N. Tziavos (Editor), Gravity and Geoid. Ziti Publishing, Thessaloniki, pp. 432–438.

Fleming K, Lambeck K, 2004. Constraints on the Greenland Ice Sheet since the Last Glacial Maximum from sea-level observations and glacial-rebound models. Quaternary Science Reviews, 23 (9–10): 1053–1077.

Forte A M, Mitrovica J X, 1996. New inferences of mantle viscosity from joint inversion of long-wavelength mantle convection and post-glacial rebound data. Geophysical Research Letters, 23 (10): 1147–1150.

Forte A M, Woodward R L, 1997. Seismic-geodynamic constraints on three-dimensional structure, vertical flow, and heat transfer in the mantle. Journal of Geophysical Research, 102 (B8): 17981–17994.

Fung Y C, 1965. Foundation of Solid Mechanics. Prentice-Hall, Englewood Cliffs, New Jersey.

Gasperini P, Sabadini R, Yuen D A, 1986. Excitation of earth's rotational axis by recent glacial discharges. Geophysical Research Letters 13: 533–536.

Gasperini P, Sabadini R, 1989. Lateral heterogeneities in mantle viscosity and post-glacial rebound. Geophysical Journal International, 98 (3): 413–428.

Gasperini P, Sabadini R, 1990. Finite-element modelling of lateral viscosity heterogeneities and postglacial rebound. Tectonophysics, 179 (1–2): 141–149.

Gasperini P, Dal Forno G, Boschi E, 2004. Linear or non-linear rheology in the Earth's mantle: the prevalence of power-law creep in postglacial isostatic readjustment of Laurentia. Geophysical Journal International, 157 (3): 1297–1302.

Gehrels W R, Milne G A, Kirby J R, Patterson R T, Belknap D F, 2004. Late Holocene sea-level changes and isostatic crustal movements in Atlantic Canada. Quaternary International, 120: 79–89.

Giunchi C, Spada G, Sabadini R, 1997. Lateral viscosity variations and post-glacial rebound: Effects on present-day VLBI baseline. Geophysical Research Letters, 24 (1): 13–16.

Giunchi C, Spada G, 2000. Postglacial rebound in a non – Newtonian spherical Earth. Geophysical Research Letters. 27 (14): 2065–2068.

Gold T, 1955. Instability of the Earth's axis of rotation. Nature, 175: 526–529.

Gregersen S, 1992. Crustal Stress Regime in Fennoscandia from focal mechanisms. Journal of Geophysical Research, 97 (B8): 11821–11827.

Hagedoorn J M, Wolf D, Martinec Z, 2007. An estimate of global mean sea-level rise inferred from tide-gauge measurements using glacial-isostatic models consistent with the relative sea-level record. Pure and Applied Geophysics, 164 (4): 791–818.

Hallet B, Hunter L, Bogen J, 1996. Rates of erosion and sediment evacuation by glaciers: A review of field data and their implications. Global and Planetary Change, 12 (1–4): 213–235.

Han D, Wahr J, 1989. Post-glacial rebound analysis for a rotating Earth. In: S Cohen, P Vanicek (Editors), Slow Deformations and Transmissions of Stress in the Earth. AGU Monograph Series 49, pp. 1–6.

Hanebuth T, Stattegger K, Grootes P M, 2000. Rapid flooding of the Sunda Shelf: a late glacial sea-level record. Science, 288: 1033–1035.

Hibbit D, Karlsson B, Sorensen P, 2005. Getting started with ABAQUS-Version (6.5). Hibbit, Karlsson and Sorensen Inc.

Huybrechts P, 1990. The Antarctic Ice Sheet during the last glacial-interglacial cycle: a three-dimensional experiment. Annals of Glaciology, 14: 115–119.

Huybrechts P, 2002. Sea-level changes at the LGM from ice-dynamic reconstructions of the Greenland and Antarctic ice sheets during the glacial cycles. Quaternary Science Reviews, 21 (1–3): 203–231.

IPCC, 2007. Climate Change 2007: The Physical Science Basis. Contribution of Working Group I to the Fourth Assessment Report of the Intergovernmental Panel on Climate Change [Solomon S, Qin D, Manning M, Chen Z, Marquis M, Averyt K B, Tignor M and Miller H L (eds.)/. Cambridge University Press, Cambridge, United Kingdom and New York, NY, USA, 996 pp.

Ishii M, Kimoto M, Sakamoto K, Iwasaki S I, 2006. Steric sea level changes estimated from historical ocean subsurface temperature and salinity analyses. Journal of Oceanography, 62 (2): 155–170.

Ivins E R, Sammis C G, 1995. On lateral viscosity contrast in the mantle and the rheology of low-frequency geodynamics. Geophysical Journal International, 123 (2): 305–322.

Ivins E R, James T S, 2005. Antarctic glacial isostatic adjustment: a new assessment. Antarctic Science, 17 (4): 541–553.

Jackson J, Mckenzie D, Priestley K, Emmerson B, 2008. New views on the structure and rheology of the lithosphere. Journal of the Geological Society, 165: 453–465.

James T S, Lambert A, 1993. A comparison of VLBI data with the ICE-3G rebound model. Geophysical Research Letters, 20 (9): 871–874.

James T S, Ivins E R, 1997. Global geodetic signatures of the Antarctic ice sheet. Journal of Geophysical Research, 102 (B1): 605–633.

James T S, Ivins E R, 1998. Predictions of Antarctic crustal motions driven by present-day ice sheet evolution and by isostatic memory of the Last Glacial Maximum. Journal of Geophysical Research, 103 (B3): 4993–5017.

Johansson J M, Davis J L, Scherneck H G, Milne G A, Vermeer M, Mitrovica J X, Bennett R A, Jonsson B, Elgered G, Elosegui P, Koivula H, Poutanen M, Ronnang B O, Shapiro II, 2002. Continuous GPS measurements of postglacial adjustment in Fennoscandia – 1. Geodetic results. Journal of Geophysical Research, 107 (B8): 2157, doi: 10.1029/2001JB000400.

Johnston P, 1993. The effect of spatially non-uniform water loads on prediction of sea-level change. Geophysical Journal International, 114 (3): 615–634.

Johnston P, Wu P, Lambeck K, 1998. Dependence of horizontal stress magnitude on load dimension in glacial rebound models. Geophysical Journal International, 132 (1): 41–60.

Johnston P, Lambeck K, 1999. Postglacial rebound and sea level contributions to changes in the geoid and the Earth's rotation axis. Geophysical Journal International, 136 (3): 537–558.

Johnston P J, Lambeck K, 2000. Automatic inference of ice models from postglacial sea level observations: Theory and application to the British Isles. Journal of Geophysical Research, 105 (B6): 13179–13194.

Kaufmann G, Wolf D, 1996. Deglacial land emergence and lateral upper-mantle heterogeneity in the Svalbard Archipelago 2. Extended results for high-resolution load models. Geophysical Journal International, 127 (1): 125–140.

Kaufmann G, 1997. The onset of Pleistocene glaciation in the Barents Sea: implications for glacial isostatic adjustment. Geophysical Journal International, 131 (2): 451–465.

Kaufmann G, Wu P, Wolf D, 1997. Some effects of lateral heterogeneities in the upper mantle on postglacial land uplift close to continental margins. Geophysical Journal International, 128: 175–187.

Kaufmann G, Wu P, 1998. Lateral asthenospheric viscosity variations and postglacial rebound: a case study for the Barents Sea. Geophysical Research Letters, 25 (11): 1963–1966.

Kaufmann G, Wolf D, 1999. Effects of lateral viscosity variations on postglacial rebound: an analytical approach. Geophysical Journal International, 137 (2): 489–500.

Kaufmann G, Lambeck K, 2000. Mantle dynamics, postglacial rebound and the radial viscosity profile. Physics of the Earth and Planetary Interiors, 121 (3–4): 301–324.

Kaufmann G, Wu P, Li G, 2000. Glacial isostatic adjustment in Fennoscandia on a laterally heterogeneous Earth. Geophysical Journal International, 143 (1): 262–273.

Kaufmann G, Lambeck K, 2002. Glacial isostatic adjustment and the radial viscosity profile from inverse modelling. Journal of Geophysical Research, 107 (B11): 2280.

Kaufmann G, Wu P, 2002. Glacial isostatic adjustment in Fennoscandia with a three-dimensional viscosity structure as an inverse problem. Earth and Planetary Science Letters, 197 (1): 165–181.

Kaufmann G, Wu P, Ivins E R, 2005. Lateral viscosity variations beneath Antarctica and their implications on regional rebound motions and seismotectonics. Journal of Geodynamics, 39 (2): 165–181.

Kendall R, Mitrovica J X, Sabadini R, 2003. Lithospheric thickness inferred from Australian post-glacial sea-level change: The influence of a ductile crustal zone. Geophysical Research Letters, 30 (9): 1461.

Kendall R A, Mitrovica J X, Milne G A, 2005. On post-glacial sea level – II. Numerical formulation and comparative results on spherically symmetric models. Geophysical Journal International, 161 (3): 679–706.

Kendall R A, Latychev K, Mitrovica J X, Davis J E, Tamisiea M E, 2006. Decontaminating tide gauge records for the influence of glacial isostatic adjustment: The potential impact of 3-D Earth structure. Geophysical Research Letters, 33 (24): L24318.

Klemann V, Wolf D, 1998. Modelling of stresses in the Fennoscandian lithosphere induced by Pleistocene glaciations. Tectonophysics, 294 (3–4): 291–303.

Klemann V, Wolf D, 1999. Implications of a ductile crustal layer for the deformation caused by the Fennoscandian ice sheet. Geophysical Journal International, 139 (1): 216–226.

Klemann V, Wu P, Wolf D, 2003. Compressible viscoelasticity: stability of solutions for homogeneous plane-Earth models. Geophysical Journal International, 153 (3): 569–585.

Klemann V, Wolf D, 2005. The eustatic reduction of shoreline diagrams: implications for the inference of relaxation-rate spectra and the viscosity stratification below Fennoscandia. Geophysical Journal International, 162 (1): 249–256.

Klemann V, Wolf D, 2007. Using fuzzy logic for the analysis of sea-level indicators with respect to glacio-isostatic adjustment: An application to the Richmond Gulf region, Hudson Bay. Pure and Applied Geophysics, 164 (4): 683–696.

Koohzare A, Vaníček P, Santos M, 2008. Pattern of recent vertical crustal movements in Canada. Journal of Geodynamics, 45: 133–145.

Kuo C Y, Shum C K, Braun A, Mitrovica J X, 2004. Vertical crustal motion determined by satellite altimetry and tide gauge data in Fennoscandia. Geophysical Research Letters, 31 (1): L01608.

Lambeck K, 1980. The Earth's variable rotation. New Scientist, 88 (1227): 426–429.

Lambeck K, 1990. Glacial rebound, sea-level change and mantle viscosity. Quarterly Journal of the Royal Astronomical Society, 31 (1): 1–30.

Lambeck K, Nakada M, 1990. Late Pleistocene and Holocene sea-level change along the Australian coast. Global and Planetary Change, 3 (1–2): 143–176.

Lambeck K, Johnston P, Nakada M, 1990. Holocene glacial rebound and sea-level change in NW Europe. Geophysical Journal International, 103 (2): 451–468.

Lambeck K, 1991. Glacial rebound and sea-level change in the British-Isles. Terra Nova, 3 (4): 379–389.

Lambeck K, 1993a. Glacial rebound of the British-Isles. 1. Preliminary model results. Geophysical Journal International, 115 (3): 941–959.

Lambeck K, 1993b. Glacial rebound of the British-Isles. 2. A high-resolution, high-precision model. Geophysical Journal International, 115 (3): 960–990.

Lambeck K, 1993c. Glacial rebound and sea-level change – an example of a relationship between mantle and surface processes. Tectonophysics, 223 (1–2): 15–37.

Lambeck K, 1995a. Constraints on the Late Weichselian ice-sheet over the Barents Sea from observations of raised shorelines. Quaternary Science Reviews, 14 (1): 1–16.

Lambeck K, 1995b. Late Devensian and Holocene shorelines of the British-Isles and North-Sea from models of glacio-hydro-isostatic rebound. Journal of the Geological Society, 152: 437–448.

Lambeck K, 1995c. Late Pleistocene and Holocene sea-level change in Greece and south-western Turkey – a separation of eustatic, isostatic and tectonic contributions. Geophysical Journal International, 122 (3): 1022–1044.

Lambeck K, 1996a. Glaciation and sea-level change for Ireland and the Irish Sea since Late Devensian/Midlandian time. Journal of the Geological Society, 153: 853–872.

Lambeck K, 1996b. Limits on the areal extent of the Barents Sea ice sheet in Late Weichselian time. Global and Planetary Change, 12 (1–4): 41–51.

Lambeck K, Johnston P, Smither C, Nakada M, 1996. Glacial rebound of the British Isles. 2. Constraints on mantle viscosity. Geophysical Journal International, 125 (2): 340–354.

Lambeck K, Smither C, Johnston P, 1998a. Sea-level change, glacial rebound and mantle viscosity for northern Europe. Geophysical Journal International, 134 (1): 102–144.

Lambeck K, Smither C, Ekman M, 1998b. Tests of glacial rebound models for Fennoscandinavia based on instrumented sea- and lake-level records. Geophysical Journal International, 135 (2): 375–387.

Lambeck K, 1999. Shoreline displacements in southern-central Sweden and the evolution of the Baltic Sea since the last maximum glaciation. Journal of the Geological Society, 156: 465–486.

Lambeck K, Yokoyama Y, Johnston P, Purcell A, 2000. Global ice volumes at the Last Glacial Maximum and early Lateglacial. Earth and Planetary Science Letters, 181 (4): 513–527.

Lambeck K, Chappell J, 2001. Sea level change through the last glacial cycle. Science, 292 (5517): 679–686.

Lambeck K, Purcell A, 2001. Sea-level change in the Irish Sea since the last glacial maximum: constraints from isostatic modelling. Journal of Quaternary Science, 16 (5): 497–506.

Lambeck K, 2002. Sea-level change from Mid-Holocene to Recent time: an Australian example with global implications. In: JX Mitrovica, BLA Vermeersen (Editors), Ice Sheets, Sea Level and the Dynamic Earth. AGU Geodynamics Series, Washington DC, vol. 29, pp. 33–50.

Lambeck K, Esat T M, Potter E K, 2002a. Links between climate and sea levels for the past three million years. Nature, 419 (6903): 199–206.

Lambeck K, Yokoyama Y, Purcell T, 2002b. Into and out of the Last Glacial Maximum: sea-level change during Oxygen Isotope Stages 3 and 2. Quaternary Science Reviews, 21 (1–3): 343–360.

Lambeck K, Purcell A, Johnston P, Nakada M, Yokoyama Y, 2003. Water-load definition in the glacio-hydro-isostatic sea-level equation. Quaternary Science Reviews, 22 (2–4): 309–318.

Lambeck K, Anzidei M, Antonioli F, Benini A, Esposito A, 2004a. Sea level in Roman time in the Central Mediterranean and implications for recent change. Earth and Planetary Science Letters, 224 (3–4): 563–575.

Lambeck K, Antonioli F, Purcell A, Silenzi S, 2004b. Sea-level change along the Italian coast for the past 10,000 yr. Quaternary Science Reviews, 23 (14–15): 1567–1598.

Lambeck K, Purcell A, 2005. Sea-level change in the Mediterranean Sea since the LGM: model predictions for tectonically stable areas. Quaternary Science Reviews, 24 (18–19): 1969–1988.

Lambeck K, Purcell A, Funder S, Kjaer K H, Larsen E, Moller P, 2006. Constraints on the Late Saalian to early Middle Weichselian ice sheet of Eurasia from field data and rebound modelling. Boreas, 35 (3): 539–575.

Lambert A, Courtier N, Sasagawa G S, Klopping F, Winester D, James T S, Liard J O, 2001. New constraints on Laurentide postglacial rebound from absolute gravity measurements. Geophysical Research Letters, 28 (10): 2109–2112.

Latychev K, Mitrovica J X, Tromp J, Tamisiea M E, Komatitsch D, Christara C C, 2005a. Glacial isostatic adjustment on 3-D earth models: a finite-volume formulation. Geophysical Journal International, 161: 421–444.

Latychev K, Mitrovica J X, Tamisiea M E, Tromp J, Moucha R, 2005b. Influence of lithospheric thickness variations on 3-D crustal velocities due to glacial isostatic adjustment. Geophysical Research Letters, 32 (1): L01304.

Latychev K, Mitrovica J X, Tamisiea M E, Tromp J, Christara C C, Moucha R, 2005c. GIA-induced secular variations in the Earth's long wavelength gravity field: Influence of 3-D viscosity variations. Earth and Planetary Science Letters, 240 (2): 322–327.

Lee H, Shum C K, Kuo C Y, Yi Y, Braun A, 2008. Application of TOPEX altimetry for solid earth deformation studies. Terrestrial, Atmospheric and Oceanic Sciences, 19 (1–2): 37–46.

Lidberg M, Johansson J M, Scherneck H G, Davis J L, 2007. An improved and extended GPS-derived 3D velocity field of the glacial isostatic adjustment (GIA) in Fennoscandia. Journal of Geodesy, 81 (3): 213–230.

Lombard A, Garcia D, Ramillien G, Cazenave A, Biancale R, Lemome J M, Flechtner F, Schmidt R, Ishii M, 2007. Estimation of steric sea level variations from combined GRACE and Jason-1 data. Earth and Planetary Science Letters, 254 (1–2): 194–2002.

Love A E H, 1909. The yielding of the Earth to disturbing forces. Proceedings of the Royal Society of London, 82: 73–88.

Lund B, Zoback M D, 1999. Orientation and magnitude of in situ stress to 6.5 km depth in the Baltic Shield. International Journal of Rock Mechanics and Mining Sciences, 36 (2): 169–190.

Lund B, 2005. Effects of deglaciation on the crustal stress field and implications for endglacial faulting: A parametric study of simple Earth and ice models. SKB Report TR-05-04.

Mainville A, Craymer M, 2005. Present-day tilting of the Great Lakes region based on water level gauges. Geological Society of America Bulletin, 117: 1070–1080.

Martinec Z, 1999. Spectral, initial value approach for viscoelastic relaxation of a spherical earth with a three-dimensional viscosity – I. Theory. Geophysical Journal International, 137 (2): 469–488.

Martinec Z, 2000. Spectral-finite element approach to three-dimensional viscoelastic relaxation in a spherical earth. Geophysical Journal International, 142 (1): 17–141.

Martinec Z, Cadek O, Fleitout L, 2001. Can the 1D viscosity profiles inferred from postglacial rebound data be affected by lateral viscosity variations in the tectosphere? Geophysical Research Letters, 28 (23): 4403–4406.

Martinec Z, Hagedoorn J, 2005. Time-domain approach to linearized rotational response of a three-dimensional viscoelastic earth model induced by glacial-isostatic adjustment: I. Inertia-tensor perturbations. Geophysical Journal International, 163 (2): 443–462.

Martinec Z, Wolf D, 2005. Inverting the Fennoscandian relaxation-time spectrum in terms of an axisymmetric viscosity distribution with a lithospheric root. Journal of Geodynamics, 39 (2): 143–163.

McCarthy D D, Luzum B J, 1996. Path of the mean rotational pole from 1899 to 1994. Geophysical Journal International, 125: 623–629.

McConnell R K, 1968. Viscosity of the Mantle from Relaxation Time Spectra of Isostatic Adjustment. Journal of Geophysical Research, 73 (22): 7089–7105.

Melosh H J, Raefsky A, 1980. The dynamical origin of subduction zone topography, collocation method for the solution of partial differential equations. Geophysical Journal of the Royal Astronomical Society, 60: 333–354.

Melosh H J, Raefsky A, 1983. Anelastic response of the Earth to a dip slip earthquake. Journal of Geophysical Research, 88 (NB1): 515–526.

Miller L, Douglas B C, 2004. Mass and volume contributions to twentieth-century global sea level rise. Nature, 428 (6981): 406–409.

Milne G A, Mitrovica J X, 1996. Postglacial sea-level change on a rotating Earth: First results from a gravitationally self-consistent sea-level equation. Geophysical Journal International, 126 (3): F13–F20.

Milne G A, 1998. Refining models of the glacial isostatic adjustment process. PhD thesis, University of Toronto, Toronto.

Milne G A, Mitrovica J X, 1998a. Postglacial sea-level change on a rotating Earth. Geophysical Journal International, 133 (1): 1–19.

Milne G A, Mitrovica J X, 1998b. The influence of time-dependent ocean-continent geometry on predictions of post-glacial sea level change in Australia and New Zealand. Geophysical Research Letters, 25 (6): 793–796.

Milne G A, Mitrovica J X, Forte A M, 1998. The sensitivity of glacial isostatic adjustment predictions to a low-viscosity layer at the base of the upper mantle. Earth and Planetary Science Letters, 154 (1–4): 265–278.

Milne G A, Mitrovica J X, Davis J L, 1999. Near-field hydro-isostasy: the implementation of a revised sea-level equation. Geophysical Journal International, 139 (2): 464–482.

Milne G A, Davis J L, Mitrovica J X, Scherneck H G, Johansson J M, Vermeer M, Koivula H, 2001. Space-geodetic constraints on glacial isostatic adjustment in Fennoscandia. Science, 291 (5512): 2381–2385.

Milne G A, Mitrovica J X, Schrag D P, 2002. Estimating past continental ice volume from sea-level data. Quaternary Science Reviews, 21 (1–3): 361–376.

Milne G A, Mitrovica J X, Scherneck H G, Davis J L, Johansson J M, Koivula H, Vermeer M, 2004. Continuous GPS measurements of postglacial adjustment in Fennoscandia: 2. Modeling results. Journal of Geophysical Research, 109 (B2): B02412.

Milne G A, Long A J, Bassett S E, 2005. Modelling Holocene relative sea-level observations from the Caribbean and South America. Quaternary Science Reviews, 24 (10–11): 1183–1202.

Milne G A, Shennan I, Youngs B A R, Waugh A I, Teferle F N, Bingley R M, Bassett S E, Cuthbert-Brown C, Bradley S L, 2006. Modelling the glacial isostatic adjustment of the UK region. Philosophical Transactions of the Royal Society, Series A, 364 (1841): 931–948.

Mitrovica J X, Peltier W R, 1991a. On postglacial geoid subsidence over the equatorial oceans. Journal of Geophysical Research, 96 (B12): 20053–20071.

Mitrovica J X, Peltier W R, 1991b. A complete formalism for the inversion of postglacial rebound data – resolving power analysis. Geophysical Journal International, 104 (2): 267–288.

Mitrovica J X, Peltier W R, 1991c. Free air gravity-anomalies associated with glacial isostatic disequilibrium – load history effects on the inference of deep mantle viscosity. Geophysical Research Letters, 18 (2): 235–238.

Mitrovica J X, Peltier W R, 1992a. A comparison of methods for the inversion of viscoelastic relaxation spectra. Geophysical Journal International, 108 (2): 410–414.

Mitrovica J X, Peltier W R, 1992b. Constraints on mantle viscosity from relative sea-level variations in Hudson-Bay. Geophysical Research Letters, 19 (12): 1185–1188.

Mitrovica J X, Peltier W R, 1993a. The inference of mantle viscosity from an inversion of the Fennoscandian relaxation spectrum. Geophysical Journal International, 114 (1): 45–62.

Mitrovica J X, Peltier W R, 1993b. Present-day secular variations in the zonal harmonics of Earth's geopotential. Journal of Geophysical Research, 98 (B3): 4509–4526.

Mitrovica J X, Davis J L, Shapiro I I, 1993. Constraining proposed combinations of ice history and Earth rheology using VLBI determined baseline length rates in North America. Geophysical Research Letters, 20 (21): 2387–2390.

Mitrovica J X, Davis J L, Shapiro I I, 1994a. A spectral formalism for computing 3-dimensional deformations due to surface loads 1. Theory. Journal of Geophysical Research, 99 (B4): 7057–7073.

Mitrovica J X, Davis J L, Shapiro I, 1994b. A spectral formalism for computing 3-dimensional deformations due to surface loads 2. Present-day glacial isostatic-adjustment. Journal of Geophysical Research, 99 (B4): 7075–7101.

Mitrovica J X, Davis J L, 1995a. The influence of a finite glaciation phase on predictions of post-glacial isostatic adjustment. Earth and Planetary Science Letters, 136 (3–4): 343–361.

Mitrovica J X, Davis J L, 1995b. Present-day postglacial sea-level change far from the Late Pleistocene ice sheets – implications for recent analyses of tide-gauge records. Geophysical Research Letters, 22 (18): 2529–2532.

Mitrovica J X, Forte A M, 1995. Pleistocene glaciation and the Earth's precession constant. Geophysical Journal International, 121 (1): 21–32.

Mitrovica J X, Peltier W R, 1995. Constraints on mantle viscosity based upon the inversion of postglacial uplift data from the Hudson-Bay region. Geophysical Journal International, 122 (2): 353–377.

Mitrovica J X, 1996. Haskell [1935/ revisited. Journal of Geophysical Research, 101 (B1): 555–569.

Mitrovica J X, Forte A M, 1997. Radial profile of mantle viscosity: Results from the joint inversion of convection and postglacial rebound observables. Journal of Geophysical Research, 102 (B): 2751–2769.

Mitrovica J X, Milne G A, 1998. Glaciation-induced perturbations in the Earth's rotation: A new appraisal. Journal of Geophysical Research, 103 (B1): 985–1005.

Mitrovica J X, Milne G A, Davis J L, 2001a. Glacial isostatic adjustment on a rotating earth. Geophysical Journal International, 147 (3): 562–578.

Mitrovica J X, Tamisiea M E, Davis J L, Milne G A, 2001b. Recent mass balance of polar ice sheets inferred from patterns of global sea-level change. Nature, 409 (6823): 1026–1029.

Mitrovica J X, Forte A M, 2002. On the radial profile of mantle viscosity. In: JX Mitrovica, BLA Vermeersen (Editors), Ice Sheets, Sea Level and the Dynamic Earth. AGU Geodynamics Series, Washington DC, vol. 29, pp. 187–199.

Mitrovica J X, Milne G A, 2002. On the origin of late Holocene sea-level highstands within equatorial ocean basins. Quaternary Science Reviews, 21 (20–22): 2179–2190.

Mitrovica J X, 2003. Recent controversies in predicting post-glacial sea-level change. Quaternary Science Reviews, 22 (2–4): 127–133.

Mitrovica J X, Milne G A, 2003. On post-glacial sea level: I. General theory. Geophysical Journal International, 154 (2): 253–267.

Mitrovica J X, Forte A M, 2004. A new inference of mantle viscosity based upon joint inversion of convection and glacial isostatic adjustment data. Earth and Planetary Science Letters, 225 (1–2): 177–189.

Mitrovica J X, Wahr J, Matsuyama I, Paulson A, 2005. The rotational stability of an ice-age Earth. Geophysical Journal International, 161 (2): 491–506.

Mohammed N, 2003. An investigation into the Effects of Glacial-Induced Erosion on Contemporary Models of Glacial Isostatic Adjustment. Master's Thesis, Durham University.

Molnar P, England P C, 1990. Late Cenozoic uplift of mountain-ranges and global climate change – chicken or egg. Nature 346 (6279): 29–34.

MSC Marc, 2003. Version 2003. MSC. Software Corporation (NYSE: MNS), Redwood City, California.

Munk W H, MacDonald G J F, 1960. The Rotation of the Earth. Cambridge University Press, New York.

Munk W, 2002. Twentieth century sea level: An enigma. Proceedings of the National Academy of Sciences of the United States of America, 99 (10): 6550–6555.

Mäkinen J, Engfeldt A, Harsson B G, Ruotsalainen H, Strykowski G, Oja T, Wolf D, 2005. The Fennoscandian land uplift gravity lines 1966–2003. In: C Jekeli, L Bastos, J Fernades (Editors), Gravity, Geoid and Space Missions. Springer Berlin Heidelberg, pp. 328–332.

Mäkinen J, Amalvict M, Shibuya K, Fukuda Y, 2007. Absolute gravimetry in Antarctica: Status and prospects. Journal of Geodynamics, 43: 339–357.

Nakada M, Lambeck K, 1987. Glacial rebound and relative sea-level variations – A new appraisal. Geophysical Journal of the Royal Astronomical Society, 90 (1): 171–224.

Nakada M, Lambeck K, 1988. The melting history of the Late Pleistocene Antarctic ice-sheet. Nature, 333 (6168): 36–40.

Nakada M, Lambeck K, 1989. Late Pleistocene and Holocene sea-level change in the Australian region and mantle rheology. Geophysical Journal International, 96: 497–517.

Nakada M, Lambeck K, 1991. Late Pleistocene and Holocene sea-level change: Evidence for lateral mantle viscosity structure? In: R. Sabadini, K. Lambeck, and E. Boschi (Editors), Glacial Isostasy, Sea Level and Mantle Rheology. Springer, New York, pp. 79–94.

Nakiboglu S M, Lambeck K, 1980. Deglaciation effects on the rotation of the Earth. Geophysical Journal of the Royal Astronomical Society, 62 (1): 49–58.

Nakiboglu S M, Lambeck K, 1981. Deglaciation related features of the Earth's gravity-field. Tectonophysics, 72 (3–4): 289–303.

Nataf H C, Ricard Y, 1996. 3SMAC: An a priori tomographic model of the upper mantle based on geophysical modelling. Physics of the Earth and Planetary Interiors, 95 (1–2): 101–122.

Nerem R S, Mitchum G T, 2002. Estimates of vertical crustal motion derived from differences of TOPEX/POSEIDON and tide gauge sea level measurements. Geophysical Research Letters, 29 (19): 1934, doi: 10.1029/2002GL015037.

Nocquet J-M, Calais E, Parsons B, 2005. Geodetic constraints on glacial isostatic adjustment in Europe. Geophysical Research Letters, 32: L06308, doi: 10.1029/2004GL022174.

Nunn P D, Peltier W R, 2001. Far-field test of the ICE-4G model of global isostatic response to deglaciation using empirical and theoretical Holocene sea-level reconstructions for the Fiji Islands, southwestern Pacific. Quaternary Research, 55 (2): 203–214.

Nygård A, Sejrup H P, Haflidason H, Bryn P, 2005. The glacial North Sea Fan, southern Norwegian Margin: architecture and evolution from the upper continental slope to the deep-sea basin. Marine and Petroleum Geology, 22 (1–2): 71–84.

Pagiatakis S D, Salib P, 2003. Historical relative gravity observations and the time rate of change of gravity due to postglacial rebound and other tectonic movements in Canada. Journal of Geophysical Research, 108 (B9): 2406.

Pagli C, Sigmundsson F, 2008. Will present day glacier retreat increase volcanic activity? Stress induced by recent glacier retreat and its effect on magnetism at the Vatnajokull ice cap, Iceland. Geophysical Research Letters, 35 (9): L09304.

Park K D, Nerem R S, Davis J L, Schenewerk M S, Milne G A, Mitrovica J X, 2002. Investigation of glacial isostatic adjustment in the northeast US using GPS measurements. Geophysical Research Letters, 29 (11): 1509.

Parsons B D, 1972. Changes in the Earth's shape. PhD Thesis, Cambridge University, Cambridge.

Paulson A, Zhong S J, Wahr J, 2005. Modelling post-glacial rebound with lateral viscosity variations. Geophysical Journal International, 163 (1): 357–371.

Paulson A, Zhong S J, Wahr J, 2007. Limitations on the inversion for mantle viscosity from postglacial rebound. Geophysical Journal International, 168 (3): 1195–1209.

Peltier W R, 1974. Impulse response of a Maxwell Earth. Reviews of Geophysics, 12 (4): 649–669.

Peltier W R, 1976. Glacial-isostatic adjustment. 2. Inverse Problem. Geophysical Journal of the Royal Astronomical Society, 46 (3): 605–646.

Peltier W R, Andrews J T, 1976. Glacial-isostatic adjustment. 1. Forward Problem. Geophysical Journal of the Royal Astronomical Society, 46 (3): 605–646.

Peltier W R, Farrell W E, Clark J A, 1978. Glacial isostasy and relative sea-level – global finite-element model. Tectonophysics, 50 (2–3): 81–110.

Peltier W R, 1985. New constraints on transient lower mantle rheology and internal mantle buoyancy from glacial rebound data. Nature, 318 (6047): 614–617.

Peltier W R, 1988. Global sea-level and Earth rotation. Science, 240 (4854): 895–901.

Peltier W R, Tushingham A M, 1991. Influence of glacial isostatic-adjustment on tide-gauge measurements of secular sea-level change. Journal of Geophysical Research, 96 (B4): 6779–6796.

Peltier W R, 1994. Ice age paleotopography. Science, 265: 195–201.

Peltier W R, 1995. VLBI Baseline Variations from the ICE-4G Model of Postglacial Rebound. Geophysical Research Letters, 22 (4): 465–468.

Peltier W R, 1996a. Mantle viscosity and ice-age ice sheet topography. Science, 273 (5280): 1359–1364.

Peltier W R, 1996b. Global sea level rise and glacial isostatic adjustment: An analysis of data from the east coast of North America. Geophysical Research Letters, 23 (7): 717–720.

Peltier W R, Jiang X H, 1996a. Glacial isostatic adjustment and Earth rotation: Refined constraints on the viscosity of the deepest mantle. Journal of Geophysical Research, 101 (B2): 3269–3290.

Peltier W R, Jiang X H, 1996b. Mantle viscosity from the simultaneous inversion of multiple data sets pertaining to postglacial rebound. Geophysical Research Letters, 23 (5): 503–506.

Peltier W R, 1998a. Postglacial variations in the level of the sea: Implications for climate dynamics and solid-earth geophysics. Reviews of Geophysics, 36 (4): 603–689.

Peltier W R, 1998b. "Implicit ice" in the global theory of glacial isostatic adjustment. Geophysical Research Letters, 25 (21): 3955–3958.

Peltier W R, 1998c. A space geodetic target for mantle viscosity discrimination: Horizontal motions induced by glacial isostatic adjustment. Geophysical Research Letters, 25 (4): 543–546.

Peltier W R, 1999. Global sea level rise and glacial isostatic adjustment. Global and Planetary Change, 20 (2–3): 93–123.

Peltier W R, 2001. Global glacial isostatic adjustment and modern instrumental records of relative sea level history. In: B.C. Douglas, M.S. Kearney, and S.P. Leatherman (Editors), Sea Level Rise. Elsevier, New York, pp. 65–93.

Peltier W R, 2002a. Global glacial isostatic adjustment: palaeogeodetic and space-geodetic tests of the ICE-4G (VM2) model. Journal of Quaternary Science, 17 (5–6): 491–510.

Peltier W R, 2002b. On eustatic sea level history: Last Glacial Maximum to Holocene. Quaternary Science Reviews, 21 (1–3): 377–396.

Peltier W R, Drummond R, 2002. A "broad-shelf effect" upon postglacial relative sea level history. Geophysical Research Letters, 29 (8): 1169, doi: 10.1029/2001GL014273.

Peltier W R, Shennan I, Drummond R, Horton B, 2002. On the postglacial isostatic adjustment of the British Isles and the shallow viscoelastic structure of the Earth. Geophysical Journal International, 148 (3): 443–475.

Peltier W R, 2004. Global glacial isostasy and the surface of the ice-age earth: The ice-5G (VM2) model and GRACE. Annual Review of Earth and Planetary Science, 32: 111–149.

Peltier W R, 2005. On the hemispheric origins of meltwater pulse 1a. Quaternary Science Reviews, 24 (14–15): 1655–1671.

Peltier W R, Fairbanks R G, 2006. Global glacial ice volume and Last Glacial Maximum duration from an extended Barbados sea level record. Quaternary Science Reviews, 25 (23–24): 3322–3337.

Pérez-Gussinyé M, Lowry A, Watts A B, Velicogna I, 2004. On the recovery of the effective elastic thickness using spectral methods: examples from synthetic data and the Fennoscandian shield. Journal of Geophysical Research, 109: 10.1029/2003JB002788.

Poudjom Djomani Y H, Fairhead J D, Griffin W L, 1999. The flexural rigidity of Fennoscandia: reflection of the tectonothermal age of the lithospheric mantle. Earth and Planetary Science Letters, 174: 139–154.

Ramillien G, Bouhours S, Lombard A, Cazenave A, Flechtner F, Schmidt R, 2008. Land water storage contribution to sea level from GRACE geoid data over 2003–2006. Global and Planetary Change, 60 (3–4): 381–392.

Rasmussen E, Fjeldskaar W, 1996. Quantification of the Pliocene-Pleistocene erosion of the Barents Sea from present-day bathymetry. Global and Planetary Change, 12 (1–4): 119–133.

Ricard Y, Sabadini R, Spada G, 1992. Isostatic deformations and polar wander induced by internal mass redistribution. Journal of Geophysical Research, 97: 14223–14236.

Ricard Y, Spada G, Sabadini R, 1993. Polar wandering of a dynamic Earth. Geophysical Journal International, 113 (2): 284–298.

Richards M A, Hager B H, 1984. Geoid anomalies in a dynamic Earth. Journal of Geophysical Research, 89 (B7): 5987–6002.

Riis F, Fjeldskaar W, 1992. On the magnitude of the Late Tertiary and Quaternary erosion and its significance for the uplift of Scandinavia and the Barents Sea. In: RM Larsen et al. (Editors), Structural and Tectonic Modelling and its Application to Petroleum Geology. Nor. Pet. Soc. Spec. Publ., 1: 163–185.

Ritsema J, van Heijst J H, Woodhouse J H, 1999. Complex shear wave velocity structure imaged beneath Africa and Iceland. Science, 286: 1925–1928.

Ritsema J, van Heijst J H, Woodhouse J H, 2004. Global transition zone tomography. Journal of Geophysical Research, 109, B02302, doi. 10.1029/2003JB002610.

Rostami K, Peltier W R, Mangini A, 2000. Quaternary marine terraces, sea-level changes and uplift history of Patagonia, Argentina: comparisons with predictions of the ICE-4G (VM2) model of the global process of glacial isostatic adjustment. Quaternary Science Reviews, 19 (14–15): 1495–1525.

Sabadini R, Peltier W R, 1981. Pleistocene deglaciation and the Earth's rotation – implications for mantle viscosity. Geophysical Journal of the Royal Astronomical Society, 66 (3): 553–578.

Sabadini R, Yuen D A, Boschi E, 1982. Polar wandering and the forced responses of a rotating, multilayered, viscoelastic planet, Journal of Geophysical Research, 87: 2885–2903.

Sabadini R, Yuen D A, Portney M, 1986. The effect of upper mantle lateral heterogeneities on post-glacial rebound. Geophysical Research Letters, 13: 337–340.

Sabadini R, Doglioni C, Yuen D A, 1990. Eustatic sea-level fluctuations induced by polar wander. Nature, 345 (6277): 708–710.

Sabadini R, Vermeersen L L A, 2002. Long-term rotation instabilities of the Earth: a reanalysis. In: JX Mitrovica, BLA Vermeersen (Editors), Ice Sheets, Sea Level and the Dynamic Earth. AGU Geodynamics Series, Washington DC, vol. 29, pp. 51–67.

Sabadini R, Marotta A M, De Franco R, Vermeersen L L A, 2002. Style of density stratification in the mantle and true polar wander induced by ice loading. Journal of Geophysical Research, 107 (B10): 2258.

Sasgen I, Martinec Z, Fleming K, 2007. Regional ice-mass changes and glacial-isostatic adjustment in Antarctica from GRACE. Earth and Planetary Science Letters, 264 (3–4): 391–401.

Sauber J M, Molnia B F, 2004. Glacier ice mass fluctuations and fault instability in tectonically active Southern Alaska. Global and Planetary Change, 42 (1–4): 279–293.

Scherneck H G, Johansson J M, Vermeer M, Davis J L, Milne G A, Mitrovica J X, 2001. BIFROST project: 3-D crustal deformation rates derived from GPS confirm postglacial rebound in Fennoscandia. Earth, Planets and Space, 53 (7): 703–708.

Schotman H H A, Vermeersen L L A, 2005. Sensitivity of glacial isostatic adjustment models with shallow low-viscosity earth layers to the ice-load history in relation to the performance of GOCE and GRACE. Earth and Planetary Science Letters, 236 (3–4): 828–844.

Sella G F, Stein S, Dixon T H, Craymer M, James T S, Mazzotti S, Dokka R K, 2007. Observation of glacial isostatic adjustment in "stable" North America with GPS. Geophysical Research Letters, 34 (2): L02306.

Shennan I, Peltier W R, Drummond R, Horton B, 2002. Global to local scale parameters determining relative sea-level changes and the post-glacial isostatic adjustment of Great Britain. Quaternary Science Reviews, 21 (1–3): 397–408.

Simons M, Hager B H, 1997. Localization of the gravity field and the signature of glacial rebound. Nature, 390: 500–504.

SKB, 2006. Climate and climate-related issues for the safety assessment SR-Can. SKB TR-06-23, Svensk Kärnbränslehantering AB.

Spada G, Antonioli A, Boschi L, Brandi V, Cianetti S, Galvani G, Giunchi C, Perniola B, Agostinetti N P, Piersanti A, Stocchi P, 2004. Modeling earth's post-glacial rebound. EOS, Transactions, AGU, 85 (6): 62–64.

Spada G, Antonioli A, Cianetti S, Giunchi C, 2006. Glacial isostatic adjustment and relative sea-level changes: the role of lithospheric and upper mantle heterogeneities in a 3-D spherical Earth. Geophysical Journal International, 165: 692–702.

Spada G, Stocchi P, 2007. SELEN: A Fortran 90 program for solving the "sea-level equation". Computers and Geosciences, 33 (4): 538–562.

Steffen H, Kaufmann G, 2005. Glacial isostatic adjustment of Scandinavia and northwestern Europe and the radial viscosity structure of the Earth's mantle. Geophysical Journal International, 163 (2): 801–812.

Steffen H, Kaufmann G, Wu P, 2006. Three-dimensional finite-element modeling of the glacial isostatic adjustment in Fennoscandia. Earth and Planetary Science Letters, 250 (1–2): 358–375.

Steffen H, Wu P, Kaufmann G, 2007. Sensitivity of crustal velocities in Fennoscandia to radial and lateral viscosity variations in the mantle. Earth and Planetary Science Letters, 257 (3–4): 474–485.

Steinberger B, O'Connell R J, 1997. Changes of the Earth's rotation axis owing to advection of mantle density heterogeneities. Nature, 387: 169–173.

Stewart I S, Sauber J, Rose J, 2000. Glacio-seismotectonics: ice sheets, crustal deformation and seismicity. Quaternary science Reviews, 19 (14–15): 1367–1389.

Svendsen J I, Astakhov V I, Bolshiyanov D Y, Demidov I, Dowdeswell J A, Gataullin V, Hjort C, Hubberten H W, Larsen E, Mangerud J, Melles M, Moller P, Saarnisto M, Siegert M J, 1999. Maximum extent of the Eurasian ice sheets in the Barents and Kara Sea region during the Weichselian. Boreas, 28 (1): 234–242.

Tamisiea M E, Mitrovica J X, Milne G A, Davis J L, 2001. Global geoid and sea level changes due to present-day ice mass fluctuations. Journal of Geophysical Research, 106 (B12): 30849–30863.

Tamisiea M E, Mitrovica J X, Davis J L, Milne G A, 2003. Long wavelength sea level and solid surface perturbations driven by polar ice mass variations: Fingerprinting Greenland and Antarctic ice sheet flux. Space Science Reviews, 108 (1–2): 81–93.

Tamisiea M E, Mitrovica J X, Davis J L, 2007. GRACE gravity data constrain ancient ice geometries and continental dynamics over Laurentia. Science, 316 (5826): 881–883.

Tarasov L, Peltier W R, 2002. Greenland glacial history and local geodynamical consequences. Geophysical Journal International, 150 (1): 198–229.

Tarasov L, Peltier W R, 2004. A geophysically-constrained large ensemble analysis of the deglacial history of the North American ice-sheet complex. Quaternary Science Reviews, 23 (3–4): 359–388.

Tarasov L, Peltier W R, 2006. A calibrated deglacial drainage chronology for the North America continent: evidence of an Arctic trigger for the Younger Dryas. Quaternary Science Reviews, 25 (7–8): 659–688.

Teller J T, 1995. History and drainage of large ice-dammed lakes along the Laurentide Ice Sheet. Quaternary International, 28: 83–92.

Tromp J, Mitrovica J X, 1999a. Surface loading of a viscoelastic earth – I. General theory. Geophysical Journal International, 137 (3): 847–855.

Tromp J, Mitrovica J X, 1999b. Surface loading of a viscoelastic earth – II. Spherical models. Geophysical Journal International, 137 (3): 856–872.

Tromp J, Mitrovica J X, 2000. Surface loading of a viscoelastic planet – III. Aspherical models. Geophysical Journal International, 140 (2): 425–441.

Tushingham A M, Peltier W R, 1991. ICE-3G – A new global-model of Late Pleistocene deglaciation based upon geophysical predictions of postglacial relative sea-level change. Journal of Geophysical Research, 96 (B3): 4497–4523.

Tushingham A M, Peltier W R, 1992. Validation of the ICE-3G model of Wurm-Wisconsin deglaciation using a global data-base of relative sea-level histories. Journal of Geophysical Research, 97 (B3): 3285–3304.

Tushingham A M, Peltier W R, 1993. Relative Sea Level Database. IGPB PAGES/World Data Center-A for Paleoclimatology Data Contribution Series # 93-016, NOAA/NGDC Paleoclimatology Program, Boulder, Colorado.

Törnqvist T E, Bick S J, van der Borg K, de Jong A F M, 2006. How stable is the Mississippi Delta? Geology, 34 (8): 697–700.

Van de Plassche O, 1986. Sea-Level Research: A Manual for the Collection and Evaluation of Data. GeoBooks, Norwich.

Van der Lee, 2002. High-resolution estimates of lithospheric thickness from Missouri to Massachusetts, USA. Earth and Planetary Science Letters, 203 (1): 15–23.

Van der Wal W, Schotman H H A, Vermeersen L L A, 2004. Geoid heights due to a crustal low viscosity zone in glacial isostatic adjustment modelling: A sensitivity analysis for GOCE. Geophysical Research Letters, 31 (5): L05608.

Velicogna I, Wahr J, 2002. A method for separating Antarctic postglacial rebound and ice mass balance using future ICESat Geoscience Laser Altimeter System, Gravity Recovery and Climate Experiment, and GPS satellite data. Journal of Geophysical Research, 107 (B10): 2263, doi: 10.1029/2001JB000708.

Vermeersen L L A, Sabadini R, Spada G, Vlaar N J, 1994. Mountain building and Earth rotation. Geophysical Journal International, 117: 610–624.

Vermeersen L L A, Sabadini R, Spada G, 1996. Analytical visco-elastic relaxation models. Geophysical Research Letters, 23: 697–700.

Vermeersen L L A, Sabadini R, 1997. A new class of stratified viscoelastic models by analytical techniques. Geophysical Journal International, 129 (3): 531–570.

Vermeersen L L A, Fournier A, Sabadini R, 1997. Changes in rotation induced by Pleistocene ice masses with stratified analytical Earth models. Journal of Geophysical Research, 102 (B12): 27689–27702.

Vermeersen L L A, Sabadini R, 1999. Polar wander, sea-level variations and ice age cycles. Surveys in Geophysics, 20 (5): 415–440.

Vermeersen L L A, 2003. The potential of GOCE in constraining the structure of the crust and lithosphere from post glacial rebound. Space Science Reviews, 108 (1–2): 105–113.

Vestøl O, 2006. Determination of postglacial land uplift in Fennoscandia from levelling, tide-gauges and continuous GPS stations using least squares collocation. Journal of Geodesy 80: 248–258.

Walcott R I, 1972. Past sea levels, eustasy and deformation of the Earth. Quaternary Research, 2: 1–14.

Wang H, Wu P, 2006. Effects of lateral variations in lithospheric thickness and mantle viscosity on glacially-induced surface motion on a spherical, self-gravitating Maxwell Earth. Earth and Planetary Science Letters, 244 (3–4): 576–589.

Watts A B, Zhong S, 2000. Observations of flexure and the rheology of oceanic lithosphere. Geophysical Journal International, 142 (3): 855–875.

Watts A B, 2001. Isostasy and Flexure of the Lithosphere. Cambridge University Press, New York.

Whitehouse P, Latychev K, Milne G A, Mitrovica J X, Kendall R, 2006. Impact of 3-D Earth structure on Fennoscandian glacial isostatic adjustment: implication for space-geodetic estimates of present-day crustal deformations. Geophysical Research Letters, 33, L13502, doi: 10.1029/2006GL026568.

Whitehouse P, 2007. A relative sea-level data base for Fennoscandia. Unpublished database available at SKB.

Whitehouse P L, Allen M B, Milne G A, 2007. Glacial isostatic adjustment as a control on coastal processes: An example from the Siberian Arctic. Geology, 35 (8): 747–750.

Wieczerkowski K, Mitrovica J X, Wolf D, 1999. A revised relaxation-time spectrum for Fennoscandia. Geophysical Journal International, 139 (1): 69–86.

Willis J K, Roemmich D, Cornuelle B, 2004. Interannual variability in upper ocean heat content, temperature, and thermosteric expansion on global scales. Journal of Geophysical Research, 109 (C12): C12036.

Wolf D, 1984. The relaxation of spherical and flat Maxwell Earth models and effects due to the presence of the lithosphere. Journal of Geophysics, 56 (1): 24–33.

Wolf D, Kaufmann G, 2000. Effects due to compressional and compositional density stratification on load-induced Maxwell viscoelastic perturbations. Geophysical Journal International, 140 (1): 51–62.

Wu P, 1978. The response of a Maxwell Earth to applied surface mass loads: Glacial isostatic adjustment. MSc Thesis. University of Toronto, Toronto.

Wu P, Peltier W R, 1978. Glacial isostasy and relative sea-level – Global finite-element model. Transactions – American Geophysical Union, 59 (12): 1028–1028.

Wu P, Peltier W R, 1982. Viscous gravitational relaxation. Geophysical Journal of the Royal Astronomical Society, 70: 435–486.

Wu P, Peltier W R, 1983. Glacial isostatic-adjustment and the free air gravity-anomaly as a constraint on deep mantle viscosity. Geophysical Journal of the Royal Astronomical Society, 74 (2): 377–449.

Wu P, Peltier W R, 1984. Pleistocene deglaciation and the Earth's rotation – a new analysis. Geophysical Journal of the Royal Astronomical Society, 76 (3): 753–791.

Wu P, 1992a. Viscoelastic versus viscous deformation and the advection of pre-stress. Geophysical Journal International, 108 (1): 136–142.

Wu P, 1992b. Deformation of an incompressible viscoelastic flat earth with power-law creep: a finite element approach. Geophysical Journal International, 108 (1): 35–51.

Wu P, 1993. Postglacial rebound in a power-law medium with axial symmetry and the existence of the transition zone in relative sea-level data. Geophysical Journal International, 114 (3): 417–432.

Wu P, 1995. Can observations of postglacial rebound tell whether the rheology of the mantle is linear or nonlinear? Geophysical Research Letters, 22 (13): 1645–1648.

Wu P, 1996. Changes in orientation of near-surface stress field as constraints to mantle viscosity and horizontal stress differences in Eastern Canada. Geophysical Research Letters, 23 (17): 2263–2266.

Wu P, Hasegawa H S, 1996a. Induced stresses and fault potential in eastern Canada due to a realistic load: A preliminary analysis. Geophysical Journal International, 127 (1): 215–229.

Wu P, Hasegawa H S, 1996b. Induced stresses and fault potential in eastern Canada due to a disc load: A preliminary analysis. Geophysical Journal International, 125 (2): 415–430.

Wu P, Ni Z H, 1996. Some analytical solutions for the viscoelastic gravitational relaxation of a two-layer non-self-gravitating incompressible spherical earth. Geophysical Journal International, 126 (2): 413–436.

Wu P, 1997. Effect of viscosity on fault potential and stress orientations in eastern Canada. Geophysical Journal International, 130 (2): 365–382.

Wu P, Johnston P, 1998. Validity of using flat-earth finite element models in the study of postglacial rebound. In: Wu, P (Editor), Dynamics of the Ice Age Earth: A Modern Perspective. Trans. Tech. Pub., Zurich, Switzerland, pp.191–202.

Wu P, Ni Z, Kaufmann G, 1998. Postglacial rebound with lateral heterogeneities: from 2D to 3D modeling. In: Wu, P (Editor), Dynamics of the Ice Age Earth: A Modern Perspective. Trans. Tech. Pub., Zurich, Switzerland, pp.557–582.

Wu P, 1999. Modelling postglacial sea levels with power-law rheology and a realistic ice model in the absence of transient tectonic stress. Geophysical Journal International, 139 (3): 691–702.

Wu P, Johnston P, Lambeck K, 1999. Postglacial rebound and fault instability in Fennoscandia. Geophysical Journal International, 139 (3): 657–670.

Wu P, Johnston P, 2000. Can deglaciation trigger earthquakes in N. America? Geophysical Research Letters, 27 (9): 1323–1326.

Wu P, 2001. Postglacial induced surface motion and gravity in Laurentia for uniform mantle with power-law rheology and ambient tectonic stress. Earth and Planetary Science Letters, 186 (3–4): 427–435.

Wu P, 2002a. Effects of mantle law stress exponent on postglacial induced surface motion and gravity in Laurentia. Geophysical Journal International, 148 (3):676–686.

Wu P, 2002b. Mode coupling in a viscoelastic self-gravitating spherical earth induced by axisymmetric loads and lateral viscosity variations. Earth and Planetary Science Letters, 197 (1–2): 1–10.

Wu P, van der Wal W, 2003. Postglacial sealevels on a spherical, self-gravitating viscoelastic earth: effects of lateral viscosity variations in the upper mantle on the inference of viscosity contrasts in the lower mantle. Earth and Planetary Science Letters, 211: 57–68.

Wu P, 2004. Using commercial finite element packages for the study of earth deformations, sea levels and the state of stress. Geophysical Journal International, 158 (2): 401–408.

Wu P, 2005. Effects of lateral variations in lithospheric thickness and mantle viscosity on glacially induced surface motion in Laurentia. Earth and Planetary Science Letters, 235 (3–4):549–563.

Wu P, Wang H, Schotman H, 2005. Postglacial induced surface motions, sea-levels and geoid rates on a spherical self-gravitating laterally heterogeneous earth. Journal of Geodynamics, 39:127–142.

Wu P, 2006. Sensitivity of relative sea levels and crustal velocities in Laurentide to radial and lateral viscosity variations in the mantle. Geophysical Journal International, 165 (2): 401–413.

Wu P, Wang H, 2008. Postglacial isostatic adjustment in a self-gravitating spherical earth with power-law rheology. Journal of Geodynamics, in press.

Yokoyama Y, Lambeck K, De Dekker P, Johnston P, Fifield L K, 2000. Timing of the Last Glacial Maximum from observed sea-level minima. Nature, 406 (6797): 713–716.

Yokoyama Y, Esat T M, Lambeck K, 2001a. Last glacial sea-level change deduced from uplifted coral terraces of Huon Peninsula, Papua New Guinea. Quaternary International, 83–85: 275–283.

Yokoyama Y, De Dekker P, Lambeck K, Johnston P, Fifield L K, 2001b. Sea-level at the Last Glacial Maximum: evidence from northwestern Australia to constrain ice volumes for oxygen isotope stage 2. Palaeogeography, Palaeoclimatology, Palaeoecology, 165 (3–4): 281–297.

Yokoyama Y, Purcell A, Lambeck K, Johnston P, 2001c. Shore-line reconstruction around Australia during the Last Glacial Maximum and Late Glacial Stage. Quaternary International, 83–85: 9–18.

Yokoyama Y, Purcell A, Marshall J F, Lambeck K, 2006. Sea-level during the early deglacial period in the Great Barrier Reef, Australia. Global and Planetary Change, 53 (1–2): 147–153.

Zhong S J, Zuber M T, Moresi L, Gurnis M, 2000. Role of temperature-dependent viscosity and surface plates in spherical shell models of mantle convection. Journal of Geophysical Research, 105 (B5): 11063–11082.

Zhong S, Paulson A, Wahr J, 2003. Three-dimensional finite-element modelling of Earth's viscoelastic deformation: effects of lateral variations in lithospheric thickness. Geophysical Journal International, 155 (2): 679–695.

Zoback M L, 1992. First- and Second-Order Patterns of Stress in the Lithosphere: The World Stress Map Project. Journal of Geophysical Research, 97 (B8): 11703–11728.

Zweck C, Huybrechts P, 2005. Modeling of the northern hemisphere ice sheets during the last glacial cycle and glaciological sensitivity. Journal of Geophysical Research, 110 (D7): D07103.

Acronyms and selected abbreviations

BIFROST	Baseline Inferences for Fennoscandian Rebound Observations, Sea-level, and Tectonics
BP	Before present
CLFE	Coupled-Laplace Finite Element
FE	Finite Element
GIA	Glacial Isostatic Adjustment
GOCE	Gravity field and steady-state Ocean Circulation Explorer
GPS	Global Positioning System
GRACE	Gravity Recovery and Climate Experiment
IPCC	Intergovernmental Panel on Climate Change
ka	thousand years
LGM	Last Glacial Maximum
Ma	million years
mGal	milligals
Pa s	pascal seconds
PREM	Preliminary Reference Earth Model
RSL	relative sea-level
SLR	Satellite Laser Ranging
SLVZ	Shallow low viscosity zone
VLBI	Very Long Baseline Interferometry